University of Nevada, Reno

Collective Force Generator Model of Muscle Contraction:
Theoretical and Experimental Support for Factors Beyond Detachment Kinetics that Influence Unloaded Shortening Velocities of Muscle

A dissertation submitted in partial fulfillment of the
requirements for the degree of Doctor of Philosophy in
Biomedical Engineering

by

Del Ray Jackson, Jr.

Dr. Jonathan E. Baker/Dissertation Advisor

May, 2013

University of Nevada, Reno
Statewide • Worldwide

THE GRADUATE SCHOOL

We recommend that the dissertation
prepared under our supervision by

DEL RAY JACKSON, JR.

entitled

Collective Force Generator Model Of Muscle Contraction: Theoretical And Experimental Support For Factors Beyond Detachment Kinetics That Influence Unloaded Shortening Velocities Of Muscle

be accepted in partial fulfillment of the
requirements for the degree of

DOCTOR OF PHILOSOPHY

Jonathan E. Baker, Ph. D., Advisor

Christine Cremo, Ph. D., Committee Member

Frederick C Harris, Jr., Ph. D., Committee Member

Nelson G. Publicover, Ph. D., Committee Member

Karen Schlauch, Ph. D., Graduate School Representative

Marsha H. Read, Ph. D., Dean, Graduate School

May, 2013

Abstract

This dissertation covers three related approaches to developing a more complete understanding of how single molecule properties of muscle myosin collectively generate unloaded shortening velocities, *V*. Theory, experimentation, and simulation results all contributed to answering fundamental muscle research questions. These questions focused on addressing how single myosin molecule properties scale in an ensemble to collectively perform work that results in *V* and how attachment kinetics affect *V*. Our work has resulted in the development of a model, based on quantifiable kinetic and physical parameters of myosin and actin, which provides a set of mechanisms to describe experimental data that the predominate models of muscle contraction are unable to.

Acknowledgements

I must acknowledge the critical role teachers have had in inspiring and preparing me for a life of scientific discovery. From my 7th grade science teacher, Mr. Waltz, who assigned me a special assignment to study the effects of pine tree needles on our school tennis courts, to my thesis advisor, Dr. Josh Baker. I am the product of a society that funds, and hopefully continues to appreciate the importance of, education. I therefore gratefully acknowledge the monetary support I have received from society by way of the NIH and NSF.

I am grateful for the contributions of my fellow Baker lab mates to the work outlined in this dissertation as well as the years of camaraderie and encouragement. There are countless moments where impromptu science discussions and white board sessions reinforced and corrected understanding of physical and chemical concepts. All of the Baker lab members have in some way contributed to this work, but special distinction is owed to Dr. Kevin Facemyer, Travis Stewart, Travis Phillips, and Alan Stickney. I also owe much to the one collaborator who was my most ardent challenger and cheerleader, Milad Webb.

The support from the University of Nevada, Reno, in the form of other graduate students, professors, department heads, and department administrative assistants was extremely helpful. My committee members were a distilled demonstration of the help available at UNR. My department chair, Dr. Nelson Publicover, is a fine example of an extremely knowledgeable and extremely compassionate person. Thanks for teaching me the finer points of critical thinking required to evaluate scientific literature. Dr. Fred

Harris has taught me the basics of computer science, starting with data structures, to more advanced concepts such as parallel computing, and did all of it with a cheerful demeanor despite my sometimes thick-headedness. Dr. Christine Cremo has been a fantastic resource for everything from basic muscle concepts to kinetics and scientific writing. I feel very fortunate to have, in addition to my advisor, another muscle research heavyweight on my committee. The graduate experience can be emotionally taxing, and I am grateful for Dr. Karen Schlauch for not only her mathematical expertise, but also for her overwhelming encouragement.

Finally, I have to acknowledge that without the mentorship of Dr. Josh Baker, I definitely would not be where I am. I may have pursued a Ph.D. in another lab, but I don't think I would have gained the same appreciation for the fundamental importance of the first principles in science. These first principles are not just physics and thermodynamics, but also the first principles of curiosity and the drive for understanding. Dr. Baker has been a fantastic mentor, teacher, collaborator, inspiration, and friend.

Dedication

This dissertation is dedicated to my wife, Tracey Jackson, who has been the best funding body a scientist could ever ask for. Besides the physical support, her emotional support has made my journey from graduate student to Ph.D. possible.

Table of Contents

Abstract i
Acknowledgements ii
Dedication iv
Table of Contents v
List of Tables ix
List of Figures x
Chapter 1 Dissertation Introduction 1
BACKGROUND 1
Actin details. 3
Myosin structure. 4
Muscle structure. 4
Strain dependent kinetics. 6
METHODS 7
Stopped flow. 7
In vitro motility assay. 8
Breaking assay. 9
Single Molecule Binding Assay. 9
OVERVIEW 12
Relationship between chemistry, strain, and movement. 12
Justification. 15
References 15
Chapter 2 The Energetics of Allosteric Regulation of ADP Release From Myosin Heads 20
ABSTRACT 20
INTRODUCTION 21
METHODS 24
Protein purification 24
Buffers 24
Activity assays 25
RESULTS and DISCUSSION 26

CONCLUSIONS 39
REFERENCES 40
Chapter 3 Sucrose Increases the Activation Energy Barrier for Actin-Myosin Strong Binding 44
ABSTRACT 44
INTRODUCTION 45
MATERIALS AND METHODS 48
Protein purification. 48
Motility assay. 48
Breaking assay. 49
Single molecule binding assay (SiMBA). 49
Stopped flow fluorimetry. 51
Steady-state actin-activated S1 ATPase assay. 52
RESULTS 52
Sucrose slows *V* but not through a viscous drag on actin filaments. 52
Sucrose decreases both katt(-ATP) and katt(+ATP) in SiMBA. 55
Sucrose decreases kdet(-ATP) in SiMBA. 57
Sucrose has a minimal effect on the diffusion coefficient of actin fragments. 57
Sucrose decreases kcat and has minimal effects on Km 58
Sucrose slows katt(-ATP) in bulk solution. 59
Sucrose slows kdet(-ATP) in bulk solution. 61
Sucrose decreases kT but has little effect on KADP in bulk solution studies. 63
Sucrose inhibits Vmax without significantly altering the detachment kinetics underlying *V*. 64
Sucrose significantly increases Ea for strong binding but not for rigor detachment. 66
DISCUSSION 67
Sucrose has little effect on detachment kinetics at physiological conditions. 68
Mechanism by which sucrose inhibits A-M strong binding. 68
A-M strong binding kinetics, katt(-ATP), influences kcat. 69
The kinetics of A-M strong binding, katt(-ATP), influence actin sliding velocities, *V*. 70
A comparison of single molecule and bulk kinetic parameters. 72
CONCLUSIONS 73

REFERENCES 74

Chapter 4 Factors beyond detachment kinetics that influence unloaded shortening velocities of muscle 78

ABSTRACT 78

INTRODUCTION 79

METHODS 81

Mechanochemical coupling. 83

Myosin step partitioning. 84

Myosin binding site saturation. 86

Efficiency of force transmission. 86

Asymmetric myosin stiffness. 87

Theoretical attachment and detachment models of *V*. 87

RESULTS 89

Rationale. 89

Model. 91

Saturation of myosin binding sites on actin. 91

Persistence length and force transmission. 92

Asymmetric myosin head stiffness. 93

Accelerated detachment kinetics. 95

Model simulations compared to experimental data. 98

DISCUSSION 98

Efficiency of force transmission modulates step size. 99

Saturation of available binding sites. 100

Mechanochemical coupling at system level limits attachment kinetics and accelerates detachment kinetics 100

Collective force. 101

CONCLUSION 102

REFERENCES 103

Supplement 108

Chapter 5 Dissertation conclusion 115

SUMMARY 115

CONCLUSIONS 115
Medical Implications. 118
RECOMMENDATIONS 118
Future work. 118
Reflections on graduate work in the Baker Lab. 119
Reflections on biological modeling. 120
Reflections on muscle modeling. 120
REFERENCES 121
Supplement 108
Description of code in model 108

List of Tables

Table 3-1 Summary of kinetic parameters measured from in vitro motility, actin-activated S1 ATPase, single molecule binding, and stopped-flow spectroscopy assays. 74
Table 4-1 Partial table of model parameters. The full table of parameters is reported in the supplement. 89
Table S-1 Simulation constants. 113
Table S-2 Time Step Variables. 114

List of Figures

1-1 Acto-myosin four state ATPase cycle. 3
1-2 The different levels of organization for skeletal muscle. 6
1-3 In vitro motility assay. 9
1-4 Single molecule binding assay setup. 10
1-5 SiMBA τ_{On} and τ_{Off} results for control conditions of varying ATP and varying S1. 11
1-6 A conceptual representation of the chemical and mechanical (strain) potentials and the movement landscape of myosin binding. 14

2-1 Kinetic and physical models for allosteric regulation of ADP release from myosin. 27
2-2 Multiple kinetic pathways of myosin V. 31
2-3 Depiction of how the average myosin head strain changes over the course of its actin-attachment time, τon, in an unloaded in vitro motility assay. 34
2-4 The effect of [ATP] on actin sliding velocities 36
2-5 The [ATP]-dependence of average actin filament length (□) measured in a skeletal muscle myosin II-based motility assay. 38

3-1 Kinetic schemes of strong A-M acto-myosin binding in the (A) presence and (B) absence of ATP (rigor condition). 46
3-2 The effects of sucrose and phosphate, Pi, on actin sliding velocities, *V*. 54
3-3 The effects of sucrose on the rate of breaking of actin filaments during a motility assay. 55
3-4 A-M attachment and detachment kinetics measured using a single molecule binding assay (SiMBA). 56
3-5 The effects of sucrose on the diffusion coefficient of actin fragments in SiMBA. 58
3-6 The effects of sucrose on actin-activated S1 ATPase activity. 59
3-7 The effects of sucrose on A-M rigor binding attachment kinetics measured using stopped flow. 61
3-8 The effects of sucrose on A-M detachment kinetics measured using stopped flow fluorimetry. 62
3-9 The effects of [MgADP] on actin sliding velocities, V. 65
3-10 The effects of temperature on (A) kdet(-ATP) and (B) katt(-ATP). 67

4-1 Acto-myosin kinetic scheme. 82
4-2 Relationship of persistence length to transmitted step and attachment kinetics on distance between binding sites. 85
4-3 Detachment limited model of velocity and CFG simulated V as a function of k_{Att}. 90
4-4 Simulated velocities over different actin lengths and simulated velocities demonstrating saturation at different attachment rates. 93
4-5 Comparison of the effects of increasing myosin density under different models of *V* (V_{max}, V_{Att}, V_{Det}) at equal driving and resistive stiffness. 95

4-6 Hypermotility at different [P_i] and k_{Det} dependence of simulated *V* on [P*i*]..... 96
4-7 Model simulation results of number of strongly bound heads, system stiffness, kAtt, and kDet at varying kAtt. 97
4-8 Model simulations compared to experimental data of the myosin concentration depence of varying kAtt. 98
S-1 Algorithm overview of our stochastic collective force generator model of muscle contraction. 109
S-2 Kinetic scheme of collective force generator model. 111

Chapter 1

Dissertation Introduction

BACKGROUND

Motor proteins, by their definition, convert chemical energy into mechanical energy to accomplish many necessary biological functions. These functions include cell division, cellular trafficking, axonal transport, and muscle contraction (*1*). Motor proteins are either rotary in nature, such as the ATP synthase, or translational, like kinesin (*2*, *3*). The family of motors is largely composed of myosins, kinesins, and dyneins (*4*). The motors interact with "tracks" which they either move along or translocate. Muscle myosins interact with the actin filament track.

There are at least 18 distinct classes of myosin (*4*). Myosin class V is a notable transport myosin (*5*). Myosin class II has both muscle and non-muscle forms. Cardiac, skeletal, and smooth muscle tissues are in part composed of muscle myosin. Throughout this dissertation, the term myosin will refer to the muscle form of myosin. Myosins can be distinguished by their physical parameters, such as the size of their mechanical step and their kinetics of ATP hydrolysis. In 1971, a formal model of the kinetic cycle was introduced (*6*). A description is given in the legend of Fig. 1-1. The sum of the time myosin is strongly bound to actin in the A.M.D. and A.M. states is τ_{On}, and the time myosin is detached and weakly bound in the A+M.T. and A+M.D.P_i. is τ_{Off}.

The duty ratio of myosin, *r*, is the fraction of time myosin spends strongly bound to actin in the course of its cyclic reactions is:

$$r = \frac{\tau_{On}}{\tau_{On}+\tau_{Off}}. \quad [1]$$

Transport myosins are considered high duty ratio motors, with an $r \approx 50\%$, whereas muscle myosin is a low duty ratio motor with an $r \approx$ 5-10% (*7*). Myosins also differ in terms of the force they generate upon binding to actin and their step sizes. Muscle myosin has a step size ~10 nm and a stiffness of ~1 pN·nm^{-1} (*7*).

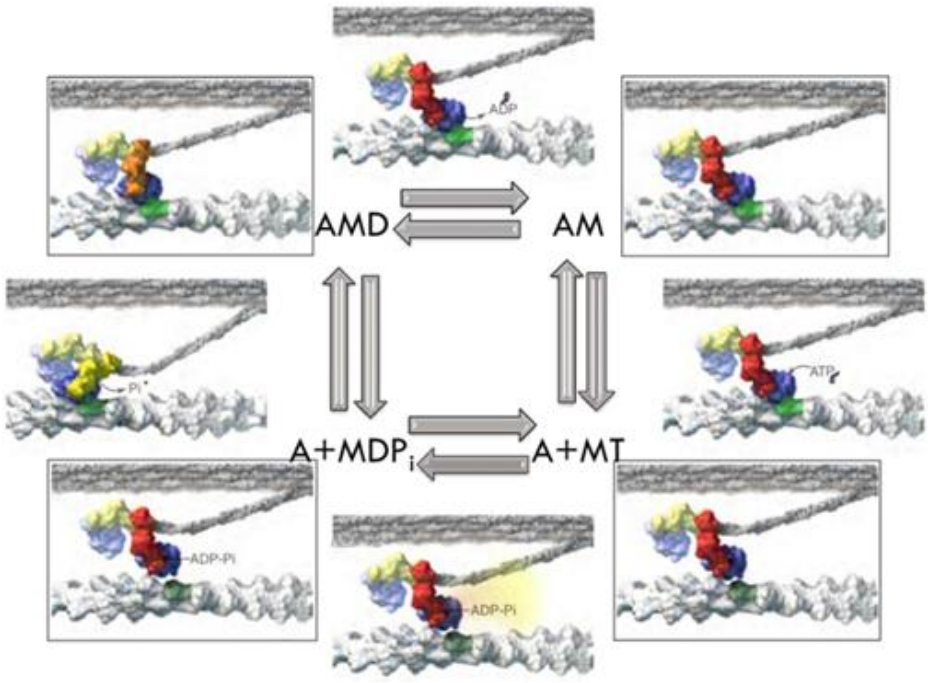

1-1 Acto-myosin four state ATPase cycle. Actin is designated by A. Myosin is designated as M. The nucleotide ATP is designated as T. Its products are designated as follows: ADP as D and inorganic phosphate as P_i. Kinetic states are enclosed in boxes. One of the two heads of skeletal muscle myosin (blue) binds to the actin filament (shown in green) at a time. The strongly bound states are AMD and AM. Detached states are the A+MT and A+MDP$_i$ states. Starting in the upper right in AM, when ATP binds to myosin it induces rapid dissociation into the A+MT state. Here, ATP hydrolysis is in rapid equilibrium between the A+MT and A+MDP$_i$ states. The weak-to-strong binding step occurs with or before P_i release and myosin is strongly bound to actin with ADP (AMD). Upon ADP release, myosin returns to the strongly bound state in absence of nucleotide (AM). The strain sensitive transitions are the A+MDPi → AMD and AMD → AM transitions. Images adopted from: Copyright © 2002 Garland Publishers, used with permission.

Actin details. Actin polymerizes to form thin filaments. The single monomer form of actin is referred to as G-actin (globular), and the filamentous form is referred to as F-actin (filamentous). Thin filaments are composed of about ~380 actin monomers (*8*). Actin filaments are double stranded polymers with a periodicity of 36 nm, which is

approximately the distance between myosin binding sites on actin (*9*). Actin filaments can be stabilized in vitro with phalloidin (*10*). Actin filaments can be visualized in microscopy assays when labeled with fluorophhores such as rhodamine, pyrene, and quantum dots.

Myosin structure. Myosin has the distinction of being the first purified protein; it was discovered when muscle was exposed to a salt treatment by Wilhelm "Willie" Friedrich Kühne in 1864 (*11*). It is not surprising that myosin was the first purified protein, considering it makes up about 38 percent of the total protein found in muscle (*12*). A single myosin monomer can be proteolyzed into heavy meromyosin (HMM) and light meromyosin (LMM). The aggregation of myosin into filaments depends on the LMM region (*13*). The HMM domain maintains the fundamental kinetic and mechanical behaviors of myosin, as it contains a head and neck regions in sub fragment 1 (S1) and sub fragment 2 (S2), which plays a role in the dimerization of myosin (*14*) The S1 is the myosin head, which has actin binding, converter domains, where nucleotides can bind, and light chain binding domains. When the enzyme papain cleaves (digests) myosin into S1, only a single head remains with both light chains intact. These single molecule properties of muscle myosin are maintained with only minor differences across the three types of muscle myosin: skeletal, smooth, and cardiac.

Muscle structure. Whole muscle is composed of muscle fibers, each of which is a multinucleated cell about 100 μm (micron, μm: 1 μm = 10,000 Å = 10-3 mm) in diameter (Fig. 1-2). The organization of long muscle fibers in parallel is repeated by the

constitutive element of a single muscle fiber, the myofibril. Myofibrils are about two to three microns in diameter and composed of sarcomeres, which are repeating contractile elements of two to three microns in length. The myosin and actin proteins in the sarcomeres are arranged in filaments, which give rise to the appearance of dark and light bands observed in the myofibril. The A-band, so named for the anisotropic appearance in polar microscopy, is primarily composed of myosin thick filaments that are in opposite orientation from each other at the midline of the thick filament, referred to as the M-line. An isotropic region, denoted at the I-band, lies between A-bands and contain the Z-line (German word for between, zwischen) where actin filaments are linked, also in opposite polarity on each side. The H-zone (German word for clear, hell) is where there are no actin filaments interacting with myosin filaments in the A-band. When muscle contracts, the Z-lines shorten towards the M-line as myosin heads pull actin filaments into greater overlap. There are approximately 300 myosin molecules, on each thick filament repeating every 43 nm and at an axial height of 14.3 nm (*15*, *16*). Each thick filament has six thin filaments surrounding it. For skeletal muscle, this equates to about 600 motors since each myosin molecule is a dimer and has two globular heads. Myosin thick filaments are thicker and longer, at 1.6 μm, than actin thin filaments.

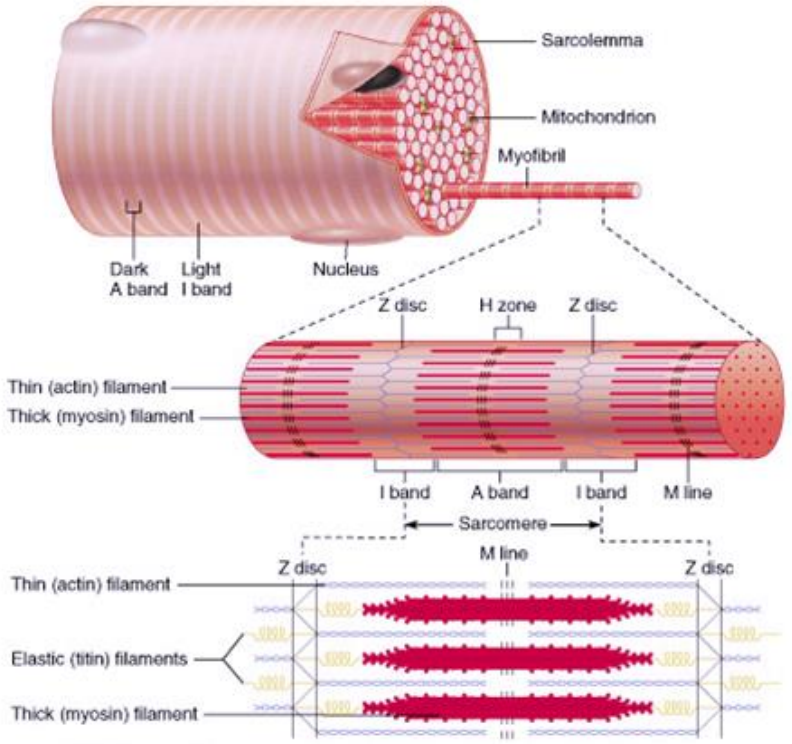

1-2 The different levels of organization for skeletal muscle. A single muscle fiber has many nuclei and mitochondria. Many myofibrils make up a muscle fiber. They are composed of myosin thick filaments and actin think filaments. Thick filaments extend from the M-line in opposite directions, as the actin thin filaments do from the Z disc. Contraction occurs as the myosin heads bind and pull the actin filaments towards the A-band. Dark bands are due to the overlap of thin and thick filaments, and the light bands (I-band) are regions composed of actin filaments. Copyright © 2001 Benjamin Cummings, used with permission.

Strain dependent kinetics. Myosin motors are a diverse class of molecules that perform work, generate force, and move at varying velocities. The strain dependence of actomyosin ATPase kinetics has been well established. (*17*). Numerous studies show a relationship between the force and velocity of muscle contraction (*18*, *19*). The muscle shortens by the overlap, or sliding, of filaments (*20*). The sliding filament model of

contraction, established in 1954, states that actin and myosin filaments stay the same length during contraction (*21*, *22*). How this relationship is understood at the molecular level is not well-detailed, but it is known that the forces myosin generates affect the kinetic rates associated with mechanical transitions (weak-to-strong binding and ADP release) (*23*–*25*). Accelerated ADP release occurs at ATP concentrations above 100 μM in an in vitro motility sliding assay to give faster, or hypermotile, velocities (*26*). At the single molecule level, individual muscle myosin heads take very discrete steps sizes on the order of eight nm for the weak-to-strong binding transition and a two nm displacement occurs with ADP release due to a rotation of the lever arm. Direct evidence at the tissue, sarcomere, and the single molecule level exists for strain dependent kinetics. At the tissue level, it was shown in 1923 that muscle generated increased heat, as a result of increased chemical activity, with higher forces (*27*). After details through x-ray crystallography and electron microscopy gave insight into structure, the strain dependence of myosin was modeled as molecular springs (*28*). The strain dependence kinetics of ADP release were directly shown for transport myosin V (*25*). The strain dependence of the weak-to-strong binding step has been suggested but has yet to be directly observed (*29*, *30*). The approach of mechanochemical coupling is a key distinction of molecular models of muscle.

METHODS

Stopped flow. A stopped flow spectrophotometer can measure the rapid kinetics of myosin attachment and detachment from actin. A solution assay, stopped flow

measures the spectroscopic signal of pyrene-labeled actin (*31*, *32*). S1 is primarily used to avoid myosin filament formation. The signal increases with S1 dissociation from actin (k_{Det}) and is quenched with S1 binding to actin (k_{Obs}). For skeletal muscle myosin, the rate of detachment, limited by ADP release, is faster than the resolution of most stopped flow instruments (~0.5 ms). In this case, the equilibrium of ADP, K_D, can be measured.

In vitro motility assay. The in vitro motility assay was developed to measure the velocity of myosin-propelled actin filaments (*33*). Fluorescently labeled actin is visualized under widefield or TIRF microscopy (Fig 1-3). In addition to measuring the velocity of actin filaments, the number of moving filaments can also be measured. This assay is convenient to measure many different types of perturbations, such as the number of myosin, varying nucleotide, kinetic inhibitors (*34–36*), and buffer conditions (*37*).

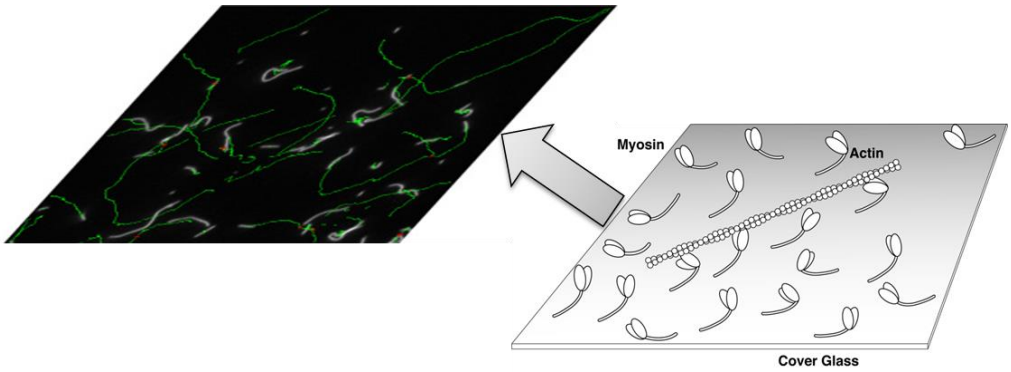

1-3 In vitro motility assay. Myosin is plated onto nitrocellulose cover slips and arranged into flow cells. Fluorescently labeled actin filaments are flowed in in the presence of ATP. Myosins cyclically bind to actin and propel it over the surface of the cover slip. All of this is visualized using widefield or TIRF microscopy. The velocity of the filaments can be measured.

Breaking assay. To qualitatively measure the changes in forces that develop between myosin heads in the in vitro motility system, a breaking assay was developed (*26*, *38*). With this assay we measure actin filament breaking events that occur during myosin propelled actin motility in an in vitro motility assay. Exponential fits to the histograms of these events yields the rate of breaking due to internal forces between myosin heads transmitted through the actin filament. The assumption is that changes that lead to changing breaking rates are correlated to changes in the internal force.

Single Molecule Binding Assay. A single molecule binding assay (SiMBA) was developed to measure the kinetics of myosin binding to and detachment from actin under the same conditions as the in vitro motility assay. It has been shown that the rate limiting steps for actin-myosin ATPase are different than the rate limiting step of velocity measured in in vitro motility assays (*39*). SiMBA determines the single molecule

kinetics of myosin binding and detachment under the same conditions as the in vitro motility assay (Fig. 1-4). Control experiments, described in Fig 1-5, were performed to validate the procedure to probe inhibitors of actin-myosin ATPase kinetics.

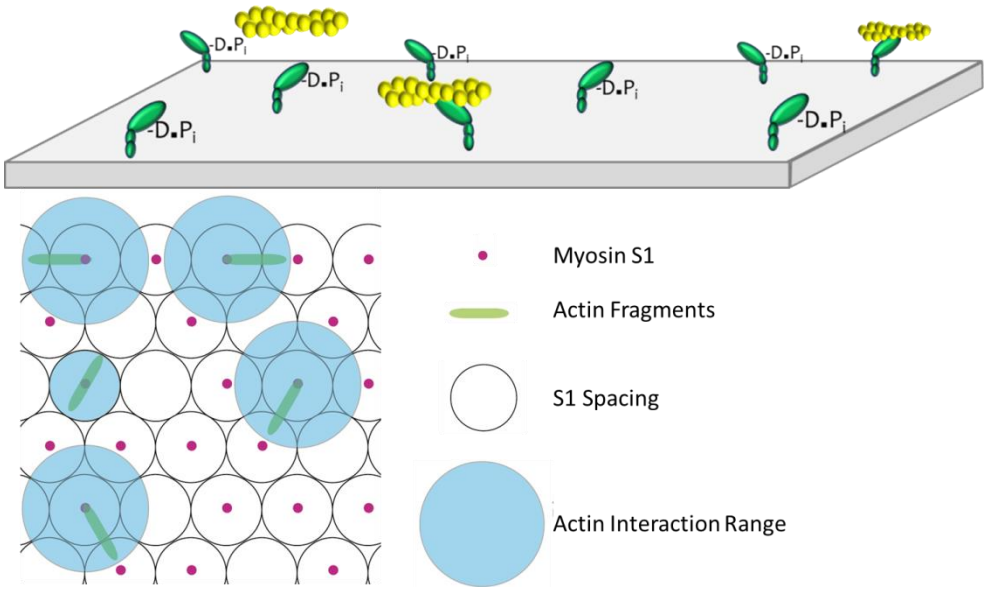

1-4 Single molecule binding assay setup. A low density of myosin S1 (in green, top) and shredded actin filaments (in yellow, top) are used to favor single molecule interactions, as indicated by the S1 spacing (black circles). The time an actin fragment is stationary in a 10 nm actin interaction range region (blue circles) for more than 2 0.1 second frames is counted as a τ_{On} event. The time myosin moves between these events are counted as τ_{Off} events. Histograms of these events are fit to exponential decays to determine the attachment and detachment rates.

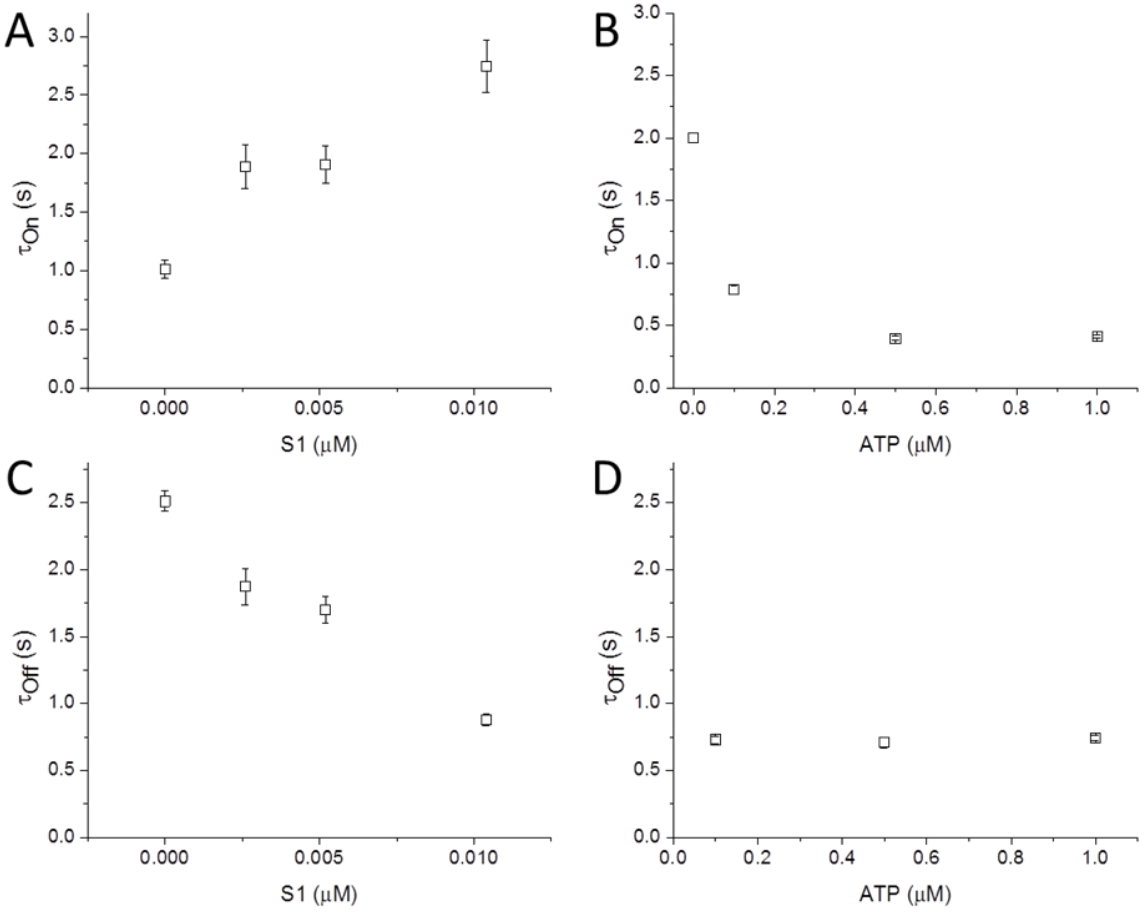

1-5 SiMBA τ_{On} and τ_{Off} results for control conditions of varying ATP and varying S1. The values for τ_{On} increase with increased S1 (A) but decrease, as expected, with increasing amounts of nucleotide (B). The values for τ_{Off} decrease with increased S1 (C) but remain the same for increasing amounts of nucleotide (D).

OVERVIEW

Relationship between chemistry, strain, and movement. A key goal of molecular models is to give insight into how chemical energy is converted into movement. Most models of muscle contraction exhibit many similarities (*40*). Hill's 1938 landmark model of muscle contraction used energetic arguments to describe muscle's force-velocity relationship (*18*). This was the first thermodynamic model of muscle as it related mechanics to heat generation. This model was semi-empirical, as it lacked any molecular detail. Almost all molecular models of muscle assume discrete biochemical states. After structural detail of crossbridges became available, Huxley's 1957 model was the first to relate molecular details to muscle contraction (*28*). The sliding filament model, as it came to be known, introduced a two state model in which myosins would displace actin filaments upon binding and formation of cross bridges. The mechanochemical coupling in the Huxley model is detailed at the level of a single molecule, and is also referred to as an independent force generator model because the chemistry of a single head is separate from the system (*41*).

Fig. 1-3 shows the chemical, strain, and movement landscapes of various models. Huxley's model, referred to as the independent force generator since the chemical and mechanical states of an individual molecule is isolated from the system, assumes the intermolecular strain is locked into place by the weak-to-strong binding transition before movement occurs (Fig. 1-6B). A later refinement to this model (Fig. 1-6A) combined the chemical and mechanical potentials to occur simultaneously (*42*). A

subset of molecular motor models is Brownian thermal-ratchet motor models (Fig. 1-6D), which decouple movement from ATP hydrolysis (*44*, *45*). In the models classified in Fig 1-6A-D, chemistry is essentially uncoupled from movement. This movement is coupled to the collection of motor molecules in a system. Therefore, these models are uncoupled from the mechanics of the system.

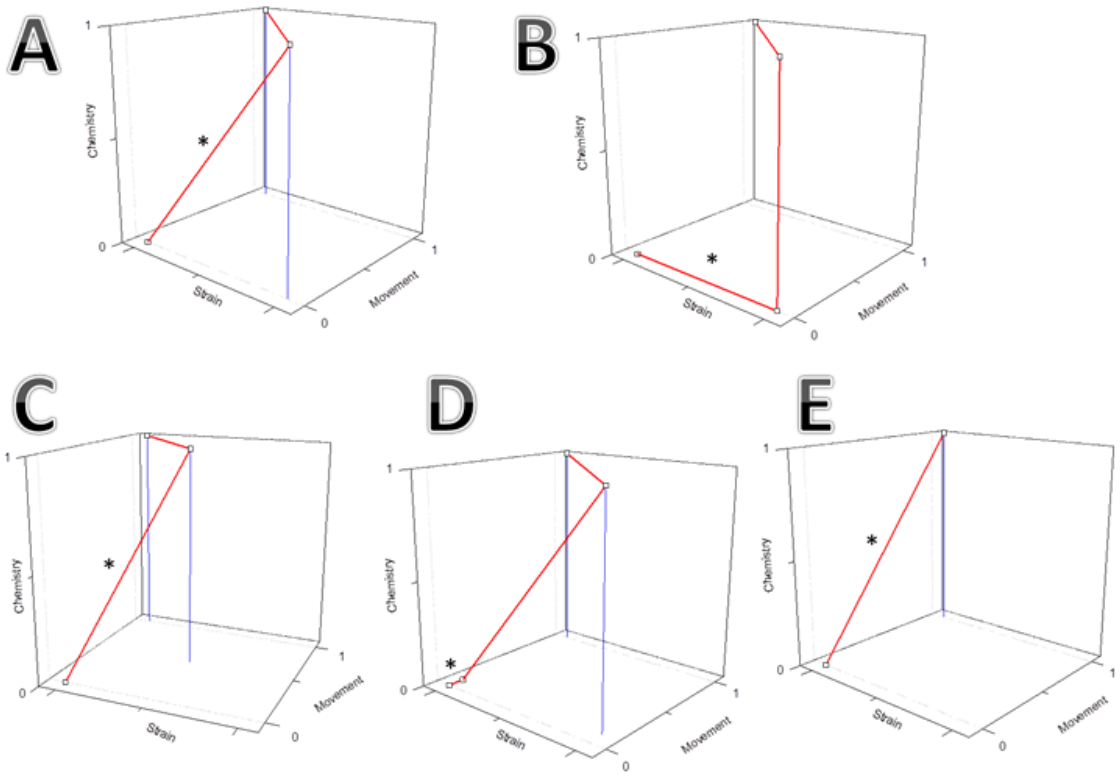

1-6 A conceptual representation of the chemical and mechanical (strain) potentials and the movement landscape of myosin binding. Each are plotted on a 3 dimensional grid to indicate the order each model of muscle contraction predicts their weak-to-strong (i.e. movement-related).The asterisk represents the transitions Brownian forces contribute to. (A) Huxley-Simmons 1971 posits that thermal fluctuations push the myosin from its chemical position and pull out internal compliances before movement occurs. (B) Huxley ’57 is similar, but assumes the strain of the motor is shifted to a different energetic level and then captured by a chemical transition to finally allow movement. (C) The collective force generator model resembles Huxley-Simmons, except as the vertical blue lines indicate, the strain of the molecule can vary, which affects the amount of movement. (D) A Brownian thermal-ratchet model requires a small amount of movement initiated by thermal fluctuations that then shift the chemical and mechanical state of the molecule simultaneously before movement occurs. (E) Chemical motor models, in general, do not account for intermolecular strain and assume the chemical transition and movement occur concurrently.

Justification. The work described in this dissertation provides a model that accurately describes how mechanochemical coupling occurs between myosins in an ensemble or collection of muscle myosin molecules (*5*, *29*). As Fig. 1-6E shows, our motor model integrates the mechanical and chemical transitions into a simultaneous transition (*43*). Chapter 2 outlines the theoretical basis for interhead forces, as opposed to intrahead forces, as the work that affects the strain dependent kinetics of myosin attachment and detachment. The mechanism of how a known inhibitor of acto-myosin ATPase is established in Chapter 3. The dependence of the number of myosin molecules in determining muscle shortening velocity (*29*) is discussed in Chapter 4 in terms of how factors beyond detachment kinetics can influence velocity.

References

1. Alberts, B., Bray, D., Lewis, J., Raff, M., Roberts, K., and Watson., J. D. (1994) Cell junctions, cell adhesion, and the extracellular matrix, in *Molecular biology …*, pp 1059–1524.

2. Vale, R. D., and Milligan, R. a. (2000) The way things move: looking under the hood of molecular motor proteins., *Science (New York, N.Y.) 288*, 88–95.

3. Yoshida, M., Muneyuki, E., and Hisabori, T. (2001) ATP synthase--a marvellous rotary engine of the cell., *Nature reviews. Molecular cell biology 2*, 669–77.

4. Schliwa, M., and Woehlke, G. (2003) Molecular motors., *Nature 422*, 759–65.

5. Vermeulen, K. C., Stienen, G. J. M., and Schmid, C. F. (2002) Cooperative behavior of molecular motors., *Journal of muscle research and cell motility 23*, 71–9.

6. Lymn, R. W., and Taylor, E. W. (1971) Mechanism of adenosine triphosphate hydrolysis by actomyosin., *Biochemistry 10*, 4617–24.

7. Block, S. M. (1996) Fifty ways to love your lever: myosin motors., *Cell 87*, 151–7.

8. Chase, P. B., Macpherson, J. M., and Daniel, T. L. (2004) A spatially explicit nanomechanical model of the half-sarcomere: myofilament compliance affects Ca(2+)-activation., *Annals of biomedical engineering 32*, 1559–68.

9. Steffen, W., Smith, D., Simmons, R., and Sleep, J. (2001) Mapping the actin filament with myosin., *Proceedings of the National Academy of Sciences of the United States of America 98*, 14949–54.

10. Cooper, J. a. (1987) Effects of cytochalasin and phalloidin on actin., *The Journal of cell biology 105*, 1473–8.

11. Holmes, K. C. (2004) Introduction., *Philosophical transactions of the Royal Society of London. Series B, Biological sciences 359*, 1813–8.

12. Squire, J. (1986) Muscle: Design, diversity, and disease, p 381. Benjamin/Cummings, Menlo Park, Calif.

13. Burns, C. G., Reedy, M., Heuser, J., and De Lozanne, A. (1995) Expression of light meromyosin in Dictyostelium blocks normal myosin II function., *The Journal of cell biology 130*, 605–12.

14. Tama, F., Feig, M., Liu, J., Brooks, C. L., and Taylor, K. a. (2005) The requirement for mechanical coupling between head and S2 domains in smooth muscle myosin ATPase regulation and its implications for dimeric motor function., *Journal of molecular biology 345*, 837–54.

15. Sellers, J. (1999) Myosins. Oxford University Press, Oxford; New York.

16. Zoghbi, M. E., Woodhead, J. L., Moss, R. L., and Craig, R. (2008) Three-dimensional structure of vertebrate cardiac muscle myosin filaments., *Proceedings of the National Academy of Sciences of the United States of America 105*, 2386–90.

17. Nishikawa, M., Takagi, H., Shibata, T., Iwane, A., and Yanagida, T. (2008) Fluctuation Analysis of Mechanochemical Coupling Depending on the Type of Biomolecular Motors, *Physical Review Letters 101*, 2–5.

18. Hill, A. V. (1938) The Heat of Shortening and the Dynamic Constants of Muscle, *Proceedings of the Royal Society B: Biological Sciences 126*, 136–195.

19. Wilkie, D. R. (1949) The relation between force and velocity in human muscle., *The Journal of physiology 110*, 249–80.

20. Huxley, H. E. (1969) The mechanism of muscular contraction., *Science (New York, N.Y.) 164*, 1356–65.

21. Huxley, A. F., and Niedergerke, R. (1954) Structural changes in muscle during contraction; interference microscopy of living muscle fibres., *Nature 173*, 971–3.

22. Huxley, H., and Hanson, J. (1954) Changes in the cross-striations of muscle during contraction and stretch and their structural interpretation., *Nature 173*, 973–6.

23. Cremo, C. R., and Geeves, M. a. (1998) Interaction of actin and ADP with the head domain of smooth muscle myosin: implications for strain-dependent ADP release in smooth muscle., *Biochemistry 37*, 1969–78.

24. Duke, T. (2000) Cooperativity of myosin molecules through strain-dependent chemistry., *Philosophical transactions of the Royal Society of London. Series B, Biological sciences 355*, 529–38.

25. Veigel, C., Wang, F., Bartoo, M. L., Sellers, J. R., and Molloy, J. E. (2002) The gated gait of the processive molecular motor, myosin V., *Nature cell biology 4*, 59–65.

26. Hooft, A. M., Maki, E. J., Cox, K. K., and Baker, J. E. (2007) An accelerated state of myosin-based actin motility., *Biochemistry 46*, 3513–20.

27. Fenn, W. O. (1923) A quantitative comparison between the energy liberated and the work performed by the isolated sartorius muscle of the frog., *The Journal of physiology 58*, 175–203.

28. Huxley, A. F. (1957) Muscle structure and theories of contraction., *Progress in biophysics and biophysical chemistry 7*, 255–318.

29. Baker, J. E., LaConte, L. E., Brust-Mascher, I., and Thomas, D. D. (1999) Mechanochemical coupling in spin-labeled, active, isometric muscle., *Biophysical journal 77*, 2657–64.

30. Baker, J. E., Brosseau, C., Joel, P. B., and Warshaw, D. M. (2002) The biochemical kinetics underlying actin movement generated by one and many skeletal muscle myosin molecules., *Biophysical journal 82*, 2134–47.

31. Criddle, a H., Geeves, M. a, and Jeffries, T. (1985) The use of actin labelled with N-(1-pyrenyl)iodoacetamide to study the interaction of actin with myosin subfragments and troponin/tropomyosin., *The Biochemical journal 232*, 343–9.

32. Geeves, M. A. (1983) The limiting rate of the ATP-mediated dissociation of actin from rabbit skeletal muscle myosin subfragment 1, *FEBS Letters 160*.

33. Uyeda, T., Warrick, H., Kron, S., and Spudich, J. (1991) Quantized velocities at low myosin densities in an in vitro motility, *Nature 352*, 307–311.

34. Cheung, a, Dantzig, J. a, Hollingworth, S., Baylor, S. M., Goldman, Y. E., Mitchison, T. J., and Straight, a F. (2002) A small-molecule inhibitor of skeletal muscle myosin II., *Nature cell biology 4*, 83–8.

35. Shaw, M. A., Ostap, E. M., and Goldman, Y. E. (2003) Mechanism of inhibition of skeletal muscle actomyosin by N-benzyl-p-toluenesulfonamide., *Biochemistry 42*, 6128–35.

36. Ostap, E. M. (2002) 2,3-Butanedione monoxime (BDM) as a myosin inhibitor., *Journal of muscle research and cell motility 23*, 305–8.

37. Greenberg, M. J., and Moore, J. R. (2010) The molecular basis of frictional loads in the in vitro motility assay with applications to the study of the loaded mechanochemistry of molecular motors., *Cytoskeleton (Hoboken, N.J.) 67*, 273–85.

38. Stewart, T. J., Jackson Jr., D. R., Smith, R. D., Shannon, S. F., Cremo, C. R., and Baker, J. E. (2013) Actin sliding velocities are influenced by the driving forces of actin-myosin binding, *Cellular and Molecular Bioengineering 6*, 26–37.

39. Yengo, C. M., Takagi, Y., and Sellers, J. R. (2012) Temperature dependent measurements reveal similarities between muscle and non-muscle myosin motility., *Journal of muscle research and cell motility 33*, 385–394.

40. Clemen, A. E.-M., Vilfan, M., Jaud, J., Zhang, J., Bärmann, M., and Rief, M. (2005) Force-dependent stepping kinetics of myosin-V., *Biophysical journal 88*, 4402–10.

41. Hill, T. L. (1974) Theoretical formalism for the sliding filament model of contraction of striated muscle. Part I., *Progress in biophysics and molecular biology 28*, 267–340.

42. Huxley, A. F., and Simmons, R. M. (1971) Proposed mechanism of force generation in striated muscle., *Nature 233*, 533–8.

43. Qian, H. (1998) Vector Field Formalism and Analysis for a Class of Thermal Ratchets, *Physical Review Letters 81*, 3063–3066.

44. Krupka, R. M. (1996) Force generation, work, and coupling in molecular motors., *Biophysical journal 70*, 1863–71.

45. Reimann, P. (2002) Brownian motors: noisy transport far from equilibrium, *Physics Reports 361*, 57–265.

Chapter 2

The Energetics of Allosteric Regulation of ADP Release From Myosin Heads

Jackson, DR, Baker, JE (2009). The energetics of allosteric regulation of ADP release from myosin heads. *Physical Chemistry Chemical Physics:PCCP* 11:4808–14. doi: 10.1039/b900998a

ABSTRACT

Myosin molecules are involved in a wide range of transport and contractile activities in cells. A single myosin head functions through its ATPase reaction as a force generator and as mechanosensor, and when two or more myosin heads work together in moving along an actin filament, the interplay between these mechanisms contributes to collective myosin behaviors. For example, the interplay between force generating and force sensing mechanisms coordinates the two heads of a myosin V molecule in its hand-over-hand processive stepping along an actin filament. In muscle, it contributes to the Fenn effect and smooth muscle latch. In both examples, a key force sensing mechanism is the regulation of ADP release via interhead forces that are generated upon actin myosin binding. Here we present a model describing the mechanism of allosteric regulation of ADP release from myosin heads as a change, $\Delta\Delta G_{-D}$, in the standard free energy for ADP release that results from the work, $\Delta\mu_{mech}$, performed by that myosin head upon ADP release, or $\Delta\Delta G_{-D} = \Delta\mu_{mech}$. We show that this model is consistent with previous measurements for strain-dependent kinetics of ADP release in

both myosin V and muscle myosin II. The model makes explicit the energetic cost of accelerating ADP release, showing that acceleration of ADP release during myosin V processivity requires ~4 kT of energy whereas the energetic cost for accelerating ADP release in a myosin II-based actin motility assay is only ~0.4 kT. The model also predicts that the acceleration of ADP release involves a dissipation of interhead forces. To test this prediction, we use an in vitro motility assay to show that the acceleration of ADP release from both smooth and skeletal muscle myosin II correlates with a decrease in interhead force. Our analyses provide clear energetic constraints for models of the allosteric regulation of ADP release and provide novel, testable insights into muscle and myosin V function.

INTRODUCTION

Despite their functional differences both muscle myosin II and myosin V share many mechanochemical features. First, they both function as enzymes that catalyze the hydrolysis of ATP and bind an actin filament cofactor to further activate the hydrolysis of ATP (*1, 2*). Second, they are molecular motors that generate force upon strong binding to actin (*3-5*). Finally, they are mechanosensors with biochemical transitions that are altered by applied forces (*6, 7*). In both myosin V and muscle myosin II, the interplay between force-generating and force-sensing mechanisms is critical for their cellular function. When two or more myosin heads function together in moving along an actin filament, the force generating biochemistry of one myosin head influences the force sensing biochemistry of other myosin heads. In myosin V molecules, this

mechanochemical feedback coordinates the two heads of a processive myosin V molecule, allowing it to follow a hand-over-hand mechanism in transporting vesicles long distances along actin filaments without diffusing away from the actin filament (*8-14*). In muscle, the interplay between force-generating and force-sensing mechanisms leads to behaviors such as the Fenn effect (the force-dependence of heat output observed in all muscle types) (*7, 15*) and latch (the efficient maintenance of force observed in smooth muscle) (*16, 17*). In this paper, we propose a novel thermodynamic model to describe these effects. To test this model, we develop and implement an in vitro assay for measuring changes in both intermolecular forces and actin-myosin biochemistry during myosin-based actin motility.

Strong binding of myosin to an actin filament induces a discrete lever arm rotation, which is widely thought to be the primary mechanism by which myosin generates force and moves actin filaments (*18, 19*). Myosin undergoes an additional, smaller lever arm rotation associated with the release of ADP (*20, 21*). However, rather than acting as a force generating mechanism, this second rotation is thought to function as a force sensing mechanism; the distinction being that the former is associated with a negative (work performing) free energy change whereas the latter has a positive (work absorbing) free energy change (*17, 22*). The basic mechanism for myosin force sensing is that a force applied in a direction that assists the lever arm rotation accelerates ADP release, whereas a force applied in a direction that resists the rotation slows ADP release. The question addressed in this paper is how does the force-generating

transition of one myosin head affect the force-sensing transitions of other myosin heads?

According to early muscle models (*23*) actin-binding of a given myosin head produces a positive intrahead mechanical strain, which is subsequently relaxed upon sliding of the actin filament. Unloaded actin filament sliding decreases the strain in all myosin heads bound to that filament, eventually pulling myosin heads into regions of negative force and strain, where they resist actin movement (*24*). The effect of this variable strain on the kinetics of ADP release is historically described through arbitrarily defined strain-dependent kinetics, presumably as an estimate of the effects of strain on myosin's active site. With these models an energetic link between myosin force-generating and force-sensing transitions is muddled.

Recently, theoretical and experimental studies of smooth muscle myosin and non-muscle myosins I, V, and VI indicate that strain-dependent kinetics of ADP release and ADP binding can be described as a change in mechanical potential (or work), $\Delta\mu_{mech}$, associated with these transitions (*11, 22, 25, 26*). In these models, $\Delta\mu_{mech}$ has been described in terms of either a generalized potential or as a mean-force potential, $F \cdot d$, where upon ADP release myosin rotates a distance d against (or with) a mean interhead force, F. The problem with many of these models is that they do not explicitly describe the acceleration of ADP release as a dissipative mechanical process through which interhead forces are diminished, and thus they lack a proper description of the energetic origins, limits, and costs of the allosteric regulation of ADP release.

In this paper, extending a previous model for the interhead strain generated upon actin-myosin binding (*27*), we describe $\Delta\mu_{mech}$ as a change in interhead strain that occurs when the lever arm rotates upon ADP release. We apply this model to both myosin V processivity (a simple two-head complex) and muscle shortening (a many-head complex) and show that it is consistent with estimates of the effects of interhead strain on ADP affinity. To further test this model, we use a novel in vitro assay and show that the acceleration of ADP release observed during myosin II-based actin motility correlates with a dissipation of interhead forces. This model and supporting data provide significant new insights into the fundamental mechanism for the interplay between myosin force generating and force sensing transitions and offer potential new mechanisms for allosteric regulation of proteins in general.

METHODS

Protein purification- Skeletal muscle myosin was purified from chicken pectoralis muscle as previously described (*28*) and stored in glycerol at -20° C. Smooth muscle myosin was purified from gizzard as previously described (*29*) and stored at 4° C on ice. Actin was isolated from chicken pectoralis (*30*) and stored on ice at 4° C. For in vitro motility assays, actin was incubated with tetramethylrhodamine isothiocyanate (TRITC) phalloidin overnight.

Buffers- Myosin buffer (300mM KCl, 25mM Imidazole, 1mM EGTA, 4mM $MgCl_2$, 10mM DTT), actin buffer (50mM KCl, 50mM Imidazole, 2mM EGTA, 8mM $MgCl_2$, 10mM DTT)

and motility buffer (50mM KCl, 50mM Imidazole, 2mM EGTA, 8mM $MgCl_2$, 10mM DTT, 0.007 to 1mM ATP, 0.5% Methyl Cellulose) were prepared and stored at 4° C.

Activity assays- The velocity of fluorescently-labeled actin filaments sliding over a bed of myosin molecules was measured using an in vitro motility assay at 25° C. Flow cells were prepared by attaching a nitrocellulose-coated cover slip to a microscope slide with 0.125 mm shim spacers. Flow cells for the motility assay were prepared as follows; 2 x 40 µl washes of myosin with a one minute incubation period, 2 x 40 µl washes with 0.5 mg/ml BSA, 2 x 40 µl washes of actin with a one minute incubation period, 2 x 40 µl washes with actin buffer, and 2 x 40 µl washes with motility buffer. Experiments were performed with myosin preparations that were less than two months old. With these preparations we found little if any effect of purification of "dead head" myosin through actin spin down or actin blocking protocols, indicating actin motility was unaffected by dead heads, thus in these experiments we did not further purify dead heads prior to our experiments. Motility assays were performed using a Nikon TE2000 epifluorescence microscope with fluorescent images digitally acquired with a Roper Cascade 512B (Princeton Instruments, Trenton, NJ) camera. For each flow cell, we recorded three 30-second image sequences from three different fields, each containing approximately 10 to 15 actin filaments. Data obtained from these three fields constitutes one (n = 1) experiment. For each image sequence, we analyzed actin movement using Simple PCI tracking software (Compix, Sewickley, PA) to obtain actin sliding velocities, V. Objects were defined by applying an exclusionary area threshold to minimize background noise. Intersect filters were applied to exclude intersecting filaments. The velocities of the

moving actin filaments were plotted as a histogram and fitted to a Gaussian distribution. The average velocity, *V*, for the field was taken from the mean of the Gaussian fit. Velocities obtained from the Gaussian distributions of the three image fields per flow cell were used to calculate an average velocity for the flow cell. These experiments were repeated at least three times for each condition. To measure the extent to which actin filaments break over time, we used ImageJ (*31*) to measure the average actin filament length within a single image obtained both at the beginning of a motility experiment and after five minutes of myosin-based actin motility.

RESULTS and DISCUSSION

From a purely biochemical perspective, the allosteric regulation of myosin's ADP affinity by actin binding can be depicted by the cartoon in Figure 2-1a. Briefly, an actin filament acts as an allosteric effector, which upon binding both heads of a myosin dimer decreases ADP affinity for one head and increases ADP affinity for the other head. In myosin, our understanding of this cooperative mechanism is enhanced by our ability to measure myosin mechanical transitions.

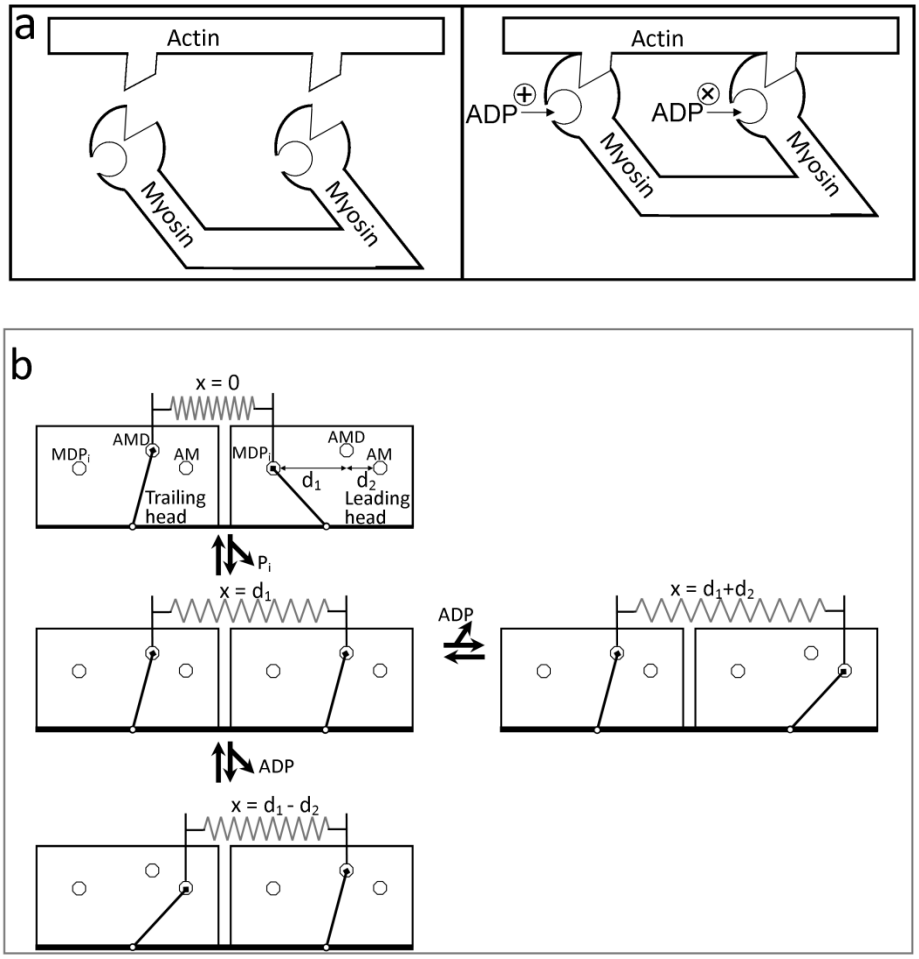

2-1 Kinetic and physical models for allosteric regulation of ADP release from myosin. (a) Actin binding to two myosin heads (left to right) increases the ADP affinity for one head and decreases the ADP affinity for the second head. (b) A four state mechanochemical model accounts for the allosteric regulation illustrated in (a) in terms of an interhead strain (spring) that changes with changes in the biochemistry of either head (A = actin, M = myosin, D = ADP, and Pi = inorganic phosphate). With one myosin head bound to actin in the A.M.D state (top), interhead strain is generated when a second head strongly binds to actin (top to middle left), stretching a compliant element (spring) a discrete distance d1. Here the spring represents the effective stiffness of all compliant elements that exist between the two heads (e.g., actin, flexible lever arm, myosin coiled coil, etc.). When both myosin heads are bound to actin in the A.M.D state, ADP release can occur either from the trailing head (middle left to bottom), relaxing the compliant element a distance d2, or from the leading head (middle left to right), stretching the compliant element a distance d2. If ADP is released from the trailing head, as seen in the bottom pathway, strain is dissipated in assisting ADP release. The pathway to the right depicts the release of ADP from the leading head, which requires work to generate strain thereby slowing the ADP release rate.

Figure 2-1b makes explicit a model – implied by numerous studies (*11, 22, 25, 26*) – for the regulation of ADP release. Specifically, with one myosin head (the trailing head) bound to an actin filament (Fig. 2-1b, top), the binding of a second (leading) myosin head to that same filament (Fig. 2-1b, top to middle left) induces a discrete structural change, generating mechanical strain, $\mu_{mech} = \frac{1}{2}\kappa \cdot d_1^2$, between the two heads, where κ is the stiffness of the linking mechanical element and d_1 is the distance the element is stretched upon strong actin binding. This strain can be generated between the two heads of a myosin dimer or between two or more myosin heads in muscle or an in vitro motility assay. Upon ADP release from the leading head (Fig. 2-1b, middle left to right), the interhead strain increases to $\mu_{mech} = \frac{1}{2}\kappa \cdot (d_1+d_2)^2$, where d_2 is the distance the spring is stretched with the second lever arm rotation associated with ADP release. The work, $\Delta\mu_{mech}$, performed by the leading (positively strained) myosin head with this transition is

$$\Delta\mu_{mech} = -\left[{}^1\!/_2\,\kappa \times {d_1}^2 - {}^1\!/_2\,\kappa \times (d_1 + d_2)^2\right] \qquad (1)$$

If ADP is released from the trailing head (Fig. 2-1b, middle left to bottom) rather than the leading head the interhead strain decreases to $\mu_{mech} = \frac{1}{2}\kappa \cdot (d_1 - d_2)^2$, and the work performed with this transition is

$$\Delta\mu_{mech} = -\left[{}^1\!/_2\,\kappa \times {d_1}^2 - {}^1\!/_2\,\kappa \times (d_1 - d_2)^2\right] \qquad (2)$$

similar to the mechanochemical formalism put forth by Huxley and Hill (*23, 32*) – only here $\Delta\mu_{mech}$ is a change in interhead strain rather than intrahead strain – the mechanical work ($\Delta\mu_{mech}$) performed with a biochemical transition contributes to the standard free

energy (i.e., the work that can be extracted from the system) for that biochemical transition. Thus the free energy change for ADP release, ΔG_{-D°, is made more negative (more favorable) by $\Delta\mu_{mech}$ when ADP is released from the trailing head, or

$\Delta G_{-D} = \Delta G_{-D^\circ} - (\frac{1}{2}\kappa \cdot d_1^{\,2} - \frac{1}{2}\,\kappa \cdot (d_1 - d_2)^2)$,

whereas when ADP is released from the leading head, the standard free energy change for ADP release,

$$\Delta G_{-D} = \Delta G_{-D^\circ} - ({}^{1}\!/_{2}\,\kappa \times d_1^{\,2} - {}^{1}\!/_{2}\,\kappa \times (d_1 + d_2)^2),$$

is made energetically less favorable by $\Delta\mu_{mech}$. In contrast to many models of allosteric regulation, here the allosteric effects of actin binding on ADP release do not result from altering the active site of myosin. Rather the standard free energy for ADP release is altered by the work performed on myosin ($\Delta\mu_{mech}$) upon ADP release, or $\Delta\Delta G_{-D} = \Delta\mu_{mech}$. The source for this energy ($\Delta\mu_{mech}$) is well defined as the free energy for actin-myosin binding. The fraction, a, of $\Delta\mu_{mech}$ performed before the activation energy barrier for the lever arm rotation dictates the extent to which $\Delta\mu_{mech}$ affects the rate for ADP release,

$$k_{-D} = k_{-D^\circ} \times e^{(-a \times \Delta\mu_{mech})} \qquad (3)$$

and ADP binding

$$k_{+D} = k_{+D^\circ} \times e^{((1-a) \times \Delta\mu_{mech})} \qquad (4)$$

This model makes explicit the energetic costs and constraints for allosteric regulation. Although the work performed by a single actin-myosin binding event is not in theory limited; the average work performed by an ensemble of binding events (either many sequential single molecule events or binding events of many myosin heads) is

limited by the actin-myosin binding energy (*13, 33*). As previously described, this binding energy can be partitioned between interhead work ($\Delta\mu_{mech}$) and the external work performed in moving an external load along an actin filament (*27*). Thus the work ($\Delta\mu_{mech}$) performed in accelerating ADP release diminishes the capacity of myosin to perform external work. Although not the focus of this paper, this point is best illustrated by considering the different ways in which an external load can affect $\Delta\mu_{mech}$. An external load would have no effect on $\Delta\mu_{mech}$ if it pulls on the leading-head side of the interhead compliance (Fig. 2-1b). In this case the acceleration of ADP release from the trailing head would be unaltered by an external load at the expense of the energy available to perform work in moving against that load. In contrast, if applied to the trailing-head side of the interhead compliance, an external load would diminish $\Delta\mu_{mech}$, disrupting ADP regulation while restoring the energy available to perform external work. We begin by applying this model to myosin V. Figure 2-2 shows a multi-pathway kinetic scheme for myosin V processivity, previously proposed based on measurements of the ADP dependence of myosin V processivity. According to this model, during the processive stepping of myosin V along an actin filament, ADP release can occur from the trailing head with the leading head either dissociated from (Fig. 2-2, top left to right) or bound to actin (Fig. 2-2, bottom left to right). Consistent with single-headed myosin V kinetic studies (*1*), the ADP binding constant for the top (unstrained) transition was estimated to be 1 μM whereas the ADP binding constant for the bottom (strained) transition was shown to be 60 μM (*11*). This reflects a difference in the standard free energy change for ADP release of $\Delta\Delta G_{-D} = -kT\cdot\ln(60/1) \approx -4kT$. The above model

predicts that $\Delta\Delta G_{-D}$ equals the work (Eq. 2) performed by the trailing myosin head upon ADP release (Fig. 2-2, bottom left to right). Single molecule studies indicate that upon actin binding a myosin head displaces an actin filament a distance d_1 = 25 nm and then further moves a distance d_2 = 5 nm upon ADP release (*6*). Using these values to solve for $\Delta\Delta G_{-D} = \Delta\mu_{mech} = -4kT$, we obtain an interhead stiffness, κ, of 0.14 pN/nm, consistent with experimental studies (*26*). As discussed above, the work performed upon actin binding of the leading head ($\frac{1}{2}\kappa \cdot d_2^2$) is limited by the actin-myosin binding energy. Here 44 pN·nm ≈ 11 kT of the actin-myosin binding energy is used to generate interhead strain, and roughly 36% of this energy is used to accelerate ADP release. The remaining energy is available for use with the powerstroke that occurs upon ATP-induced detachment of the trailing head (*27*).

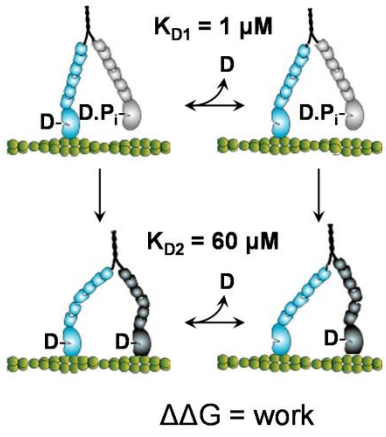

2-2 Multiple kinetic pathways of myosin V. During its hand-over-hand processive walking along an actin filament, the trailing head of myosin V can release ADP either with or without the leading head bound to actin. When ADP dissociation from the trailing head occurs before the leading head strongly binds to actin (top), no strain is imposed on the trailing head. The binding constant for this transition is 1 μM (*11*). When ADP dissociation from the trailing head occurs with the leading head strongly bound to actin (bottom) intrahead strain makes this transition more favorable. The binding constant for this transition is 60 μM (*11*).

Strain dependent kinetics are not unique to myosin V. It has long been argued that because there is no net force on an actin filament during unloaded sliding, the positive forces (and strain) generated by actin-myosin binding must be offset by negative forces (and strain) that resist actin movement (*23, 24*). According to most muscle models, this change in strain alters the rate of ADP release. However whether the strain that affects the rate of ADP release is intrahead as described in Huxley-like models (*23*) or interhead like in Fig. 2-1b and as described in collective force generating models of muscle contraction (*34*) remains unclear. In the former intrahead model, forces equilibrate within a myosin head and the force generated by one myosin head does not affect the mechanics of neighboring myosin heads. In the latter interhead model, forces equilibrate among myosin heads and the force generated by one myosin head influences the mechanics of neighboring myosin heads.

To study the effect of myosin head strain on the rate of ADP release from muscle myosin II heads and to better characterize the mechanism by which the variable strain generated during unloaded actin sliding alters ADP release from these heads, we use an in vitro motility assay. Figure 2-3 illustrates how myosin head strain changes over the time, τ_{on}, it remains bound to an actin filament during muscle shortening or in an in vitro motility assay. When a myosin head binds to an actin filament (Fig. 2-3, left) it generates a positive strain in a direction that assists actin movement. As the actin filament moves with time (Fig 2-3, left to right), the strain associated with the bound head decreases and eventually becomes negatively strained. Finally, ATP binding to myosin induces dissociation from actin (Fig. 2-3, right). The actin-myosin attachment time is the sum of

the time myosin spends waiting for ADP release, $T_{-D} = 1/k_{-D}$, and the time myosin spends waiting for ATP to bind, $T_{+T} = 1/k_{+T}[ATP]$, where k_{-D} is the ADP release rate and k_{+T} is the second order ATP-induced actin-myosin dissociation rate. The model in Fig. 2-3 predicts that by altering the ATP concentration, we can vary the average strain at which ADP release occurs. At high ATP concentrations ($[ATP] >> k_{-D}/k_{+T}$), most of the actin-myosin attachment time, τ_{on}, is spent waiting for ADP to be released, or $\tau_{on} \sim T_{-D}$. In this case ADP release occurs on average from negatively strained heads. In contrast, at low ATP concentrations ($[ATP] << k_{-D}/k_{+T}$), most of the actin-myosin attachment time, τ_{on}, is spent waiting for ATP to bind, or $\tau_{on} \sim T_{+T}$. In this case, ADP release occurs on average from positively strained heads. Thus we would expect actin sliding velocities obtained at low [ATP] to exhibit an ADP release rate that is slowed by positive strain, and actin sliding velocities obtained at high [ATP] to exhibit an ADP release rate that is accelerated by negative strain. A transition between these two extreme strain-dependent ADP release rates is predicted to occur at $[ATP] = k_{-D}/k_{+T}$.

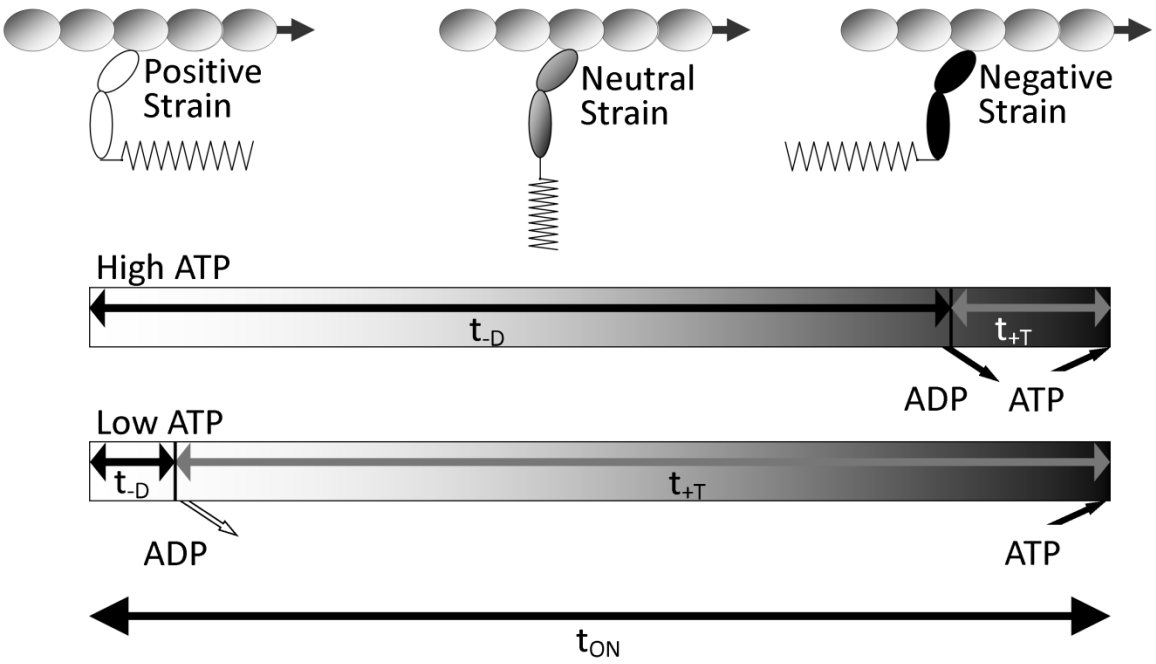

2-3 Depiction of how the average myosin head strain changes over the course of its actin-attachment time, τon, in an unloaded in vitro motility assay. Upon strong binding to actin (left), a myosin head generates a positive strain (in the direction of actin movement). Over time (left to right), actin movement decreases this strain eventually pulling the myosin head so that it becomes negatively strained before detaching from actin (right) (*24*). This balance of forces is required in an unloaded motility assay at any ATP concentration. At high [ATP] (top time line), most of a myosin head's actin attachment time is spent waiting for ADP to be released and ATP binding quickly follow. Under these conditions ADP release occurs, on average, from negatively strained heads. At low [ATP] (bottom time line), most of a myosin head's actin attachment time is spent waiting for ATP to bind. Under these conditions ADP release occurs, on average, from positively strained heads. The scale of the low [ATP] time line is roughly 10-fold smaller than that of the high [ATP] time line.

In fact, an [ATP]-dependent shift in the kinetics underlying actin sliding velocities has been reported (*35*), but until now has not been analyzed in terms of strain-dependent kinetics. Using an in vitro motility assay, we obtain actin sliding velocities at different ATP concentrations for both skeletal and smooth muscle myosin. In Fig. 2-4 we graph, in a double reciprocal plot, the ATP-dependence of actin sliding velocities, V, for both

muscle myosin types. It is widely assumed that V varies inversely with the actin-myosin attachment time, τ_{on}, or

$d/V = \tau_{on} = (1/k_{-D} + 1/k_{+T}[ATP])$,

where d is a proportionality constant often equated with myosin's step size (~8 nm) (*24*). Fitting low [ATP] velocity data to this equation (dashed lines, Fig. 2-4), we obtain values for $k_{-D(+strain)}$ of 55 s^{-1} for smooth and 174 s^{-1} for skeletal muscle myosin. At saturating [ATP], $1/V_{max} = 1/k_{-D}$, and from V_{max} we estimate values for $k_{-D(-strain)}$ of 96 s^{-1} for smooth muscle myosin and 291 s^{-1} for skeletal myosin. For both smooth and skeletal muscle myosin, there is roughly a two-fold difference between $k_{-D(-strain)}$ and $k_{-D(+strain)}$. According to a simple physical model (Eqs. 1 thru 3), this two-fold change in k_{-D} results from a two-fold difference between

$\exp[(½a\cdot\kappa\cdot d_1^2 – ½a\cdot\kappa\cdot(d_1 – d_2)^2)/kT]$ and

$\exp[(½a\cdot\kappa\cdot d_1^2 – ½\ a\cdot\kappa\cdot(d_1 + d_2)^2)/kT]$.

If we assume that d_1 = 8 nm and d_2 = 2 nm for a muscle myosin head (*7, 36*), we obtain a value for $a\cdot\kappa$ of approximately 0.1 pN/nm. This is similar to the interhead stiffness estimated above for myosin V, but it is significantly less than the intrahead stiffness estimates of 1 – 2 pN/nm for a single skeletal muscle myosin head (*37*). One possible explanation for this discrepancy is that the strain that influences ADP release is interhead rather than intrahead. In other words, Eq. 2 describes the net change in strain in all compliant elements (head-head linkages, myosin-surface linkages, S2 hinge, etc.) that are affected when ADP is released from a given head. In this case, κ in Eq. 2 represents an effective interhead stiffness.

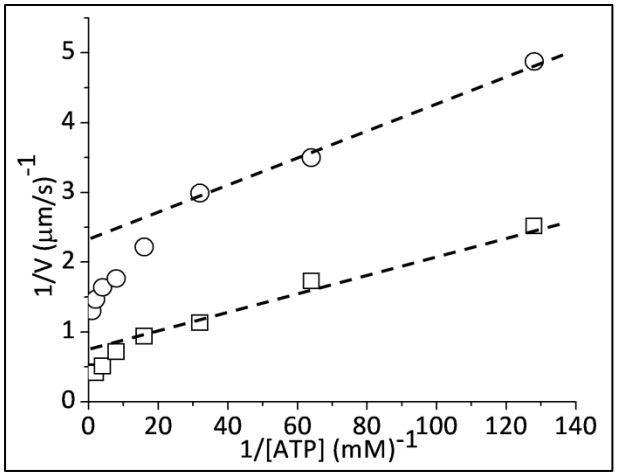

2-4 The effect of [ATP] on actin sliding velocities . V measured in a motility assay using smooth (○) and skeletal (□) muscle myosin and graphed in a double reciprocal plot. The dashed lines are a linear fit of velocities obtained at low [ATP].

According to the above analysis, in a motility assay at high [ATP] the average work performed in accelerating ADP release from a single smooth or skeletal myosin head is $½\kappa \cdot d_1^2 - ½\kappa \cdot (d_1 - d_2)^2 \approx 0.35$ kT, assuming a = 1. Interestingly, the energetic cost for accelerating ADP release from muscle myosin (0.35 kT) is considerably less than that estimated above for myosin V (4 kT), consistent with the coordination of heads being more critical for the function of myosin V. The strain used to accelerate ADP release is ultimately generated by the weak-to-strong binding transition. For muscle myosin the energetic cost for the strain generated with the weak-to-strong transition is $½\kappa \cdot d_1^2 = 3.2$ pN·nm ≈ 0.8 kT, of which ~45% is used to accelerate ADP release.

As discussed above, a strain-dependent model for allosteric regulation of ADP release from myosin predicts that the acceleration of ADP release involves a relaxation of interhead strain and a dissipation of interhead forces (Fig. 2-1b). Specifically, our

model (Fig. 2-3) predicts that in a motility assay performed at high [ATP], the acceleration of ADP release would involve a dissipation of interhead forces; whereas at low [ATP], the slowing of ADP release would involve an increase in interhead forces. Consistent with this prediction, we have shown previously that at high [ATP], the acceleration of ADP release coincides with P_i-independent actin sliding velocities, consistent with low interhead forces. Whereas at low [ATP], the transition to slower ADP release rates accompanies a shift to P_i-dependent sliding velocities, consistent with a shift to high interhead forces (*35*).

To further test the model prediction that acceleration of ADP release at high [ATP] coincides with a dissipation of interhead forces, we studied the rate at which actin filaments break in a motility assay as an indicator of the interhead forces exerted on the actin filament. Figure 2-5 shows the ATP-dependence of average actin filament lengths measured in a skeletal muscle myosin-based motility assay five minutes after flow cells were incubated with actin filaments and motility buffer. These data show a sudden transition from long filaments at ATP concentrations above approximately 100 μM to short filaments at ATP concentrations below 100 μM, indicating a transition from high interhead forces to low interhead forces when ATP concentrations are increased above 100 μM. In this assay, we observed little or no breaking of actin filaments over a five minute period in the absence of myosin, indicating that actin filament breaking is myosin dependent. We observed no effect of ATP on actin filament lengths in the absence of myosin, indicating that the ATP-dependence of actin filament breaking is also myosin-dependent. We observed little or no actin filament re-annealing during these

experiments, indicating that re-annealing does not contribute to the observed change in actin filament lengths over time. Finally, when 10 nM TRITC-actin, 100 μg/ml myosin, and 10 μM ATP are mixed in motility buffer and imaged in a flow cell, we observe that actin filament breaking occurs primarily during myosin-based motility and not through actin-myosin interactions in solution. These results suggest that actin filament breaking observed in a motility assay at low [ATP] results from ATP- and myosin-dependent mechanics.

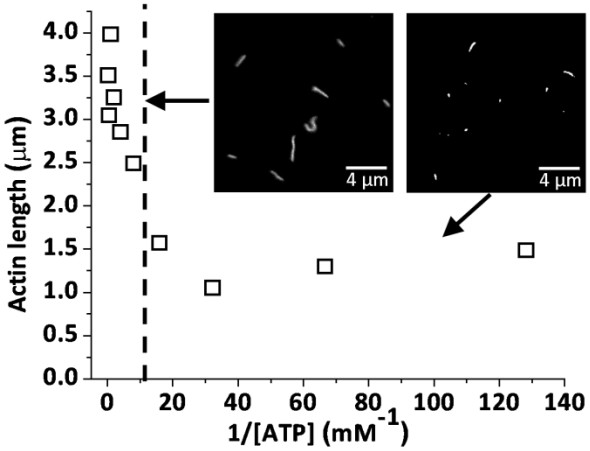

2-5 The [ATP]-dependence of average actin filament length (□) measured in a skeletal muscle myosin II-based motility assay. Measurements were made five minutes after incubation in a motility assay. The vertical dashed line marks the approximate [ATP] above which we observe an accelerated ADP release rate (*35*), a loss of Pi-dependence of V (*35*), and minimal filament breaking, all consistent with the acceleration of ADP release being involving dissipation of interhead forces. The mean filament length at high [ATP] (left of the dashed line) is 3.18 μm. The mean filament length at low [ATP] (right of the dashed line) is 1.35 μm. The insets are characteristic images of fluorescently labeled actin filaments obtained at 1 mM ATP (left) and 10 μM ATP (right).

The ATP concentration (~100 μM) above which we observe diminished actin filament breaking (Fig. 2-5) is remarkably similar to the critical [ATP] at which we observe a

transition from a slow ADP release rate to an accelerated ADP release rates in Fig. 4. Likewise, it is the ATP concentration above which actin sliding velocities, V, become independent of P_i (*35*). Together these results provide strong support for the hypothesis in Fig. 1b that ADP release is accelerated by the work performed on myosin through the relaxation of interhead strain.

CONCLUSIONS

We propose a model that describes the allosteric regulation of ADP release as a change in the free energy for ADP release, $\Delta\Delta G_{-D}$, caused by the mechanical work performed, $\Delta\mu_{mech}$, with this transition in stretching interhead compliant elements, or $\Delta\Delta G_{-D} = \Delta\mu_{mech}$. This model is consistent with estimates for $\Delta\Delta G_{-D}$ in myosin V and accurately describes the acceleration of ADP release measured herein using an in vitro motility assay. Most notably, the prediction that the acceleration of ADP release is a mechanically dissipative process is consistent with our observations of a correlation between the acceleration of ADP release and the dissipation of interhead forces. This model presents an intriguing alternative to allosteric models that involve an altered active site. Although we cannot rule out the possibility that interhead strain can alter the active site of myosin, our analysis suggests that inter-molecular mechanical work is the predominant mechanism for allosteric regulation of ADP release from myosin. The model of interhead strain dependent kinetics makes several interesting predictions. For example, the model predicts that a change in interhead compliance will alter ADP release kinetics in a well-defined way (Eq. 2). The model presented herein describes a

one-dimensional strain; however, models of three-dimensional strain, which would be most applicable to the lattice spacing in muscle, might reveal additional insights into the strain-dependence of ADP release in muscle.

REFERENCES

1. De La Cruz, E. M., Wells, A. L., Rosenfeld, S. S., Ostap, E. M., and Sweeney, H. L. (1999) The kinetic mechanism of myosin V, *Proc Natl Acad Sci U S A 96*, 13726-31.

2. Lymn, R. W., and Taylor, E. W. (1971) Mechanism of adenosine triphosphate hydrolysis by actomyosin, *Biochemistry 10*, 4617-24.

3. Mehta, A. D., Rock, R. S., Rief, M., Spudich, J. A., Mooseker, M. S., and Cheney, R. E. (1999) Myosin-V is a processive actin-based motor, *Nature 400*, 590-3.

4. Eisenberg, E., and Hill, T. L. (1985) Muscle contraction and free energy transduction in biological systems, *Science 227*, 999-1006.

5. Moore, J. R., Krementsova, E. B., Trybus, K. M., and Warshaw, D. M. (2001) Myosin V exhibits a high duty cycle and large unitary displacement, *J Cell Biol 155*, 625-35.

6. Veigel, C., Wang, F., Bartoo, M. L., Sellers, J. R., and Molloy, J. E. (2002) The gated gait of the processive molecular motor, myosin V, *Nat Cell Biol 4*, 59-65.

7. Veigel, C., Molloy, J. E., Schmitz, S., and Kendrick-Jones, J. (2003) Load-dependent kinetics of force production by smooth muscle myosin measured with optical tweezers, *Nat Cell Biol 5*, 980-6.

8. Yildiz, A., Forkey, J. N., McKinney, S. A., Ha, T., Goldman, Y. E., and Selvin, P. R. (2003) Myosin V walks hand-over-hand: single fluorophore imaging with 1.5-nm localization, *Science 300*, 2061-5.

9. Rief, M., Rock, R. S., Mehta, A. D., Mooseker, M. S., Cheney, R. E., and Spudich, J. A. (2000) Myosin-V stepping kinetics: a molecular model for processivity, *Proc Natl Acad Sci U S A 97*, 9482-6.

10. Uemura, S., Higuchi, H., Olivares, A. O., De La Cruz, E. M., and Ishiwata, S. (2004) Mechanochemical coupling of two substeps in a single myosin V motor, *Nat Struct Mol Biol 11*, 877-83.

11. Baker, J. E., Krementsova, E. B., Kennedy, G. G., Armstrong, A., Trybus, K. M., and Warshaw, D. M. (2004) Myosin V processivity: multiple kinetic pathways for head-to-head coordination, *Proc Natl Acad Sci U S A 101*, 5542-6.

12. Rosenfeld, S. S., and Sweeney, H. L. (2004) A model of myosin V processivity, *J. Biol. Chem. 279*, 40100-11.

13. Kolomeisky, A. B., and Fisher, M. E. (2003) A simple kinetic model describes the processivity of myosin-v, *Biophys J 84*, 1642-50.

14. Purcell, T. J., Sweeney, H. L., and Spudich, J. A. (2005) A force-dependent state controls the coordination of processive myosin V, *Proc Natl Acad Sci U S A 102*, 13873-8.

15. Fenn, W. O. (1923) A Quantitative Comparison between the Energy Liberated and the Work Preformed by the Isolated Sartorius Muscle of the Frog, *J. Physiol. 58*, 175-203.

16. Dillon, P. F., Aksoy, M. O., Driska, S. P., and Murphy, R. A. (1981) Myosin phosphorylation and the cross-bridge cycle in arterial smooth muscle, *Science 211*, 495-7.

17. Baker, J. E., Brosseau, C., Fagnant, P., and Warshaw, D. M. (2003) The unique properties of tonic smooth muscle emerge from intrinsic as well as intermolecular behaviors of Myosin molecules, *J. Biol. Chem. 278*, 28533-9.

18. Baker, J. E., Brust-Mascher, I., Ramachandran, S., LaConte, L. E., and Thomas, D. D. (1998) A large and distinct rotation of the myosin light chain domain occurs upon muscle contraction, *Proc. Natl. Acad. Sci. U. S. A. 95*, 2944-9.

19. Rayment, I., Rypniewski, W. R., Schmidt-Base, K., Smith, R., Tomchick, D. R., Benning, M. M., Winkelmann, D. A., Wesenberg, G., and Holden, H. M. (1993) Three-Dimensional Structure of Myosin Subfragment-1: A Molecular Motor, *Science 261*, 50-58.

20. Whittaker, M., Wilson-Kubalek, E. M., Smith, J. E., Faust, L., Milligan, R. A., and Sweeney, H. L. (1995) A 35 A movement of smooth muscle myosin on ADP release, *Nature 378*, 748-751.

21. Gollub, J., Cremo, C. R., and Cooke, R. (1996) ADP Release Produces a Rotation of the Neck Region of Smooth Myosin but Not Skeletal Myosin, *Nature Struct. Biol. 3*, 796-802.

22. Cremo, C. R., and Geeves, M. A. (1998) Interaction of actin and ADP with the head domain of smooth muscle myosin: implications for strain-dependent ADP release in smooth muscle, *Biochemistry 37*, 1969-78.

23. Huxley, A. F. (1957) Muscle Structure and Theories of Contraction, *Prog Biophys 7*, 255-315.

24. Baker, J. E., Brosseau, C., Joel, P. B., and Warshaw, D. M. (2002) The biochemical kinetics underlying actin movement generated by one and many skeletal muscle myosin molecules, *Biophys J 82*, 2134-47.

25. Oguchi, Y., Mikhailenko, S. V., Ohki, T., Olivares, A. O., De La Cruz, E. M., and Ishiwata, S. (2008) Load-dependent ADP binding to myosins V and VI: implications for subunit coordination and function, *Proc Natl Acad Sci U S A 105*, 7714-9.

26. Veigel, C., Schmitz, S., Wang, F., and Sellers, J. R. (2005) Load-dependent kinetics of myosin-V can explain its high processivity, *Nat Cell Biol 7*, 861-9.

27. Baker, J. E. (2004) Free energy transduction in a chemical motor model, *J Theor Biol 228*, 467-76.

28. Warshaw, D. M., Desrosiers, J. M., Work, S. S., and Trybus, K. M. (1990) Smooth muscle myosin cross-bridge interactions modulate actin filament sliding velocity in vitro, *J Cell Biol 111*, 453-63.

29. Ikebe, M., and Hartshorne, D. J. (1985) Effects of Ca^{2+} on the Conformation and Enzymatic Activity of Smooth Muscle Myosin, *J. Biol. Chem. 260*, 13146-13153.

30. Pardee, J. D., and Spudich, J. A. (1982) Purification of muscle actin, *Methods Enzymol 85 Pt B*, 164-81.

31. Abramoff, M. D., Magelhaes, P. J., and Ram, S. J. (2004) Image Processing with ImageJ, *Biophotonics International 11*, 36-42.

32. Hill, T. L. (1974) Theoretical formalism for the sliding filament model of contraction of striated muscle. Part I, *Prog Biophys Mol Biol 28*, 267-340.

33. Baker, J. E., LaConte, L. E., Brust-Mascher, I. I., and Thomas, D. D. (1999) Mechanochemical coupling in spin-labeled, active, isometric muscle, *Biophys J 77*, 2657-64.

34. Baker, J. E., and Thomas, D. D. (2000) A thermodynamic muscle model and a chemical basis for A.V. Hill's muscle equation, *J Muscle Res Cell Motil 21*, 335-44.

35. Hooft, A. M., Maki, E. J., Cox, K. K., and Baker, J. E. (2007) An accelerated state of Myosin-based actin motility, *Biochemistry 46*, 3513-20.

36. Tyska, M. J., Dupuis, D. E., Guilford, W. H., Patlak, J. B., Waller, G. S., Trybus, K. M., Warshaw, D. M., and Lowey, S. (1999) Two heads of myosin are better than one for generating force and motion, *Proc. Natl. Acad. Sci. U. S. A. 96*, 4402-7.

37. Lewalle, A., Steffen, W., Stevenson, O., Ouyang, Z., and Sleep, J. (2008) Single-molecule measurement of the stiffness of the rigor myosin head, *Biophys J 94*, 2160-9.

Chapter 3

Sucrose Increases the Activation Energy Barrier for Actin-Myosin Strong Binding

Jackson, DR, Webb, M, Stewart, TJ, Phillips, T, Carter, M, Cremo, CR, Baker, JE (2013). Sucrose Increases the Activation Energy Barrier for Actin-Myosin Strong Binding. Manuscript submitted for publication.

ABSTRACT

To determine the mechanism by which sucrose slows in vitro actin sliding velocities, *V*, we used stopped flow kinetics and a single molecule binding assay, SiMBA. We observed that in the absence of ATP, sucrose (880 mM) slowed the rate of actin-myosin (A-M) strong binding by 71 ± 8% with a smaller inhibitory effect observed on spontaneous rigor dissociation (21 ± 3%). Similarly, in the presence of ATP, sucrose slowed strong binding associated with P_i release by 85 ± 9% with a smaller inhibitory effect on ATP-induced A-M dissociation, k_T (39 ± 2%). Sucrose had no noticeable effect on any other step in the ATPase reaction. In SiMBA, sucrose had a relatively small effect on the diffusion coefficient for actin fragments (25 ± 2%), and with stopped flow we showed that sucrose increased the activation energy barrier for A-M strong binding by 37 ± 3%, indicating that sucrose inhibits the rate of A-M strong binding by slowing bond formation more than diffusional searching. The inhibitory effects of sucrose on the rate of A-M rigor binding (71%) are comparable in magnitude to sucrose's effects on both *V*

(79 ± 33% decrease) and maximal actin-activated ATPase, k_{cat}, (81 ± 16% decrease), indicating that the rate of A-M strong bond formation significantly influences both k_{cat} and *V*.

INTRODUCTION

Muscle contraction is generated through the A-M ATPase cycle (Fig. 3-1 *A*), which modulates A-M affinity between weak- and strong-binding states. A-M binding occurs first through a weak-binding equilibrium, K_{WS}, followed by strong bond formation, k_{SB} (Fig. 3-1 *A*). But because the techniques used herein are only sensitive to strong bond formation, in our analysis we assume that A-M strong binding occurs as a single step having an effective rate constant $k_{att(+ATP)} = K_{WS} \cdot k_{SB}$ (Fig. 3-1 *A*). During muscle contraction, A-M strong bond formation is associated with a myosin lever arm rotation and phosphate, P_i, release (1–3). This mechanochemical step is the molecular mechanism for force generation in muscle (1, 4–6) and is thought to be rate-limiting for actin-activated ATPase activity (7). A-M strong binding can also occur in the absence of nucleotide, and again here we assume in our analysis a single rigor-binding step having an effective rate constant $k_{att(-ATP)}$ (Fig. 3-1 *B*). A-M detachment occurs upon ATP binding to myosin with a second-order rate constant k_T (Fig. 3-1 *A*). In the absence of nucleotide, A-M detachment can occur spontaneously with a rate $k_{det(-ATP)}$ (Fig. 3-1 *B*).

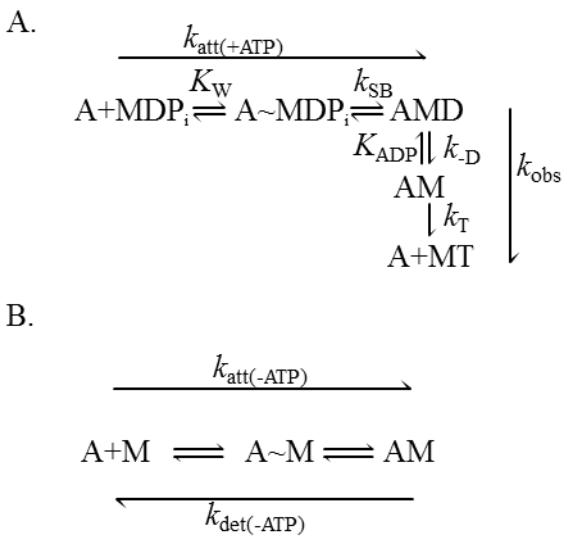

3-1 Kinetic schemes of strong A-M acto-myosin binding in the (A) presence and (B) absence of ATP (rigor condition). (A) In the presence of MgATP, A-M strong binding is a two-step process. Weak actin-myosin binding (A~MDP$_i$) is thought to occur rapidly with an equilibrium binding constant K_W. Strong A-M binding, with a rate constant k_{SB}, is associated with P_i release and a myosin lever arm rotation. The effective rate constant for this two-step binding reaction is $k_{att(+ATP)} = K_W \cdot k_{SB}$. ADP release from A-M occurs with a rate constant k_{-D} followed by ATP-induced A-M detachment with a second-order rate constant k_T. (B) Even in the absence of ATP, A-M strong binding occurs through a two-step reaction with an effective rate constant, $k_{att(-ATP)}$. A-M detachment can occur spontaneously with a rate constant $k_{det(-ATP)}$. A = actin, D = MgADP, T = MgATP, P_i = phosphate, M = myosin.

Known inhibitors of A-M strong binding such as BTS (N-benzyl-p-toluene sulphonamide), BDM (2,3-butanedione monoxime), and blebbistatin decrease k_{SB} by slowing P_i release (8–10). Specifically, they affect $k_{att(+ATP)}$ (Fig. 1 *A*) but not $k_{att(-ATP)}$ (Fig. 3-1 *B*). In order to determine the effects of strong A-M binding on A-M ATPase biochemistry and mechanics, an inhibitor that specifically slows the rate of A-M strong binding, $k_{att(-ATP)}$, is needed. Here we show that sucrose is such an inhibitor.

Sucrose inhibits the force generated by skinned muscle fibers (11) and slows in vitro actin sliding velocities, *V* (12). Sucrose has also been used to probe the kinetics of

non-muscle myosins (13). For myosin V and VI, De La Cruz and coworkers showed that sucrose slows ADP binding and detachment without affecting the ADP dissociation constant, K_{ADP} (Fig. 3-1 *A*). Although it has no known physiological significance, sucrose is an accessible, stable, and reversible (14) reagent that is useful for studying the relationship between A-M kinetics and mechanics. To date, the mechanism by which sucrose inhibits muscle contraction and *V* remains unclear.

Two possible mechanisms for inhibition of muscle mechanics by sucrose are mechanical (viscous) and chemical (ATPase). It has been argued that sucrose does not inhibit *V* by imposing a mechanical load on the actin filament (8), and data presented herein support this argument (Figs. 3-2 *B* and 3-3). It has also been shown that sucrose has no significant effect on myosin (basal) ATPase activity (9), implying that sucrose does not slow product release in the absence of actin. The effect of sucrose on ATPase activity in the presence of actin has not been previously tested. It has been suggested that sucrose inhibits ADP release from the A-M complex (12). Here we show that sucrose slows $k_{att(-ATP)}$ and to a lesser extent the rate of A-M dissociation without significantly affecting the ADP release rate.

In this paper, using both single molecule and bulk kinetic assays, we show that 880 mM sucrose inhibits A-M strong binding, slowing both $k_{att(+ATP)}$ (Fig. 3-1 *A*) and $k_{att(-ATP)}$ (Fig. 3-1 *B*) by 70 – 85%. Sucrose had a relatively small effect on the diffusion coefficient for actin fragments in our single molecule binding assay, SiMBA, and increased the activation energy barrier for A-M strong binding, indicating that sucrose inhibits the rate of A-M strong binding by slowing bond formation more than diffusional

searching. The 85% inhibition of A-M binding resembles measured effects of sucrose both on the maximal actin-activated ATPase activity k_{cat} (81%) and on V (79%), indicating that the rate of A-M strong bond formation significantly influences both k_{cat} and V.

MATERIALS AND METHODS

Protein purification. Skeletal muscle myosin was prepared from rabbit psoas muscle as previously described and stored in 50% glycerol at –20°C (15, 16). Subfragment-1 (S1) was prepared by either chymotryptic or papain digestion of myosin (16, 17). A myosin buffer of 300 mM KCl, 25 mM imidazole, 1 mM EGTA, and 4 mM $MgCl_2$ was used to dilute myosin and S1 to experimental concentrations for use in in vitro motility and single molecule binding assays. For transient kinetic experiments, S1 was diluted in 23 mM imidazole (pH 7.4), 85 mM KCl, 5 mM $MgCl_2$, 1 mM DTT, and 1 mM EGTA. Actin was isolated from rabbit psoas muscle and stored on ice at 4°C (18). An actin buffer of 50 mM KCl, 50 mM imidazole, 2 mM EGTA, 8 mM $MgCl_2$, 10 mM DTT, and an oxygen scavenger system (292 $mg \cdot mL^{-1}$ glucose, 1.63 $mg \cdot mL^{-1}$ glucose oxidase, and 2.25 $mg \cdot mL^{-1}$ catalase) was used to dilute actin used in motility and single molecule assays.

Motility assay. For in vitro motility assays, actin was incubated with a 1:1 molar ratio of TRITC (tetramethylrhodamine) phalloidin (Sigma-Aldrich, St. Louis, MO USA) overnight at 4°C. In vitro motility experiments with whole myosin were performed as previously described, except here we ignored in our analysis actin trajectories shorter than 3 µm (19). Each point is a minimum of three experiments. A sucrose stock was made from reagent grade sucrose (Sigma-Aldrich, St. Louis, MO USA) to a stock

concentration of 2.34 M. Motility buffer contained 50 mM KCl, 50 mM imidazole, 2 mM EGTA, 8 mM $MgCl_2$, 10 mM DTT, 0 – 880 mM sucrose, 1 mM MgATP, and 0.5% methylcellulose. The macroscopic viscosities of motility buffers at different sucrose concentrations without methylcellulose were measured with a rotational viscometer (DV-E, BYK Additives & Instruments, Wallingford, CT USA) and were consistent with published CRC values (20).

Breaking assay. In order to measure the rate of breaking of moving actin filaments in the motility assay, we performed breaking assays. Breaking assays were performed under the same conditions as motility assays. Actin filament breaking was measured as described previously (21). Data were analyzed using Image J (NIH, Bethesda, MD). The time it took for a filament to break, T_{break}, was calculated from the filament's origin, which is defined as either the initial frame the filament was completely visible in the field of view, the frame it entered the field of view, or the frame in which it broke from a longer filament. T_{break} values were then plotted in a histogram and fit to a single exponential equation using Origin software (Origin Lab Corporation, North Hampton, MA) to determine the breaking rate with and without 880 mM sucrose (Fig. 3). Between 86 and 107 events were measured from between 8 and 29 movies from three to five experiments.

Single molecule binding assay (SiMBA). SiMBA is a modified landing assay (22, 23) developed to determine A-M binding and dissociation kinetics under in vitro motility conditions. In SiMBA, actin fragments bind and dissociate from single S1 molecules bound to a coverslip. The duration of A-M binding was measured to

determine the rate of A-M detachment, k_{det} (Fig. 1 *B*). The duration of free actin diffusion (limited to two-dimensions with methylcellulose) was measured to determine the rate of A-M attachment, k_{att}. Actin was mixed with equimolar phalloidin-Alexa-488 (Invitrogen, Carlsbad, CA USA) and incubated overnight at 4°C. SiMBA experimental buffer was the same as our motility buffer, only it contained 1% methylcellulose and no or low MgATP as specified. Papain S1 (1 $\mu g \cdot mL^{-1}$) was applied to a glass slide in a flow chamber and incubated on ice for 20 min. Bovine serum albumin (Sigma-Aldrich, St. Louis, MO USA) at 1 $mg \cdot mL^{-1}$ in actin buffer was then incubated for the same time under the same conditions to block the glass surface. Alexa-488-labeled actin (10 nM) in motility buffer was sonicated briefly using a sonicator (Model 100 Sonic Dismembrator, Fisher Scientific, Waltham, MA USA) on ice until mean fragment lengths were ~1 µm. Actin fragment lengths and S1 surface density were adjusted to maximize single molecule interactions observed as swiveling actin fragments on S1 and minimize actin binding to multiple S1 observed as stuck fragments. Actin fragments were visualized with a TIRF microscope (488 nm excitation laser, Nikon TE-2000U, Technical Instruments, Burlingame, CA USA) and movies were recorded with a CCD (Model B-512, Roper Scientific, Tucson, AZ USA). Actin fragment trajectories were recorded over the course of 3 min in a single field (51 µm x 51 µm). Three distinct modes were observed: non-specific binding, binding to S1, or diffusing in 2D (detached from S1). Actin fragments that remained bound to the surface over the course of the entire movie were considered to be non-specifically bound to the surface and were not counted. Actin fragments that remained relatively stationary (< 300 nm motion) on the surface (bound)

for more than 2 frames (> 0.20 sec) but eventually detached were counted as binding events and the frames for the bound event were counted. Unbound events were those in which actin fragments either entered the field moving (> 1 μm) and eventually bound or moved between bound events within the field. The frequency of binding events in control experiments (no S1) was approximately 10% of the number observed in our S1 experiments. For 100 to 400 binding events gathered from a minimum of 5 experiments, we measured the durations of bound (T_{on}) and dissociated (i.e. diffusing) (T_{off}) actin fragments and plotted these values in histograms. We fit the histograms to single exponentials to obtain bound (τ_{on}) and detached (τ_{off}) lifetimes from which we calculated k_{det} (τ_{on}^{-1}) and $\rho \cdot k_{att}$ (τ_{off}^{-1}), where ρ is the effective S1 concentration in SiMBA.

Stopped flow fluorimetry. F-actin was labeled with pyrene and stabilized with phalloidin (24). Kinetic experiments, besides the varying temperature experiments, were performed at 25°C in 23 mM imidazole (pH 7.4), 85 mM KCl, 5 mM $MgCl_2$, 1 mM DTT, and 1 mM EGTA with a Hi-Tech SF-61 DX2 stopped-flow spectrophotometer equipped with a 100-watt mercury-xenon lamp and an excitation monochromator. Pyrene-actin fluorescence was excited at 365 nm and emission was detected after passing through a KV-399 cut-off filter. All of the transients shown are an average of 4 – 7 shots and all reported protein and ligand concentrations are the final, post-mixed values. For A-M binding experiments (Fig. 7, *A* and *B*), 0.25 μM S1 was rapidly mixed with 0.25 – 8 μM pyrene-actin and transients were fit to a single exponential to determine $k_{att(-ATP)}$. For A-M dissociation experiments (Fig. 8 *A*), 0.5 μM S1 and 0.5 μM pyrene-actin were preincubated for 5 – 10 min were rapidly mixed with 25 μM

unlabeled actin (25). Transients were fit to a single exponential to determine $k_{det(-ATP)}$. For ATP-induced A-M dissociation experiments (Fig. 3-8 *B*), 0.5 µM pyrene actin, 0.6 µM S1, and 0 – 400 µM MgADP were rapidly mixed with 40 µM MgATP (10) and the transients were fit to a single exponential to determine k_{obs} (Fig. 3-1 *A*). Here all protein, ligand, and sucrose concentrations refer to concentrations in the stopped flow chamber after mixing. In all sucrose experiments, sucrose concentrations were identical in both syringes.

Steady-state actin-activated S1 ATPase assay. Actin-activated S1 ATPase assays were performed at 30°C as previously described (26). A buffer solution containing 50 mM KCl, 50 mM imidazole, 2 mM EGTA, and 8 mM $MgCl_2$ was used. Reaction time points were quenched with 3% sodium citrate so that colorimetric measurements could be made at 2 min intervals over the course of 12 min after initial mixing of chymotryptic S1, phalloidin stabilized F-actin, and ATP. The intensity of the malachite green (27) was measured in a SpectraMax M5 microplate reader (Molecular Devices, Sunnyvale, CA USA). After averaging triplicate points from two experiments, the data were fit to the Michaelis-Menten equation to determine k_{cat} and K_m values.

RESULTS

Sucrose slows *V* but not through a viscous drag on actin filaments. We used an in vitro motility assay with skeletal myosin to confirm the effects of sucrose on actin sliding velocities, *V*. Fig. 3-2 *A* shows that *V* decreases with sucrose in a concentration-dependent manner by up to 80% (from 2.1 ± 0.3 to 0.43 ± 0.18 µm·sec^{-1}) at 880 mM sucrose. To determine whether or not the viscosity of the sucrose-containing

motility buffers contributes to slowing *V*, we took advantage of the phenomenon that P_i inhibits loaded but not unloaded muscle shortening velocities (28). Like in muscle, we have observed that in an in vitro motility assay, P_i inhibits loaded but not unloaded velocities (data not shown). Figure 3-1 *B* shows that *V* inhibited by 290, 730, and 1,460 mM sucrose is not further slowed upon addition of 40 mM P_i, suggesting that sucrose does not slow *V* via a viscous load.

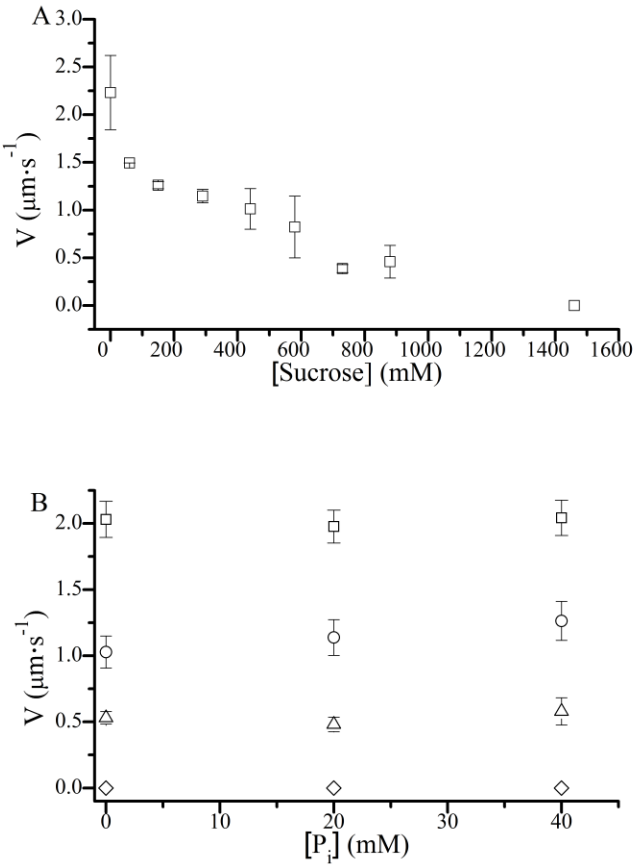

3-2 The effects of sucrose and phosphate, Pi, on actin sliding velocities, *V*. (A) 880 mM sucrose decreased *V* by 80%. (B) The addition of 20 or 40 mM P_i had no effect on actin sliding velocities at 0 (□), 290 (○), 730 (△), and 1,460 mM (◇) sucrose, indicating that sucrose does not slow *V* through a mechanical load.

In order to further test the hypothesis that sucrose does not impose an external load, we measured the effects of sucrose on the rate of actin filament breaking in an in vitro motility assay (21). Figure 3-3 shows histograms of the time it takes a given actin filament to break measured during in vitro motility assays performed both with (circle) and without (square) 880 mM sucrose. Rates for actin filament breaking were obtained from single exponential fits to these histograms, showing that the addition of sucrose decreased the rate of breaking nearly 3-fold (from 0.052 ± 0.002 to 0.017 ± 0.001 s^{-1},

SEM), indicating that sucrose does not slow *V* through an increased mechanical load or drag but instead slows *V* through a mechanism that involves inhibition of forces generated on actin filaments.

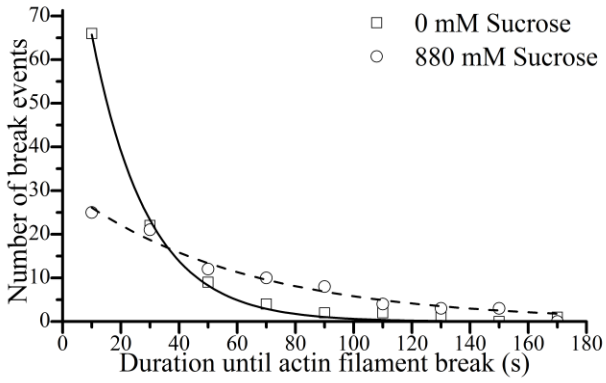

3-3 The effects of sucrose on the rate of breaking of actin filaments during a motility assay. The time it takes a given actin filament to break was measured during a motility assay. Approximately 100 measurements under each condition were plotted in a histogram and fit to a single exponential to determine filament breaking rates both in the absence (□, solid line) and presence (○, dashed line) of 880 mM sucrose. Sucrose decreased the rate of breaking from 0.052 to 0.017 s^{-1}.

Sucrose decreases both katt(-ATP) and katt(+ATP) in SiMBA. We used SiMBA to determine the effects of sucrose on A-M binding kinetics under in vitro motility conditions. Fig. 3-4 *A* shows a histogram of T_{off} values obtained in the absence of MgATP both with (circles) and without (squares) 880 mM sucrose. These histograms were to single exponentials to determine the lifetime of the detached state, $\tau_{off(-ATP)}$, from which A-M binding rates, $\rho \cdot k_{att(-ATP)} = \tau_{off(-ATP)}^{-1}$, were calculated. Here ρ is the effective S1 concentration in SiMBA, which is related to the S1 surface density and was held constant in all experiments. The data show that with addition of 880 mM sucrose, $\rho \cdot k_{att(-ATP)}$ decreases 70% (from 0.72 ± 0.02 to 0.21 ± 0.02 s^{-1}), suggesting that sucrose

directly inhibits A-M rigor strong binding. These experiments were repeated in the presence of 1 µM MgATP (Fig. 3-4 *A inset*) where most A-M binding events are associated with P_i release. Similar to its effect on rigor binding kinetics, 880 mM sucrose slowed $\rho \cdot k_{att(+ATP)}$ by 86% (from 0.97 ± 0.08 to 0.14 ± 0.01 s^{-1}), suggesting that the kinetics that limit rigor bond formation (Fig. 3-1 *B*) similarly influence actin-induced P_i release (Fig. 3-1 *A*).

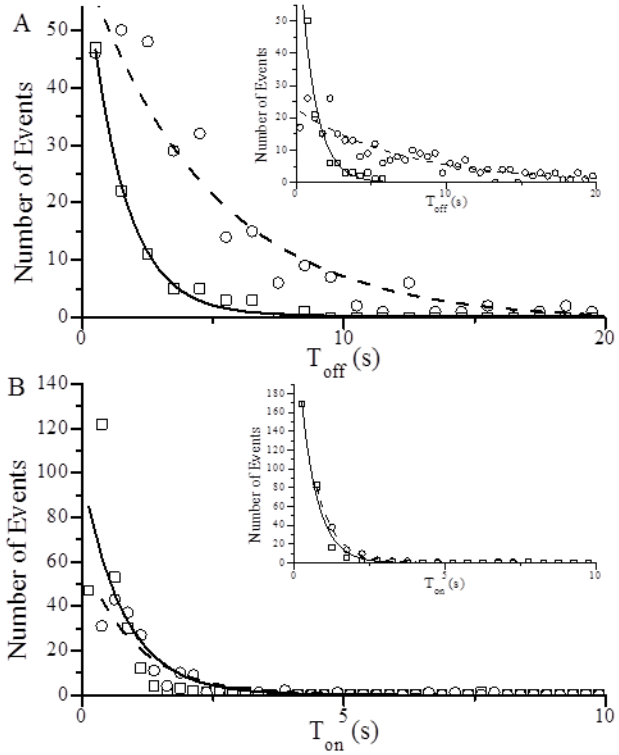

3-4 A-M attachment and detachment kinetics measured using a single molecule binding assay (SiMBA). (A) Durations of actin fragment in the detached state, T_{off}, and (B) durations of actin fragment in the attached state, T_{on}, were measured and plotted in histograms, and fit to single exponentials both with (○, dashed line) and without (□, solid line) 880 mM sucrose. Single exponential fits to these histograms gave (A) attachment ($\rho \cdot k_{att}$) and (B) detachment (k_{det}) rates both in the presence (inset) and absence of 1 µM MgATP. Results are summarized in Table 3-1.

Sucrose decreases kdet(-ATP) in SiMBA. To determine the effects of sucrose on A-M detachment kinetics, we used SiMBA to measure durations, T_{on}, of actin fragments bound to S1 affixed to a coverslip surface. In Fig. 3-4 *B*, T_{on} values obtained in the presence (circles) and absence (squares) of 880 mM sucrose are plotted in a histogram and fit to single exponentials (lines) to determine A-M bound lifetimes, τ_{on}, and A-M detachment rates, $k_{det} = \tau_{on}^{-1}$. The addition of 880 mM sucrose decreased $k_{det(-ATP)}$ by 21% (from 1.27 ± 0.15 to 1.0 ± 0.1 s^{-1}). These experiments were repeated in the presence of 1 µM ATP (Fig. 3-4 *B inset*), where the addition of 880 mM sucrose decreased the A-M detachment rate 13% (from 1.81 ± 0.06 to 1.57 ± 0.04 s^{-1}). These data show that sucrose inhibits A-M dissociation both in the presence and absence of ATP, but the magnitude of the effect was much smaller than the > 70% reduction of $k_{att(-ATP)}$ and $k_{att(+ATP)}$.

Sucrose has a minimal effect on the diffusion coefficient of actin fragments. Inhibition of k_{att} by sucrose (Fig. 3-4 *A*) might result from sucrose slowing the diffusion of actin fragments. To test this possibility, the same SiMBA assay used to measure sucrose effects on $k_{att(-ATP)}$ was used to determine the effects of sucrose on the diffusion coefficient, *D*, of actin fragments. Fig. 3-5 *A* shows mean squared displacements, MSD, (29) of ~ 1 µm actin fragments obtained at 0 (open squares), 440 (open circles), and 880 (open triangles) mM sucrose. Diffusion coefficients (*D*) were obtained from fits of these data to the equation $MSD = 4 \cdot D \cdot t^{\alpha}$ and are plotted in Fig. 3-5 *B*. Alpha values of approximately 1 were obtained from all fits, indicating that the actin fragments were undergoing free diffusion (30). These data show that the diffusion

coefficient, *D*, for actin fragments in SiMBA decreased by 25% (Table 3-1) upon addition of 880 mM sucrose, indicating that the 70 – 80% decrease in $k_{att(-ATP)}$ with addition of sucrose results primarily from slowing a non-diffusive component of k_{att}.

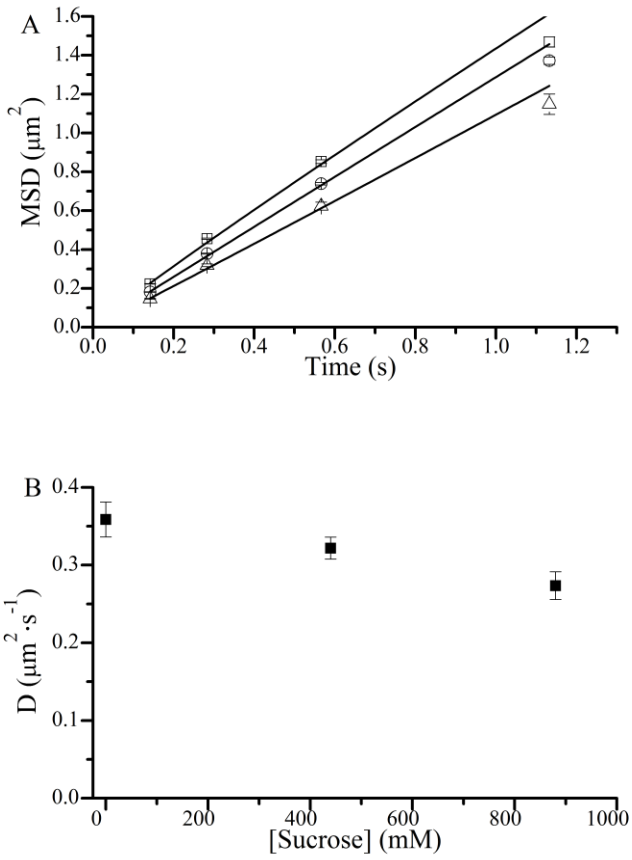

3-5 The effects of sucrose on the diffusion coefficient of actin fragments in SiMBA. (A) Mean squared displacements (MSD) from over 300 actin fragment trajectories were measured at different time windows for 0 (□), 440 (○), and 880 (△) mM sucrose. (B) Diffusion coefficients were determined at each sucrose concentration by fitting the MSD data to $4Dt^{\alpha}$ and plotted. D = diffusion coefficient, t = time, α = alpha coefficient. Results are summarized in Table 3-1.

Sucrose decreases kcat and has minimal effects on Km. To determine the effects of sucrose on A-M ATPase kinetics, we measured actin-activated S1 ATPase

activity both with and without sucrose. Figure 3-6 shows that the addition of 790 mM sucrose reduces the maximum actin-activated ATPase rate, $k_{cat,}$ 80% (from 75 ± 13 to 15 ± 1 min^{-1}) and decreases K_m from 33 ± 2 to 9 ± 1 µM. The 80% decrease in k_{cat} with sucrose correlates with the 86% inhibition of $k_{att(+ATP)}$ by sucrose, suggesting that A-M strong binding significantly influences k_{cat}. The decrease in K_m might result from sucrose slowing detachment kinetics and implies that sucrose does not decrease weak-binding affinity, K_W.

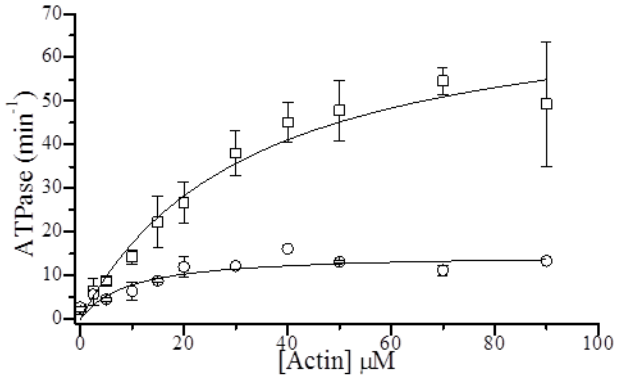

3-6 The effects of sucrose on actin-activated S1 ATPase activity. The rate of P_i release during an ATPase reaction was measured in a colorimetric assay at the indicated actin concentrations both with and without 700 mM sucrose and plotted. These data were fit to the Michaelis-Menten equation to obtain values for the maximum actin-activated ATPase activity, k_{cat}, and the K_m. The basal ATPase was 2.4 and 2.7 min^{-1} for 0 and 880 mM sucrose. In the absence of sucrose (□) we measured a k_{cat} of 75 min^{-1} and K_m of 33 µM. In the presence of 700 mM sucrose (○), we measured a k_{cat} of 15 min^{-1} and a K_m of 9 µM.

Sucrose slows katt(-ATP) in bulk solution. To verify the effects of sucrose on $\rho \cdot k_{att(-ATP)}$ measured with SiMBA, we used stopped flow fluorimetry to measure the effects of sucrose on the rate constant, $k_{att(-ATP)}$, for A-M rigor binding in solution. Fig. 3-7 *A* shows the effects of sucrose on a representative fluorescence transient following

rapid mixing of pyrene actin and S1. Fluorescence transients were fit to single exponentials to obtain binding rate constants, k_{eff}, and in Fig. 3-7 *B* values for k_{eff} obtained at different actin concentrations both with (circles) and without (squares) 880 mM sucrose are plotted. Rate constants, $k_{att(-ATP)}$, for A-M binding were obtained from the slopes of linear fits to these plots, showing that 880 mM slows $k_{att(-ATP)}$ by 80% (from 2.41 ± 0.08 to 0.48 ± 0.01 $\mu M^{-1} \cdot s^{-1}$) consistent with SiMBA results.

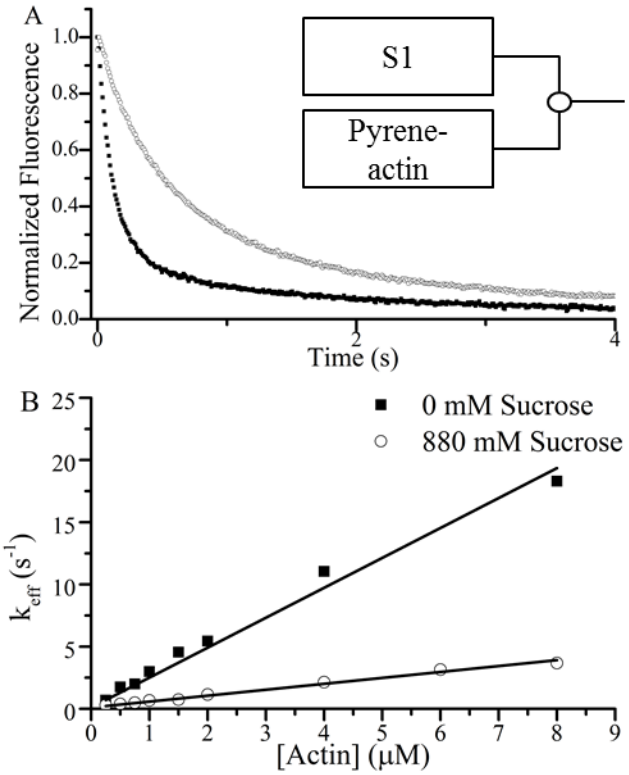

3-7 The effects of sucrose on A-M rigor binding attachment kinetics measured using stopped flow. (A) Representative fluorescence transients following rapid mixing of 0.75 μM pyrene-actin with 0.25 μM S1 (final concentrations) at 0 (■) and 880 (○) mM sucrose. (B) Single exponential fits of approximately 15 fluorescence transients averaged together from three different experiments gave a k_{eff} for each actin concentration. The [A]-dependence of k_{eff} is described by the equation $K_W \cdot k_{SB} \cdot [A]/([A] \cdot K_W + 1) + k_{det(-ATP)}$ (24). We observe a linear relationship out to the highest [A] used, indicating that under these conditions, $[A] < 1/K_w$, and $k_{eff} = K_W \cdot k_{SB} \cdot [A] = k_{att(-ATP)} \cdot [A]$. Thus rate constants for A-M binding, $k_{att(-ATP)}$ were obtained from the slope of a linear fit (line) to the data in Fig. 7 *B*, setting the y-intercept to $k_{det(-ATP)} = 0.11\ s^{-1}$ obtained in Fig. 8 *A*.

Sucrose slows kdet(-ATP) in bulk solution. To confirm the effects of sucrose on $k_{det(-ATP)}$ in SiMBA, we used stopped flow to measure the corresponding effects in bulk solution. Figure 3-8 *A* shows fluorescence transients obtained both with (open circles) and without (open squares) 880 mM sucrose following rapid mixing of pyrene-actin-S1 with excess unlabeled actin. These transients were fit to single

exponentials to determine $k_{det(-ATP)}$, showing that 880 mM sucrose slows $k_{det(-ATP)}$ by 15% (from 0.13 ± 0.06 to 0.11 ± 0.03 s^{-1}).

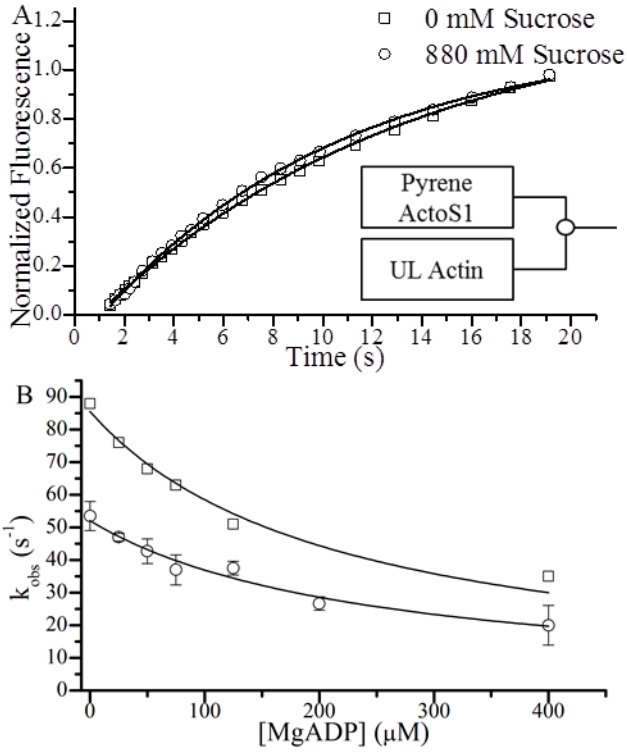

3-8 The effects of sucrose on A-M detachment kinetics measured using stopped flow fluorimetry. (A) Normalized fluorescence transients following rapid mixing of 0.5 μM S1 and 0.5 μM pyrene actin against 25 μM (final concentrations) unlabeled actin (UL) in the presence (○) and absence (□) of 880 mM sucrose here shown with every 10th point plotted. Single exponential fits (lines) yielded $k_{det(-ATP)}$ values of 0.13 and 0.11 s^{-1} for 0 and 880 mM sucrose respectively. (B) ATP-induced A-M dissociation transients were obtained when 0.5 μM pyrene actin, 0.5 μM S1, and the indicated [MgADP] were rapidly mixed with 40 μM MgATP (final concentrations) both in the presence (○) and absence (□) of 880 mM sucrose. Values for k_{obs} at each [MgADP] were obtained from single exponential fits to approximately ten transients obtained from two experiments and were plotted. These plots were fit to Eq. 1 to obtain values for k_T and K_{ADP} that are summarized in Table 3-1.

Sucrose decreases kT but has little effect on KADP in bulk solution studies. Under physiological conditions it is difficult to measure the effects of sucrose on ATP-induced A-M detachment kinetics because fast skeletal muscle myosin A-M detachment rates are too fast to measure using stopped flow. We observed no effect of 880 mM sucrose on fluorescence transients following rapid mixing of pyrene actin + S1 + 200 µM MgADP with 1 mM MgATP, suggesting that sucrose does not slow detachment kinetics enough to make the A-M detachment rate measurable (data not shown).

For fast skeletal muscle myosin, non-physiological conditions are typically used to estimate detachment kinetic parameters. To determine the effects of sucrose on ATP-induced A-M dissociation kinetics (Fig. 3-1 *A*), we used stopped flow to measure fluorescence transients at different [MgADP] following rapid mixing of S1 + pyrene actin with 40 µM MgATP. ATP-induced fluorescence transients were fit to single exponentials to determine k_{obs} at different [MgADP] both with (Fig. 3-8 *B*, open circle) and without (Fig. 3-8 *B*, open square) 880 mM sucrose. The data in Fig. 3-8 *B* were fit to the equation (10)

$$k_{obs} = \frac{k_T[\mathrm{ATP}]}{(1 + [\mathrm{ADP}]/K_{ADP})} \qquad \text{Eq. 1}$$

to determine values for the ADP dissociation constant, K_{ADP}, and the ATP-induced A-M detachment rate constant, k_T (Fig. 3-1 *A*). 880 mM sucrose slows k_T by 40% (from 2.14 ± 0.06 to 1.30 ± 0.03 $\mu M^{-1} \cdot s^{-1}$) and has little effect on K_{ADP} (Table 3-1).

Sucrose inhibits Vmax without significantly altering the detachment kinetics underlying *V*. Figure 9 *A* shows the effects of sucrose on the ADP-dependence of *V*, measured using an in vitro motility assay. In the absence of sucrose (open squares) ADP slows *V* through product inhibition of τ_{on} as previously described (31), and our data in Fig. 3-9 *A* are accurately described by the equation:

$$\frac{V}{V_{max}} = \frac{[\mathrm{ATP}]}{[\mathrm{ATP}]+\left(\frac{k_{-D}}{k_T}\right)*\left(1+\frac{[\mathrm{ADP}]}{K_{ADP}}\right)} \qquad \text{Eq. 2}$$

where V_{max} is the maximum sliding velocity and k_{-D} is the ADP release rate. The right side of this equation describes the effects of A-M detachment kinetics on *V*. Fitting the data in Fig. 3-9 *A* to Eq. 2, using the corresponding K_D and k_T values determined from stopped flow (Table 3-1), the fit value for V_{max} decreased by 70% (2.3 to 0.69 μm·s^{-1}) and k_{-D} increased (86 ± 24 and 123 ± 26 s^{-1}) with 880 mM sucrose. These k_{-D} estimates are low relative to published values, presumably because the value for k_T used in our motility analysis was estimated from stopped flow and is lower than k_T values estimated from in vitro motility experiments.

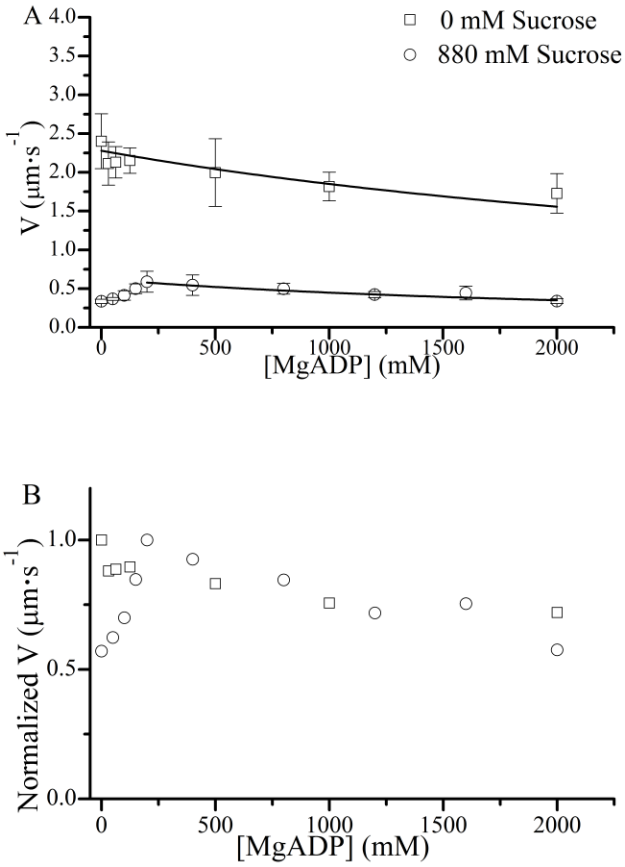

3-9 The effects of [MgADP] on actin sliding velocities, V. (A) We used an in vitro motility assay to measure the velocity, *V*, of actin filament sliding over a bed of full length skeletal muscle myosin at 1 mM MgATP and the indicated [MgADP] both with (□) and without (○) 880 mM sucrose. Plots of *V* versus [MgADP] were fit (lines) to Eq. 2, using values for k_T and K_{ADP} in Table 3-1. The sucrose data obtained below 200 mM MgADP was excluded from this fit. (B) Data obtained in the presence of sucrose was multiplied by 4, consistent with the 4-fold decrease in V_{max} observed upon addition of 880 mM sucrose. Both datasets were normalized to V_{max} in the absence of sucrose.

With 880 mM sucrose, the ADP-dependence of *V* exhibits two different phases. The recovery of *V* observed with addition of up to 200 μM MgADP (Fig. 3-9 *A*) presumably results from an increased number of actin-bound myosin heads engaging actin with the myosin surface to overcome the sucrose-inhibited diffusive component of k_{att} (Fig. 3-5). The inhibition of *V* observed above 200 μM MgADP results from the k_{det}-

dependence of *V*, illustrated in Fig. 3-9 *B*, with the normalization of the two datasets to each other. These results show that sucrose inhibits V_{max} without significantly altering the detachment kinetics underlying *V* (31). The 71% decrease in V_{max} correlates with an ~80% reduction in the rates for both maximal actin-activated ATPase and strong A-M binding observed upon addition of 880 mM sucrose, suggesting that the kinetics of A-M strong binding significantly influence *V* (32).

Sucrose significantly increases Ea for strong binding but not for rigor detachment. Consistent with the relatively small inhibitory effect on $k_{det(-ATP)}$, we observe that sucrose has little effect on the activation energy, $E_{a(det)}$, for rigor detachment (from 24 ± 3 to 28 ± 3 kJ·mol^{-1}) (Fig. 3-10 *A*). In contrast, 880 mM sucrose increased the activation energy barrier for rigor strong binding, $E_{a(att)}$, (from 49 ± 2 to 68 ± 5 kJ·mol^{-1}) consistent with our observation that sucrose significantly inhibits $k_{att(-ATP)}$ through a non-diffusive mechanism (Fig. 3-10 *B*).

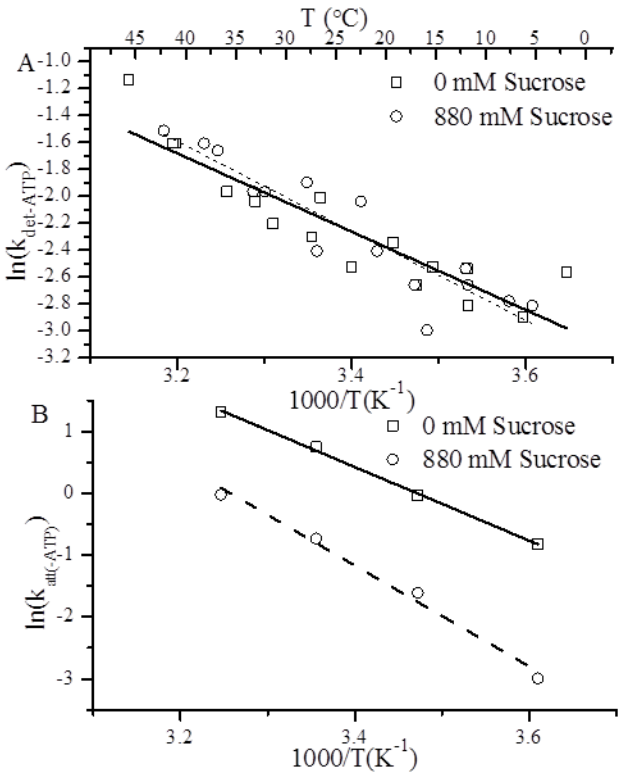

3-10 The effects of temperature on (A) kdet(-ATP) and (B) katt(-ATP). (A) Fluorescence transients were obtained following rapid mixing of 0.5 µM S1 + 0.5 µM pyrene actin with 25 µM unlabeled actin both in the presence (○) and absence (□) of 880 mM sucrose. Approximately 4-7 transients were fit to single exponentials to obtain values for $k_{det(-ATP)}$. These experiments were repeated at different temperatures and ln($k_{det(-ATP)}$) values were plotted versus inverse temperature in an Arrhenius plot. The slope of linear fits to these plots gave values for the activation energy, E_a, and showed that sucrose had no significant effect on E_a (see Table 3-1). (B) Fluorescence transients (~4-7) following rapid mixing of 0.25 µM S1 with different concentrations of pyrene actin were fit to single exponentials to obtain k_{eff}. $k_{att(-ATP)}$ was obtained from the slope of the [A]-dependence of k_{eff} as previously described (Fig. 7 *B*). These experiments were repeated at different temperatures, and the temperature-dependence of $k_{att(-ATP)}$ was plotted in Arrhenius plots (see above), showing that sucrose increases E_a for A-M strong binding (see Table 3-1).

DISCUSSION

In this paper, we show that the primary mechanism by which sucrose slows ATPase kinetics and actin sliding velocities, *V*, is inhibition of A-M strong binding, k_{att}. Muscle contraction is generated through the A-M strong binding transition (Fig. 3-1 *A*),

which occurs with P_i release and a discrete rotation of myosin's lever arm domain. Inhibitors of this mechanochemical step have proven useful for studying basic mechanisms of muscle contraction. Small molecule inhibitors of strong A-M binding, such as BDM, BTS, and blebbistatin (8–10) inhibit $k_{att(+ATP)}$ and myosin ATPase without affecting $k_{att(-ATP)}$. In contrast, here we show that sucrose inhibits $k_{att(-ATP)}$ without affecting myosin (basal) ATPase (12). Sucrose is the first (but probably not the only) effector of $k_{att(+ATP)}$ to be shown to exhibit this mechanism and as discussed below may provide an important tool for studying the effects of strong bond formation on A-M ATPase kinetics and muscle mechanics.

Sucrose has little effect on detachment kinetics at physiological conditions. From stopped flow experiments performed at low [ATP], we estimated that sucrose has little effect on the MgADP dissociation constant, K_{ADP}, and inhibits k_T by less than 40%. The lack of an effect of sucrose on $K_{ADP} = k_{-D}/k_{+D}$ suggests that sucrose affects neither rate constant or that sucrose affects both rate constants proportionally (13). Sucrose inhibition of k_T results either from sucrose decreasing the rate of MgATP binding (possibly by slowing MgATP diffusion) or from sucrose decreasing the rate of A-M detachment following MgATP binding. In either case, at saturating MgATP the effect of sucrose on k_T has little influence on τ_{on} (31) and thus accounts for neither the observed 80% inhibition of V nor the observed 80% inhibition of k_{cat}.

Mechanism by which sucrose inhibits A-M strong binding. Our results indicate that sucrose has a relatively small effect on the diffusion of actin filaments (Fig.

3-5), and that the primary mechanism by which sucrose inhibits katt (Figs. 3-4 A and 3-7 B) is through slowing A-M strong bond formation. This would be especially true in muscle and in vitro motility where contributions of the diffusive component of katt are minimized by the fixed, close proximity of actin and myosin. Observations that sucrose increases the activation energy barrier for A-M strong binding (Fig. 3-10 B) and that sucrose does not increase the Km for actin-activated ATPase (Fig. 3-6) support a conclusion that sucrose inhibits katt by slowing A-M strong bond formation. We can think of no mechanism by which sucrose would bind specific sites on actin or myosin to inhibit A-M binding, and thus we propose that the effects of sucrose on A-M binding are non-specific, much like kinetic effects of ionic strength, pH, or temperature. However, unlike these non-specific effectors, which typically alter multiple steps in the actin-myosin ATPase cycle, sucrose appears to primarily affect A-M strong binding. Because A-M binding is thought to be associated with significant redistribution of waters from the binding interface (33), desolvation is one mechanism by which sucrose might be altering the A-M binding landscape. However, the effects of sucrose on protein-protein interactions can be complex (34), and so in this paper we focus on the kinetic rather than physical-chemical effects of sucrose.

A-M strong binding kinetics, katt(-ATP), influences kcat. A-M strong binding accelerates Pi release from myosin, and so it is not surprising that slowing the kinetics of A-M strong bond formation slows kcat and possibly Pi release. The observation that inhibition of Pi release (by BDM, blebbistatin, BTS) and inhibition of A-M strong binding (by sucrose) both slow k_{att}(+ATP) supports the idea that Pi release and

A-M strong binding are tightly coupled. These studies do not rule out the possibility that Pi release precedes A-M strong binding, and sucrose can be used to test this hypothesis. Specifically, stopped flow fluorimetry can be used to measure the rate, k-Pi, of Pi release, and an observation that sucrose slows k_{att}(+ATP) but not k-Pi would indicate Pi release precedes A-M strong binding. An observation that sucrose similarly inhibits both katt(+ATP) and k-Pi would indicate that Pi release and A-M strong binding are inextricably coupled.

The kinetics of A-M strong binding, katt(-ATP), influence actin sliding velocities, *V*. Conventional models of muscle contraction posit that $V = d/\tau_{on}$, where d is the mechanical step generated by the lever arm rotation of a myosin head, and τ_{on} is the lifetime of A-M strong binding (35, 36). Using an in vitro motility assay to determine the effects of P_i and blebbistatin (a small molecule inhibitor of P_i release) on *V* (19), we previously demonstrated a correlation between the kinetics of P_i release and *V*. In this paper, our observation that sucrose has a large and proportional effect on both *V* and $k_{att(-ATP)}$ but relatively small effects on the kinetic parameters that determine τ_{on} suggest a link between the kinetics of strong A-M binding and *V* (Figs. 3-2 *A*, 3-7 *B*, and 3-8).

Consistent with solution kinetic studies, our in vitro motility data (Fig. 9) suggest that sucrose does not affect the detachment kinetics underlying *V*. The right side of Eq. 2 describes the effects of A-M detachment kinetics on *V* (31). In essence, it describes the shape of the ADP-dependence of *V* shown in Fig. 3-9. The left side of Eq. 2 describes the amplitude of these curves. We observed that sucrose slows V_{max} by approximately 4-fold, and when we multiply the sucrose data by this factor (Fig. 3-9 *B*), the two curves

(above the 200 mM MgADP needed to fully engage actin filaments with the motility surface) resemble each other, implying that sucrose inhibits V_{max} (left side of Eq. 2) and not detachment kinetics (right side of Eq. 2). This kinetic analysis of our in vitro motility data is consistent with both SiMBA and stopped flow experiments and implies that V_{max} is influenced by k_{att} (19, 36).

The hypothesis that sucrose affects V_{max} through attachment kinetics is supported by the observed effects of sucrose on actin dynamics and mechanics in the motility assay. When V is slowed through inhibition of detachment kinetics (e.g., at low [MgATP]) or by increased mechanical loads (e.g., in the presence of an alpha-actinin load), the frequency of actin filament breaking increases and actin filaments become less dynamic (21). In contrast when V is slowed through inhibition of attachment kinetics (e.g., upon addition of blebbistatin), the frequency of actin filament breaking decreases, and actin filaments become more dynamic. In the in vitro motility assay, we observed that upon addition of sucrose actin filament dynamics increased (data not shown) and the frequency of actin filament breaking decreased (Fig. 3-3).

The effects of k_{att} on V_{max} can be understood by considering that decreasing k_{att} has the same effect on the A-M binding rate, r, as decreasing myosin density, ρ (i.e., $r = \rho \cdot k_{att}$). Not surprisingly, the effects of decreasing k_{att} on motility resemble those observed when ρ is decreased. Specifically, decreasing ρ in a motility assay increases actin dynamics, decreases actin filament breaking, and results in a sub-saturating V_{max} that is influenced by detachment kinetics. What remains to be determined is why

inhibition of V_{max} resulting from a decrease in k_{att} cannot be recovered by increasing ρ (12, 19).

A comparison of single molecule and bulk kinetic parameters. We have used both single molecule (SiMBA) and bulk (stopped-flow) kinetic measurements to determine the effects of sucrose on the rate constants for A-M attachment and detachment. In general, the magnitude of the sucrose effect is comparable between the two methods; however, in certain cases the absolute values of kinetic parameters differ. The rate of A-M binding in the absence of nucleotide measured in SiMBA was $\rho \cdot k_{att(-ATP)}$ = 0.7 s^{-1} and the rate measured in stopped flow was $k_{att(-ATP)}$ = 2.4 $\mu M^{-1} \cdot s^{-1}$. The ratio of these two measurements gives an effective S1 concentration in the SiMBA assay of ρ = 290 nM.

Through a solution kinetic analysis it is well established that $k_{att} = K_W \cdot k_{SB}$. The relationship between k_{att}, K_W, and k_{SB} in single molecule binding studies is less clear. The first step in A-M binding is weak-binding which occurs with a rate constant, k_{+W}. Once in the weak state, the probability that myosin undergoes a strong binding transition is $k_{SB}/(k_{-W} + k_{SB})$, where k_{-W} is the rate constant for dissociation from the weak state. Thus $k_{att} = k_{+W} \cdot (k_{SB}/(k_{-W} + k_{SB}))$, which when $k_{-W} >> k_{SB}$ approaches $k_{att} = k_{SB} \cdot (k_{+W}/k_{-W}) = K_W \cdot k_{SB}$, and so K_W and k_{SB} have the same effect on k_{att} values obtained from both single molecule and bulk kinetic experiments. Both SiMBA and stopped flow studies show that sucrose inhibits k_{att}, but neither technique can directly show whether the mechanism is a decrease in K_W, inhibition of k_{SB}, or both. Our observations that sucrose has a relatively small effect on the diffusion coefficient for actin fragments in SiMBA and that sucrose

increases the activation energy for k_{att} indicates that sucrose slows k_{att} through a mechanism other than diffusion. The observation that sucrose inhibits k_{cat} in our actin-activated ATPase experiments suggests that sucrose inhibits k_{SB}. The observation that sucrose causes a slight increase in K_m suggests that sucrose does not inhibit K_W.

The rate of spontaneous A-M dissociation, $k_{det(-ATP)}$ was ~10-fold faster in SiMBA than in stopped flow. Possible reasons for this difference include i) the degrees of freedom of the A-M complex are more limited in SiMBA than in solution and ii) cooperative effects that exist in solution experiments but do not exist in SiMBA due to its 1:1 filament:S1 stoichiometry.

CONCLUSIONS

Sucrose inhibits A-M ATPase activity and actin sliding velocities by slowing $k_{att(+ATP)}$. The observation that sucrose specifically inhibits A-M strong bond formation, $k_{att(-ATP)}$, suggests that sucrose may be useful for determining the relationship between A-M strong binding, muscle mechanics, and A-M ATPase kinetics.

Kinetic parameters with and without sucrose		
Sucrose:	0 mM	880 mM
V, $\mu m \cdot s^{-1}$	2.05 ± 0.3 (3)	0.43 ± 0.2 (3)
D actin, $\mu m^2 \cdot s^{-1}$	0.36 ± 0.02	0.27 ± 0.02
k_{cat}*, min^{-1}	75 ± 13 (2)	15 ± 1 (2)
K_m*, µM	33 ± 2 (2)	9 ± 1 (2)
$\rho \cdot k_{att(-ATP)}$†, s^{-1}	0.72 ± 0.02	0.21 ± 0.02
$\rho \cdot k_{att(+ATP)}$†, s^{-1}	0.97 ± 0.08	0.14 ± 0.01
$k_{att(-ATP)}$‡, $\mu M^{-1} \cdot s^{-1}$	2.41 ± 0.08	0.48 ± 0.01
$k_{det(-ATP)}$‡, s^{-1}	0.13 ± 0.06 (2)	0.11 ± 0.03 (2)
$k_{det(-ATP)}$†, s^{-1}	1.3 ± 0.2	1.0 ± 0.1
k_T‡, $\mu M^{-1} \cdot s^{-1}$	2.1 ± 0.1	1.3 ± 0.1
K_{ADP}‡, µM	217 ± 30	244 ± 33
$E_{a(att)}$‡, $kJ \cdot mol^{-1}$	50 ± 2	68 ± 5
$E_{a(det)}$‡, $kJ \cdot mol^{-1}$	24 ± 3	28 ± 3
*Steady-state ATPase assays performed at 700 mM sucrose.		
†SiMBA		
‡Stopped-Flow		
N values are in parenthesis.		
Errors with (N) are ± SD. All other errors are SEM to a fit.		

Table 3-1 Summary of kinetic parameters measured from in vitro motility, actin-activated S1 ATPase, single molecule binding, and stopped-flow spectroscopy assays.

REFERENCES

1. Lymn, R.W., and E.W. Taylor. 1971. Mechanism of adenosine triphosphate hydrolysis by actomyosin. *Biochemistry*. 10: 4617–24.

2. Goldman, Y.E. 1987. Kinetics of the actomyosin ATPase in muscle fibers. *Annual Review of Physiology*. 49: 637–54.

3. Cooke, R. 1997. Actomyosin interaction in striated muscle. *Physiological Reviews*. 77: 671–97.

4. Huxley, H.E. 1969. The mechanism of muscular contraction. *Science*. 164: 1356–65.

5. Huxley, A.F. 1974. Muscular contraction. *J Physiol*. 243: 1–43.

6. Baker, J.E., I. Brust-Mascher, S. Ramachandran, L.E. LaConte, and D.D. Thomas. 1998. A large and distinct rotation of the myosin light chain domain occurs upon

muscle contraction. *Proceedings of the National Academy of Sciences of the United States of America*. 95: 2944–9.

7. Stein, L. a, L.E. Greene, P.B. Chock, and E. Eisenberg. 1985. Rate-limiting step in the actomyosin adenosinetriphosphatase cycle: studies with myosin subfragment 1 cross-linked to actin. *Biochemistry*. 24: 1357–63.

8. Kovács, M., J. Tóth, C. Hetényi, A. Málnási-Csizmadia, and J.R. Sellers. 2004. Mechanism of blebbistatin inhibition of myosin II. *The Journal of Biological Chemistry*. 279: 35557–63.

9. Ostap, E.M. 2002. 2,3-Butanedione monoxime (BDM) as a myosin inhibitor. *Journal of Muscle Research and Cell Motility*. 23: 305–8.

10. Shaw, M.A., E.M. Ostap, and Y.E. Goldman. 2003. Mechanism of inhibition of skeletal muscle actomyosin by N-benzyl-p-toluenesulfonamide. *Biochemistry*. 42: 6128–35.

11. Chase, P.B., T.M. Denkinger, and M.J. Kushmerick. 1998. Effect of viscosity on mechanics of single, skinned fibers from rabbit psoas muscle. *Biophysical Journal*. 74: 1428–38.

12. Chase, P.B., Y. Chen, K.L. Kulin, and T.L. Daniel. 2000. Viscosity and solute dependence of F-actin translocation by rabbit skeletal heavy meromyosin. *American Journal of Physiology. Cell Physiology*. 278: C1088–98.

13. Robblee, J.P., W. Cao, A. Henn, D.E. Hannemann, and E.M. De La Cruz. 2005. Thermodynamics of nucleotide binding to actomyosin V and VI: a positive heat capacity change accompanies strong ADP binding. *Biochemistry*. 44: 10238–49.

14. Ando, T., and H. Asai. 1977. The effects of solvent viscosity on the kinetic parameters of myosin and heavy meromyosin ATPase. *Journal of Bioenergetics and Biomembranes*. 9: 283–8.

15. Prochniewicz, E., D.A. Lowe, D.J. Spakowicz, L. Higgins, K. O'Conor, et al. 2008. Functional, structural, and chemical changes in myosin associated with hydrogen peroxide treatment of skeletal muscle fibers. *American Journal of Physiology. Cell Physiology*. 294: C613–26.

16. Margossian, S.S., and S. Lowey. 1982. Preparation of myosin and its subfragments from rabbit skeletal muscle. *In*: Colowick SP, NO Kaplan, editors. Methods in Enzymology. New York: Academic Press. pp. 55–71.

17. Weeds, A.G., and R.S. Taylor. 1975. Separation of subfragment-1 isoenzymes from rabbit skeletal muscle myosin. *Nature*. 257: 54–56.

18. Pardee, J.D., and J.A. Spudich. 1982. Purification of muscle actin. *Methods in Enzymology*. 85: 164–181.

19. Hooft, A.M., E.J. Maki, K.K. Cox, and J.E. Baker. 2007. An accelerated state of myosin-based actin motility. *Biochemistry*. 46: 3513–20.

20. 1984. CRC Handbook of Chemistry and Physics - 64th Edition. CRC Press.

21. Stewart, T.J., D.R. Jackson Jr., R.D. Smith, S.F. Shannon, C.R. Cremo, et al. 2013. Actin sliding velocities are influenced by the driving forces of actin-myosin binding. *Cellular and Molecular Bioengineering*. In press.

22. Hancock, W.O., and J. Howard. 1998. Processivity of the motor protein kinesin requires two heads. *The Journal of Cell Biology*. 140: 1395–405.

23. Mizuno, N., S. Toba, M. Edamatsu, J. Watai-Nishii, N. Hirokawa, et al. 2004. Dynein and kinesin share an overlapping microtubule-binding site. *The EMBO Journal*. 23: 2459–67.

24. Criddle, A.H., M.A. Geeves, and T. Jeffries. 1985. The use of actin labelled with N-(1-pyrenyl)iodoacetamide to study the interaction of actin with myosin subfragments and troponin/tropomyosin. *The Biochemical Journal*. 232: 343–9.

25. De La Cruz, E.M., and E.M. Ostap. 2009. Kinetic and equilibrium analysis of the myosin ATPase. 1st ed. Elsevier Inc.

26. Trybus, K.M. 2000. Biochemical studies of myosin. *Methods*. 22: 327–35.

27. Henkel, R.D., J.L. VandeBerg, and R.A. Walsh. 1988. A microassay for ATPase. *Analytical Biochemistry*. 169: 312–318.

28. Cooke, R., and E. Pate. 1985. The effects of ADP and phosphate on the contraction of muscle fibers. *Biophysical Journal*. 48: 789–98.

29. Qian, H., M.P. Sheetz, and E.L. Elson. 1991. Single particle tracking. Analysis of diffusion and flow in two-dimensional systems. *Biophysical Journal*. 60: 910–21.

30. Nelson, S.R., M.Y. Ali, K.M. Trybus, and D.M. Warshaw. 2009. Random Walk of Processive, Quantum Dot-Labeled Myosin Va Molecules within the Actin Cortex of COS-7 Cells. *Biophysical Journal*. 97: 509–518.

31. Baker, J.E., C. Brosseau, P.B. Joel, and D.M. Warshaw. 2002. The biochemical kinetics underlying actin movement generated by one and many skeletal muscle myosin molecules. *Biophysical Journal*. 82: 2134–47.

32. Bárány, M. 1967. ATPase activity of myosin correlated with speed of muscle shortening. *The Journal of General Physiology*. 50: Suppl:197–218.

33. Takács, B., E. O'Neall-Hennessey, C. Hetényi, J. Kardos, A.G. Szent-Györgyi, et al. 2011. Myosin cleft closure determines the energetics of the actomyosin interaction. *FASEB Journal : Official Publication of the Federation of American Societies for Experimental Biology*. 25: 111–21.

34. Frederick, K.B., D. Sept, and E.M. De La Cruz. 2008. Effects of solution crowding on actin polymerization reveal the energetic basis for nucleotide-dependent filament stability. *Journal of Molecular Biology*. 378: 540–50.

35. Huxley, A.F., and R.M. Simmons. 1971. Proposed mechanism of force generation in striated muscle. *Nature*. 233: 533–538.

36. Yengo, C.M., Y. Takagi, and J.R. Sellers. 2012. Temperature dependent measurements reveal similarities between muscle and non-muscle myosin motility. *Journal of Muscle Research and Cell Motility*. .

Chapter 4

Factors beyond detachment kinetics that influence unloaded shortening velocities of muscle

Jackson, DR, and Baker, JE (2013) Factors beyond detachment kinetics that influence unloaded shortening velocities of muscle. Manuscript to be submitted for publication.

ABSTRACT

The conventional view of muscle contraction is that actin-myosin detachment kinetics primarily determine the rate of contraction or in vitro motility velocities (*V*) under standard values of myosin concentration, myosin step size (*d*), and time strongly bound (τ_{on}) as $V = d/\tau_{on}$. We are proposing a molecular model that describes how factors beyond detachment kinetics affect *V*. These factors include attachment kinetics, myosin binding site density on actin, the persistence length of actin, and the stiffness of driving and resistive myosin heads. Simulations show that these factors affect *V* by modulating detachment kinetics and myosin step size through the mechanisms of kinetic saturation, efficiency of force transmission, and the work an individual myosin does against a collection of myosin molecules on binding and displacement of an actin filament. This model also accurately predicts that the number of available myosin (N), actin length, and nucleotide dependent *V* and gives a measure of the internal forces generated between myosin heads that result in actin breaking. This model supplies a

simple framework to interpret and predict results of experimental studies that measures changes in kinetics, myosin concentration, and actin length on *V* in terms of well-established single molecule kinetic and mechanical properties. In summary, unloaded shortening velocities can be influenced by many factors other than detachment kinetics. Thus a mutation or perturbation that results in a change in *V* need not result from a change in only *d* or τ_{on}.

INTRODUCTION

The basis of muscle contraction is the displacement of an actin thin filament by the working step of a myosin head, which happens with a conformational change in the protein induced by myosin binding actin. The velocity of actin movement, *V*, can be slowed by bound myosin heads. A maximum velocity, V_{max}, occurs in muscle when myosin thick filaments and actin thin filaments overlap sufficiently and is reached under in vitro conditions at a saturating myosin density. Most models of muscle contraction predict the internal effective stiffness of bound heads imposes a mechanical load that limits V_{max} (*1*, *2*). According to these models, actin movement can only occur when the resistive load is dissipated, which occurs at the rate of detachment of bound heads. Our simulations of a detachment-limited model demonstrate that at the detachment limit determined by the rate of ADP release, the working step of a bound myosin either generates internal force and no movement or the working step is prevented from occurring.

It has been shown that attachment kinetics influence *V* (*3*, *4*), but an explicit model showing this effect at saturating numbers of myosin is lacking. An understanding

of how attachment kinetics influence *V* at saturating numbers of myosin is crucial to be able to design ways to tune muscle function at the molecular scale (*5*). We propose a model that demonstrates how both attachment and detachment kinetics influence *V*. Our model (See Supplement) incorporates the concepts of the efficiency of force transmission of a myosin weak-to-strong binding step, actin persistence length, the saturation of myosin binding sites on actin, and differential stiffness of negatively (bound) and positively (binding) strained myosin heads (*6*).

We have previously presented an analytical model that described the effects of persistence length and myosin duty ratio on a force transmission term (*7*). The model described in this work extends these concepts by explicitly dealing with number of myosin, actin length, and mechanochemical coupling. We describe our model as a collective force generator model due to the macroscopic description of the mechanics of the system from the collected properties of single molecules that generate internal force, which ultimately determines the attachment and detachment kinetics (See Supplement). We also incorporate our three novel assumptions of efficiency of myosin step transmission, saturation of myosin binding sites on actin, and differential stiffness of binding and bound myosin.

A polymer's flexibility is measured by the persistence length, L_p, which is the length at which thermal forces can bend a polymer. Actin filaments have a relatively low L_p (*8*, *9*) compared to microtubules and are observed to bend regularly. A high degree of flexibility diminishes the ability of myosin heads to transmit forces among neighboring heads in a collection of motor proteins. The effect of actin L_p on in vitro

motility has been experimentally demonstrated (*10*) but has never been incorporated into a model of muscle shortening.

It is well established that with increasing myosin concentrations, actin-activated ATPase activity saturates at a maximal level of activity (*11*). It has been estimated that under standard in vitro motility conditions, there is approximately one myosin head bound to every available binding site on actin with approximately 36 nm spacing between binding sites (*10*, *12*). Yet, actin-myosin saturation kinetics have not been explicitly incorporated into prior models of muscle shortening.

Higuchi and colleagues have shown that when an actin-bound myosin head is pulled in a direction opposite to actin sliding movement, the stiffness of that myosin head is ~2x higher than an actin-bound myosin head pulled in the direction of actin sliding (*6*). This suggests that actin-bound myosin heads impose minimal resistance to muscle shortening, which is in agreement with the concept that resistance to unloaded shortening is energetically counterproductive and can result in actin damage (*3*, *7*, *13*, *14*). Our model is the first to explicitly incorporate the concept of minimal resistance imposed by bound myosin heads.

In this paper, we incorporate persistence length, saturation of myosin binding sites on actin, and asymmetric stiffness into a model of muscle contraction (See Supplement). This model accurately accounts for the observed effects of k_{Att} on V.

METHODS

Stochastic simulations of our model of collective force use individual myosin heads as agents in a discrete-time Markov chain with five states corresponding to

kinetic states (Fig 4-1). A description of the implementation of the model as a stochastic simulation program is provided in the supplement. A 100 nanosecond time step value, *dt*, is used to limit the number of simultaneous mechanical transitions to less than 0.00001% of the total number of available transitions. Simultaneous mechanical transitions are blocked from occurring but simultaneous kinetic transitions are permitted, since they do not affect system state variables (i.e. system stiffness, distance between strong-bound heads, and actin position).

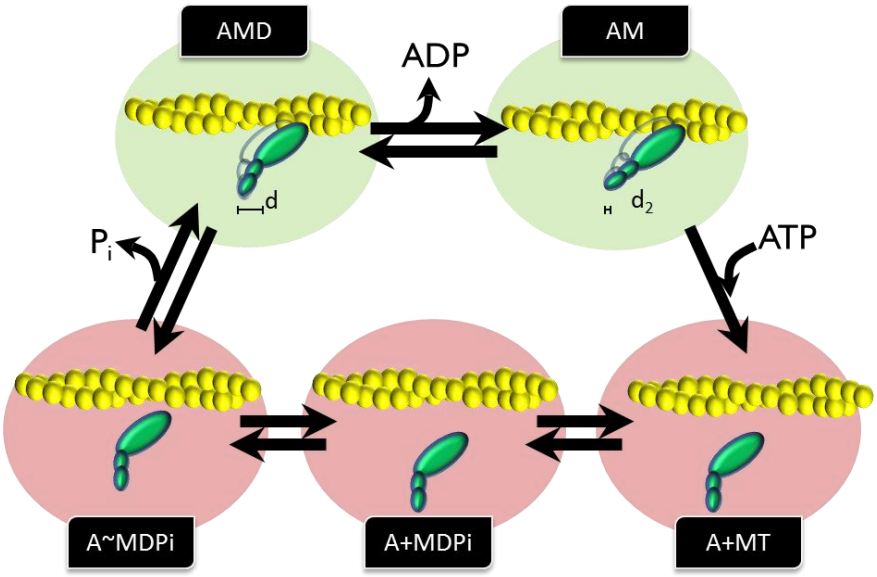

4-1 Acto-myosin kinetic scheme. A five state actin (A) myosin (M) kinetic scheme showing myosin strongly bound states (AMD, AM) that are occupied according to the slowest detachment step (ADP release at saturating ATP) a weakly bound state (A~MDPi), and detached states (A+MT, A+MDPi). In our model, the number of myosin molecules that can occupy the strongly bound and weakly bound states (AMD, AM, A~MDPi) is limited to the number of available binding sites (Nabs) which is determined by the actin length (La) and binding site density (bsd) of one binding site for every 36 nm of actin. The discrete step of 5-10 nm associated with the weak-to-strong binding transition (A~MDPi →AMD) and the additional displacement of 2 nm with ADP release are both work-dependent transitions, with the mechanics of the system affecting the forward and reverse rates of these transitions.

Mechanochemical coupling. The collective force component of our model arises from the method in which the mechanical system state variables are coupled to the chemistry of individual myosin heads. As described previously, the collective force model implies that interhead forces influence the attachment rates of individual heads (*15*). This is different from individual force generator models in which the intrahead force of an individual myosin is the sole work potential that influences the attachment rate of individual myosin heads (*5*, *16*). Each myosin head has mechanical (driving head stiffness, κ_{Drive}, resistive head stiffness, κ_{Uni}, step size, d, and ADP release step size, d_2) and kinetic (kinetic rate transitions out of and into each of the five kinetic states: A+MT, A+MDP, A~MDP, AMD, and AM) parameters (Fig. 4-1). In this model, myosin is defined as a single headed molecule, but could also be assumed to be a two headed molecule in which only a single head binds at a time. The probability of a transition between states occurring is determined from the rate constant of that transition scaled to the time step of the simulation, dt ($P_{A+MT->A+MD} = k_{A+MT->A+MD} * dt$) (*17*). If it is a work dependent transition (A~MD ↔ AMD or AMD ↔ AM), then a Bell approximation (*18*–*20*) is used to model the effects of the work with a partitioning term, p, as in the case of the weak-to-strong transition:

$$W_{WS+} = -p_{WS+} * \frac{1}{2}\kappa_{Drive}{x_{Myo}}^2 + \frac{1}{2}\kappa_{Drive}x_{Myo} \times x_{Act} \quad [1]$$

to determine the kinetics of that transition.

$$k_{WS+} = {k_{WS+}}^{\circ} \times e^{\frac{W_{WS+}}{k_B T}} \quad [2]$$

Currently, our model only considers the influence of the internal force from bound myosin heads on the work-dependent kinetics of myosin attachment (A~MDP -> AMD) and detachment (AMD -> AM). This internal force is modeled as a macroscopic property, κ_{Res}, determined by the product of strongly bound heads, N_{sb}, and κ_{Uni}.

Myosin step partitioning. Our model partitions myosin steps (1) according to how much of the step is due to the flexibility of the actin filament and (2) to how much of the working step pulls out compliance in the myosin itself and how much compliance it pulls out in the system. The distance between strong-bound myosin heads, d_{bsb}, is calculated by dividing the actin length, L_a, by N_{sb} at each time step. A worm-like chain model, incorporating a persistence length, L_p, of 20 μm and d_{bsb} is used to determine the slack of the filament, s:

$$s = d_{bsb} - \sqrt{2{L_p}^2\left(e^{\frac{-d_{bsb}}{L_P}} - 1 + \frac{d_{bsb}}{L_p}\right)} \quad [3]$$

which is the distance an actin filament flexes This slack length absorbs a portion of a myosin's working step, d. Therefore, the transmitted portion of the working step, d_{Trans}, is calculated as (See Fig. 4-2A):

$$d_{Trans} = d - s \quad [4]$$

Fig. 2B shows how d_{bsb} decreases with increasing numbers of bound heads.

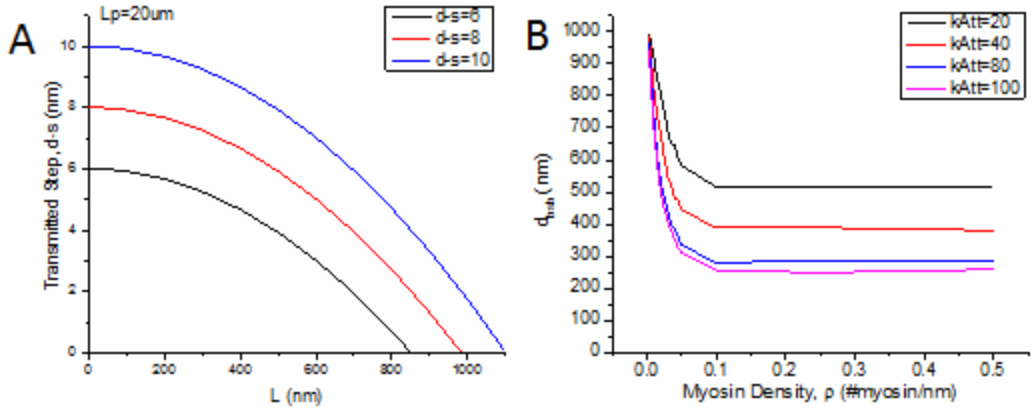

4-2 Relationship of persistence length to transmitted step and attachment kinetics on distance between binding sites. (A) The transmitted portion of myosin's step size (Eq. 4) is shown as a function of the step size (6, 8, or 10 nm) and the length of the actin filament (*L*) at a persistence length of 20 µm. The transmitted portion of the step size falls off as the actin filament length (in nm) increases. This distance, *L*, is analogous to the distance between binding strongly bound sites on actin. (B) The distance between strongly bound sites, d_{bsb}, on actin is shown to decrease in model simulations with increasing myosin density, ρ. At saturation of available binding sites, increased ρ has no effect as all available binding sites are occupied by weakly and strongly bound myosin (weakly bound myosin heads do not contribute to d_{bsb} but do occupy binding sites).

This transmitted step is partitioned into displacement of actin on attachment, Δx_{ActAtt}, and the displacement of elastic myosin components, Δx_{Myo}, according to the relative mechanics of the driving head that is binding and the mechanics of the system, a composite of the bound resistive myosin heads:

$$\Delta x_{ActAtt} = \frac{\kappa_{Drive}}{\kappa_{Drive}+\kappa_{Res}} \times d_{Trans} \quad [5]$$

$$\Delta x_{Myo} = d_{Trans} - \Delta x_{Act} \quad [6]$$

A displacement of actin upon detachment in the case of at least two strongly bound heads, Δx_{ActDet}, is determined from an average of the myosin displacement, x_{Uni}.

$$x_{Uni} = \frac{\kappa_{Drive} \times \Delta x_{Myo}}{(N_{sb}-1) \times \kappa_{Uni}} \quad [7]$$

$$\Delta x_{ActDet} = \frac{\kappa_{Uni} \times x_{Uni} \times (N_{sb} - 2) - \kappa_{Drive} \times \Delta x_{Myo}}{-\kappa_{Drive} - \kappa_{Drive} \times (N_{sb} - 2)} \quad [8]$$

Our model shows how myosin's step size partitioned first on the basis of the flexibility of the actin filament, which is a function of the persistence length of actin and distance between strongly bound myosin heads (Eqs. 3 & 4). Secondly, this transmitted step size is then partitioned between displacing actin on attachment or detachment (Eqs. 5 & 8) and pulling out myosin elastic compliance (Eq. 6). The distance the step size moves actin on detachment is determined from the relaxation of compliant components in bound myosin heads (Eq. 7).

Myosin binding site saturation. Our model is based on three novel assumptions. First we assume that actin myosin binding can saturate the number of available myosin binding sites on a fundamental actin length. The number of available binding sites, N_{abs}, is the product of the actin filament length, L_a, and the binding site density variable (simulations in this paper used a binding site density, b_{sd}, of 0.028, which is equal to 1 binding site at every 36 nm). The filament length is the total length of actin, and is not the same as the length between strongly bound myosin heads discussed in the previous section.

$$N_{abs} = L \times b_{sd} \quad [9]$$

N_{abs} limits the number of myosin heads that can occupy a weak or strong binding state (A~MDP, AMD, or AM).

Efficiency of force transmission. A second assumption is that efficiency of the force transmission generated by myosin's working step determines the fundamental length,

L_f, of actin. This length of actin is the point on Fig. 4-2A that the transmitted step is equal to zero at a given persistence length and step size. This is the maximum, or fundamental, length of actin that a single head can transmit the force from its binding step. That is, a working step of myosin is not transmitted beyond this distance.

$$L_f = L: s\left(L, L_p\right) = d \quad [10]$$

Asymmetric myosin stiffness. The third assumption is that the unitary stiffness of driving and bound myosin heads can be asymmetric as shown experimentally by Kaya and Higuchi (*6*). Positively-strained myosin heads have an approximately two times higher stiffness than negatively strained myosin heads. Myosin heads bound to actin are pulled from positively strained to negatively strained positions with the displacement of myosin by binding heads (*13*).

Theoretical attachment and detachment models of *V*. Using the above assumptions, stochastic simulations of the model calculate *V* by calculating transitions for each head in a random order at each time step. In the results of simulated data, each point in a figure is from the average of five simulations repeated under each condition, with a run length of 1 s and a time step, *dt*, of 1 μs. Additionally, the theoretical velocity of attachment, V_{Att}, and detachment, V_{Det}, are calculated for comparison. Assuming a myosin can bind actin against comparatively low resistance, V_{Att} would be determined from the transmitted step size, the rate of attachment, and the number of myosin weakly bound in the pre-power stroke state:

$$V_{Att} = N_{wb} \times k_{Att} \times d_{Trans} \quad [11]$$

For V_{Det}, it is assumed at least one strongly-bound head is required for maximal velocity (*21*). This is modeled by calculating the probability of at least one head being strong bound with the duty ratio, *r*, and number of myosin available to bind to a given actin filament, *N*:

$$r = \frac{\tau_{On}}{\tau_{On}+\tau_{Off}} \quad [12]$$

$$a = 1 - (1 - r)^N \quad [13]$$

This term modifies the *V*, determined from the product of the rate of detachment and the myosin step size:

$$V_{Det} = a \times d \times k_{Det} \quad [14]$$

An analytical expression of our model without the differential stiffness and myosin binding site saturation assumptions was previously reported and defined the contribution of attachment kinetics in the duty ratio term in *a* as affecting the d_{bsb} (*22*).

$$a_{CFG} = d - \frac{1}{\rho r} + \sqrt{2{L_p}^2\left(e^{-\frac{1}{\rho r L_p}} - 1 + \frac{1}{\rho r L_p}\right)}\Big/ d \quad [15]$$

This paper extends the analytical model with the asymmetric stiffness, myosin binding site saturation, and force transmission assumptions in a stochastic version.

$$V_{Max} = a_{CFG} \times d \times k_{Det} \quad [16]$$

Table of Values		
Persistence Length of Actin	P	20 um
Myosin weak to strong binding step size	d	8 nm
Myosin density	ρ	0.1 heads*nm-1
Basal attachment rate	kAtt°	20 s-1
Basal ADP release rate	kDet°	200 s-1
ADP release step size	d2	2 nm
Stiffness of driving (binding) myosin	kDrive	0.5 pN*nm-1
Stiffness of resistive (bound) myosin	kUni	0.1 pN*nm-1
Partition of attachment step work	partWS	0.5
Partition of ADP relase step work	partADP	0.5
ATP binding rate	kT	5000 s-1 mM-1
ATP concentration	ATP	1 mM

Table 4-1 Partial table of model parameters. The full table of parameters is reported in the supplement.

RESULTS

Rationale. Models of velocity connect measurable kinetic and mechanical parameters to muscle function. A detachment limited model of *V*, first proposed by A.F. Huxley, was developed from the observations that muscle reaches a maximum *V*, V_{max}, that fits Eq. 14 with published values for *d* and k_{det} (*23*, *24*). Assuming the formalism that at least one strong bound head is required for maximal movement (Eq. 13) (*21*), an analytical model of V_{Det} shows that a maximal *V* occurs at the detachment limited kinetic rate constant of ADP release and that decreases in V_{Det} due to decreased attachment kinetics can be overcome by increased numbers of myosin available to bind (Fig. 4-3A, arrows indicate that to recover *V* inhibited by reduced k_{Att} (vertical arrow), an increase in the number of myosin heads is required (horizontal arrow)).

This implies that the mechanism of attachment kinetics affecting *V* is through a duty ratio change (Eq. 12) on the number of available myosin heads that can bind to

actin. Recent studies challenge this with experimental data that shows that decreased *V* due to decreased attachment rate are not recovered with increasing number of heads (*3*, *25*, *26*). The theoretical basis of this is plotted in Fig 4-3B and experimental data is shown at the end of this section.

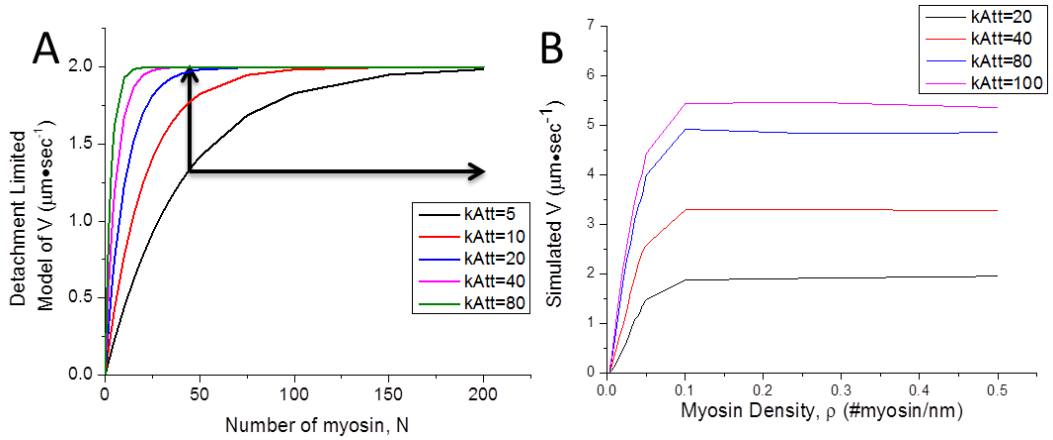

4-3 Detachment limited model of velocity and CFG simulated V as a function of k_{Att}. (A) The effect of varying attachment rates on the *N* dependence of the detachment limited model of velocity, V = a*d*k_{det}, where a is equal to the probability of at least one head being bound (a = (1-(1-r)^N)) is shown for a step size of 10 nm and a detachment rate of 200 s^{-1}. This model predicts that the effect of reduced attachment rates can be overcome with increased *N*, as demonstrated by the arrows showing the required increase in *N* to overcome the reduced V at a kAtt of 5 s-1. (B) Our analytical model of *V* shown as a function of increasing myosin density at various rates of attachment (20, 40, 80, 100 s^{-1}). Reduced *V* is not recovered with increasing numbers of myosin, unlike the detachment limited model of *V* shown in Fig. 2A.

Although numerous studies support attachment kinetics affect *V* beyond a change in duty ratio mechanism, no explicit model has been proposed (*3*, *4*, *7*, *27*, *28*). The goal of this study is to develop a model that accounts for these observations.

Model. Our model of muscle shortening accounts for observations that *V* decreases with inhibition of k_{Att} and cannot be recovered by increasing myosin density or actin length (in general, with increasing *N*). Like in many previous models, our model incorporates many well-established mechanical and kinetic properties of the actin-myosin ATPase reaction. Unique to our model are parameters that account for i) saturation of myosin binding sites on actin, ii) actin flexibility, and iii) the asymmetric stiffness of myosin. Here we focus on these parameters and their simulated effects on *V*.

Saturation of myosin binding sites on actin. In the absence of A-M saturation kinetics (Eq. 9), our simulations of *V* versus myosin density are consistent with V_{Det} (Fig. 4-3A). The reason is that without incorporating saturation kinetics, the number of strongly bound myosin heads increases without limit when myosin densities are increased, eventually reaching – regardless of myosin stiffness, actin length, attachment kinetics, etc. – a sufficient number of strongly bound myosin to completely limit actin sliding velocities. Then, actin can only move when strongly bound heads detach at which point V is detachment-limited. In short, for a model to account for the observation that inhibition of k_{Att} slows *V* at relatively high myosin densities, one must incorporate saturation of A-M binding.

Fig. 4-3B shows our simulations of *V* versus myosin density when we incorporate A-M saturation kinetics into the model (Eq. 9). In contrast to the detachment-limited model (Fig. 4-3A), *V* saturates with increasing myosin when myosin saturates binding sites on actin rather than when the number of strongly-bound myosin heads becomes

sufficient to impose a halting mechanical load. The effects of k_{Att} on V are not reversed by increasing myosin density because the effects of increasing myosin density are kinetically limited by A-M saturation binding kinetics.

Persistence length and force transmission. The number, N, of myosin heads available to bind an actin filament not only increases with myosin density (as modeled in Fig. 4-3A); N also increases with actin filament length (longer actin filaments interact with more myosin heads). While A-M saturation kinetics can account for saturation of V at high myosin densities (Fig. 4-3B), it does not account for saturation of V at high actin filament lengths, L_a. The mechanism by which V saturates at high L_a has previously been addressed (*10*). Specifically, they argue that V saturates when the actin filament length becomes longer than the distance over which a myosin head can transmit forces, which is a function of the actin filament persistence length, L_p.

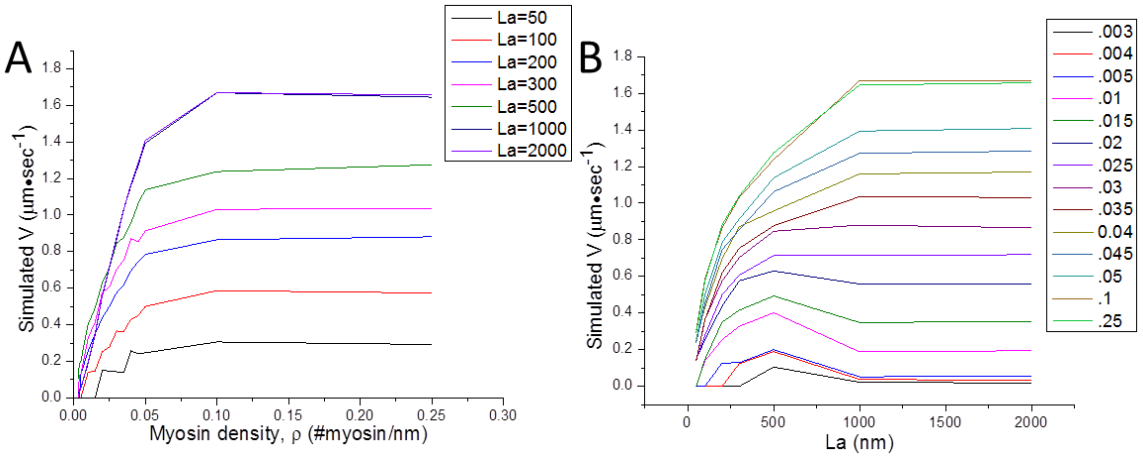

4-4 Simulated velocities over different actin lengths and simulated velocities demonstrating saturation at different attachment rates. (A) Model predictions of the effects of varying actin length, L_a, and myosin density, ρ, on simulated V. A sigmoidal shape is observed in the predicted V at low and high L_a. Velocities saturate when the number of available myosin binding sites on actin, N_{abs}, are saturated with weakly and strongly bound heads. (B) The effects of varying k_{Att} on simulated model V with increasing myosin density are similar to the model effects of varying a force transmission term, η, in Fig 2 B. Our model predicts that increasing the number of available myosin motors will not recover slower V resulting from decreased attachment kinetics.

Fig. 4 shows simulations of the combined effects of L_a and myosin density, ρ, on V. In these simulations forces cannot be transmitted beyond 1 µm. This is evident in both Figs. 4-4A and 4-4B by the saturation of V at an L_p of 1 µm.

Asymmetric myosin head stiffness. Higuchi and colleagues have shown that a myosin head has a high stiffness when it actively pushes in the direction of actin movement and a low stiffness when it is passively pulled in the direction of actin movement (*29*). These observations suggest a potential mechanism for minimizing myosin head resistance to muscle shortening. However, the manifestation of this low resistance has yet to be modeled. The reason, as described above, is that in the absence of A-M saturation kinetics, strongly bound myosin heads accumulate without limit when

myosin densities are increased. Regardless of the resistive stiffness of a myosin head, the collective resistive stiffness of myosin heads increases with the number of strongly bound heads, until strongly-bound myosin heads limit actin movement and *V* saturates at a detachment limit. Incorporating A-M saturation kinetics into a model of asymmetric myosin head stiffness gives very different results.

Fig. 4-5 shows our simulations of *V* at different myosin densities. These simulations are compared to simulations of an attachment-limited model of *V* (Eq. 11, black line) and a detachment-limited model of *V* (Eq. 14, red line). Again, V_{Att} saturates with increasing myosin density with the saturation of AMDP and V_{Det} saturates with increasing myosin density when actin-bound myosin heads fully limit actin movement. Fig. 4-5A is a simulation our model simulation of *V* with symmetric myosin head stiffness, showing that *V* saturates at a detachment-limited velocity. However, when we run the same simulation with a relatively low resistive myosin head stiffness, Fig. 4-5B shows that *V* approaches an attachment-limited *V*.

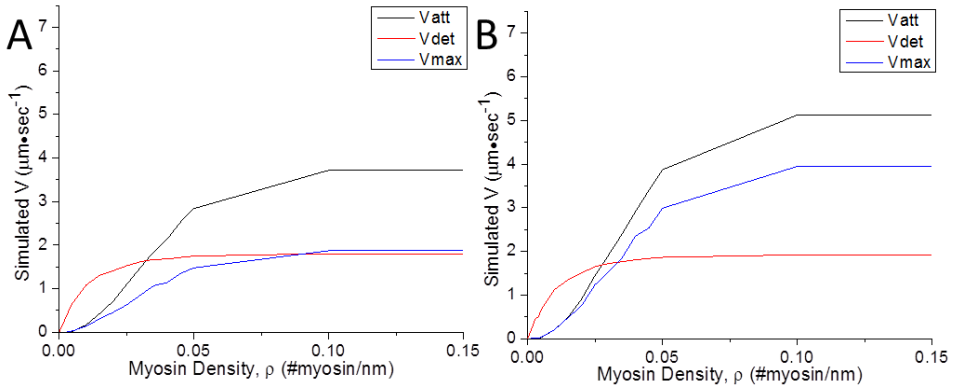

4-5 Comparison of the effects of increasing myosin density under different models of *V* (V_{max}, V_{Att}, V_{Det}) at equal driving and resistive stiffness. (A) The predictions of *V* from three different models of *V* as a function of detachment kinetics demonstrate the differences in the three models. The model of *V* from attachment kinetics is determined from $V_{Att} = N * d * k_{Att}$. The model of *V* from detachment kinetics is defined as $V_{Det} = d * k_{Det}$. Our model of collective force (V_{max}) with an explicit definition of the efficiency of force transmission as explicitly defined by attachment and detachment kinetics and with the contribution of mechanics to acto-myosin kinetics is shown as *V*. All simulated model *V* use a value for *d* that is affected by the efficiency of force transmission and mechanochemical coupled kinetics, with a major difference in the three models being that movement in V_{max} can occur with both attachment and detachment, with the mechanics of the system determining the extent. (A) shows predicted *V* with equal stiffness between driving (binding) and resistive (bound) myosin heads. (B) Comparison of different models of *V* (V_{max}, V_{Att}, V_{Det}) at higher driving stiffness. A differential stiffness between the two populations of myosin heads (driving and resistive) allows for model velocities that exceed V_{Det} at low k_{Det} but are still bounded by V_{Att}.

Accelerated detachment kinetics. Previous work showed that accelerated ADP release lead to hypermotile *V* and that P_i could affect unloaded shortening *V* at sub-maximal detachment kinetics, k_{Det} (*3*). The inverse *V* vs inverse ATP plots enables the quantification of the ADP release rate from the y-int as previously described (*3*). Linear fits of simulated *V* yield an ADP release rate of 333 s^{-1} at high ATP for both 0 and 40 μM Pi (Fig. 4-6A). At low ATP and no P_i, an ADP release rate of 222 s^{-1} was determined by extrapolating the linear fit of low ATP data to the y-intercept. For low ATP and 40 μM P_i, the ADP release rate was calculated to be about 10% slower at 200 s^{-1}. Simulated *V* at

different [Pi] and k_{Det} are shown in Fig 4-6B. At low k_{Det}, P_i decreases *V*. The effect of P_i on reducing *V* is minimized at higher k_{Det}, which is in agreement with the experimental evidence presented by Hooft et al.

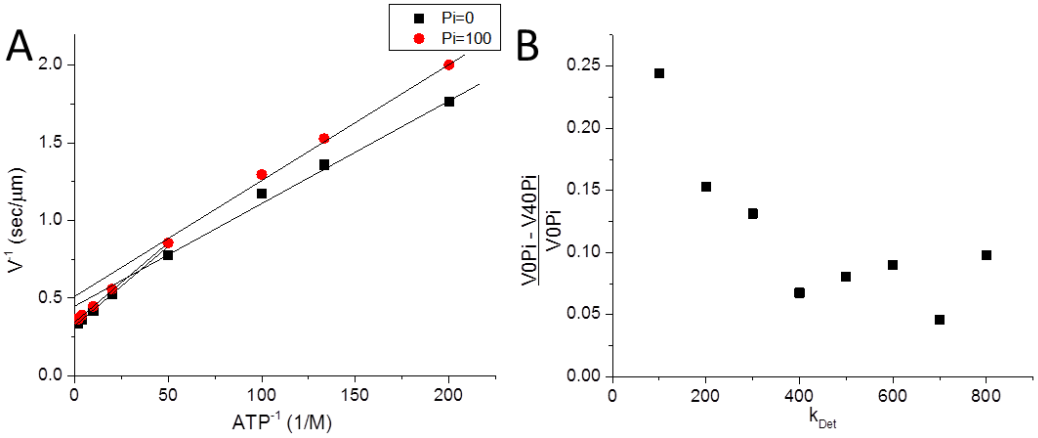

4-6 Hypermotility at different [P_i] and k_{Det} dependence of simulated *V* on [P*i*]. (A) The effect of varying [ATP] on simulated model *V* at low and high [P_i] demonstrate a possible mechanism for observed hypermotile (that is, accelerated k_{det}) *V*. Above a critical concentration of ATP, *V* are accelerated due to accelerated rates of ADP release, as measured by using the y-int of a fitted line to the linear slope of *V* above 20 uM ATP as the value for ADP release, k_{-D}, and a 10 nm step size (*3*). A k_{-D} in the absence and presence of P_i at high ATP of 333 s^{-1} was determined by this fit. In the absence of P_i, a k_{-D} of 155 s^{-1} at low ATP was determined. In the presence of P_i at low ATP, a k_{-D} of 200 s^{-1} was determined. (B) The model predictions of the P_i-effect dependence on k_{Det} are shown with the difference in simulated *V* in the absence and presence of 40 µM P_i are plotted in (B) as (VP_i=0-VP_i=40)/VP_i=0). This demonstrates the model prediction that the effect of P_i on slowing *V* is dependent on detachment kinetics, with the effect being greater at lower k_{Det}.

An examination of the underlying outputs of the simulation demonstrates the interplay of the novel model mechanisms (Fig. 4-7). The number of strongly bound myosin heads, N_{sb}, saturates with increasing number of myosin at varying values for varying k_{Att} (Fig 4-7A). As shown earlier in Fig. 4-2B, this reduces the distance between strong binding sites on actin, increasing the myosin's effective step size as myosin's

force transmission is increased (see Fig. 4-2A, $L \approx d_{bsb}$). A measure of the internal force of the system as a function of increased ρ is given by the system stiffness, κ_{Res} (Fig 4-7B). As myosin heads strongly bind to actin κ_{Res} increases. κ_{Res} is expected to perfectly correlate with N_{sb} as it is the product of N_{sb} and κ_{Uni}. The effect of ρ and k_{Att} on the mechanochemically-coupled k_{Att} and k_{Det} are seen in Figs 4-7C & 4-7D. Increased work due to the increased internal force of the system slows attachment but accelerates detachment.

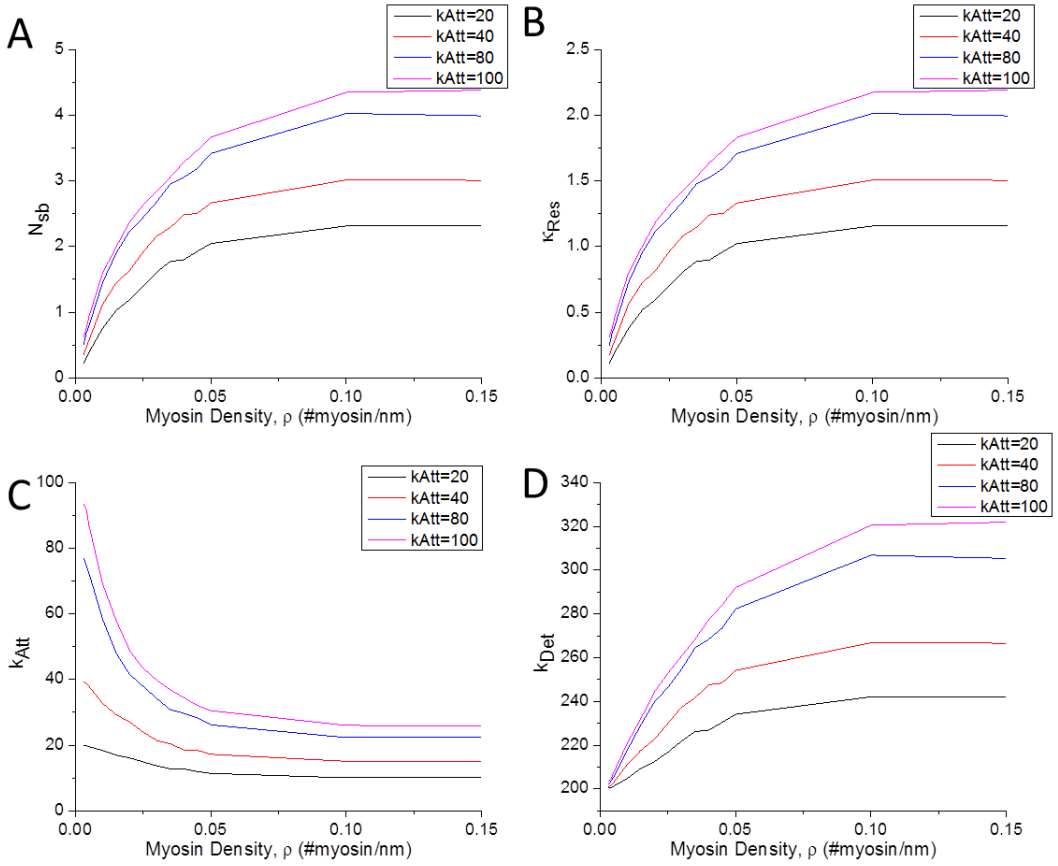

4-7 Model simulation results of number of strongly bound heads, system stiffness, kAtt, and kDet at varying kAtt. The myosin density dependence of the (A) Number of strongly bound myosin, N_{sb}, (B) system resistive element, κ_{Res}, (C) work-dependent attachment rate, k_{Att}, and (D) the work-dependent detachment rate, k_{Det}, with increasing number of myosin at different basal attachment rates (20, 40, 80, 100 s^{-1}) is shown.

Model simulations compared to experimental data. Experimental data showing the effects of an attachment inhibitor, blebbistatin, on in vitro *V* at increasing myosin concentrations shows that the inhibited *V* is not recovered with more myosin (Fig 4-8A). Our model approximates this data using the mechanisms described in this paper (Fig 4-8B).

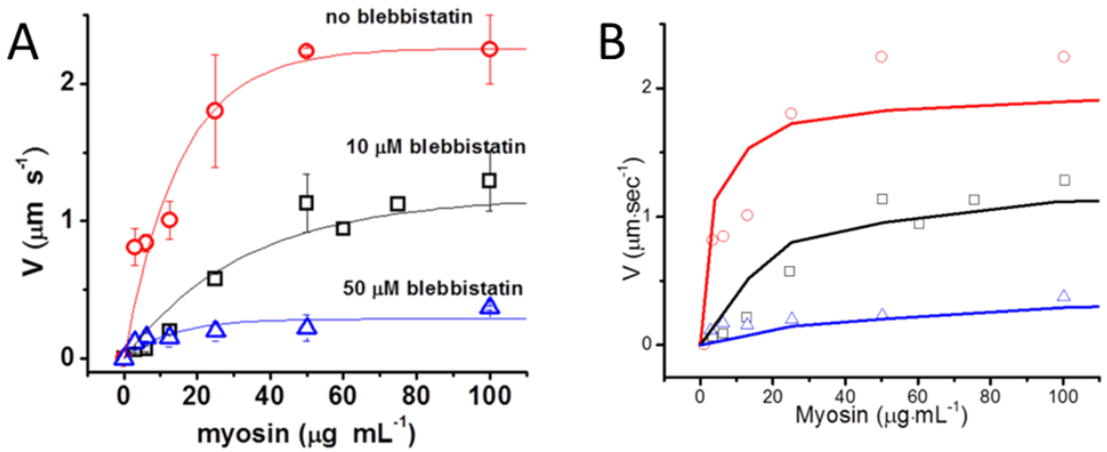

4-8 Model simulations compared to experimental data of the myosin concentration depence of varying kAtt. A comparison of (A) experimental and (B) simulation results of the effect of reduced attachment rates with increasing number of myosin. Varying concentrations of the attachment inhibitor blebbistatin (0, 10, and 50 μM) are shown to reduce in vitro actin sliding velocities. The collective force generation model demonstrates similar saturation of *V* at decreased attachment rates that are not recovered with increasing myosin concentration.

DISCUSSION

We have developed a model of unloaded shortening velocities, *V*, that accounts for the experimental observation that *V* is reduced through inhibition of k_{Att} and cannot be recovered by increasing ρ (*3*, *7*, *25*, *28*). This required the addition of three components that are unique to our model: A-M saturation kinetics, force transmission, and asymmetric myosin stiffness. Addition of these components is experimentally

justified and results in a model of muscle shortening with novel implications for our understanding of muscle contraction.

We demonstrate the predictions of our theoretical model of *V* being influenced by attachment kinetics with simulations varying *N* and asymmetric myosin stiffness (Figs. 4-3B, 4-5B). We simulate the myosin density and actin filament length-dependence of *V* to validate the assumption that myosin binding sites on actin saturate (Fig. 4-4). This model incorporates actin-myosin binding saturation by limiting weak and strong binding sites on a fundamental actin filament length, determined by the efficiency of force transmission of a myosin working step (*7*, *10*). Our model predicts that the effect of resistive stiffness of bound myosin heads (negatively strained) relative to the stiffness of binding myosin heads (positively strained) can give rise to a *V* determined by the number of weakly bound myosin heads in a fundamental actin length (Eq. 11) exceeding detachment limited *V* (Eq. 13) (Fig 4-5B). Our explicit model shows detachment limited *V* under symmetric myosin stiffness (Fig. 4-5A).

Efficiency of force transmission modulates step size. The working step of myosin has been estimated between 5 and 10 nm (*30*). The persistence length (L_p) of phalloidin stabilized actin has been estimated between 15 and 20 μm (*8*, *9*). This suggests that the working step of a myosin is not transmitted at 100% along a length of actin. Experiments have shown that there exists a minimum distance of ~130 nm between skeletal myosin available to bind an actin filament in vitro for maximal efficiency of force transmission (*10*). Our model assumes that this efficiency of force transmission, measured in terms of the transmitted portion of the working step (Eq. 4), is a function of

the distance between strongly bound myosin heads and the L_p. A worm-like chain model can be used to approximate the distance a polymer can deform due to an applied force (*31*). The fundamental length of actin, L_f, which is the maximum distance along an actin filament a working step of myosin can be transmitted, is estimated at ~1 μm for an L_p of 20 μm (Fig. 4-2A).

As an increasing number of myosin heads strongly bind to an actin filament, the average distance between strongly bound sites (d_{bsb}) decreases. As shown in Fig. 4-2B, increasing k_{Att} affects the efficiency of force transmission by increasing the number of strongly bound heads and reducing d_{bsb}.

Saturation of available binding sites. Actin activated skeletal myosinS1 ATPase saturates with a K_m of 13 μM and is limited by P_i release associated with attachment kinetics in solution (*11*). Using this same assumption, that binding sites can be saturated, in our model is a mechanism by which increased myosin density cannot compensate for decreased attachment kinetics. When binding sits are saturated, increased number of myosin are unable to recover *V* (Fig. 4-3B,4- 4).

Mechanochemical coupling at system level limits attachment kinetics and accelerates detachment kinetics. The collective mechanics of the system are modeled at the system level. In previous models the mechanics of the system with an explicit definition of spring elements (*32*–*35*). Our model uses a macroscopic resistive spring element, κ_{Res}, which is a product of the number of strongly bound myosin heads and the unitary resistive stiffness (Fig 4-7A, 4-7B). This decreases the actual rates of attachment (Fig 4-7C) and increases the detachment rates (Fig 4-7D).

Collective force. Conventional models of muscle shortening assume a mechanical limit to shortening velocity in which strongly-bound myosin heads prevent actin filament movement from the working step of binding heads. They assume actin only moves with the dissipation of resistive forces upon myosin detachment from actin. This assumption fits if force generation of a binding myosin head is assumed to precede actin movement (*23*). Yet, there is evidence that myosin's discrete lever arm rotation can displace an actin filament on binding without significant force generation (*36*–*38*).

Barany suggested that muscle shortening velocities are limited by ATPase kinetics, which are limited by actin-myosin attachment kinetics (*39*). Recent studies show a correlation between inhibitors of actin-myosin binding (blebbistatin, RTF, bts, mutation R423Q) and *V* (*3*, *26*, *28*, *40*). The temperature-dependence of V does not match the temperature-dependence of ATPase activity, indicating they are not limited by the same kinetic processes. (*4*). This suggests that *V* is not completely determined by actin-myosin detachment kinetics.

We previously proposed a mechanism by which attachment kinetics can influence *V* at mechanically limited velocities (*3*). Actin-myosin binding can accelerate the kinetics of ADP release from bound resistive myosin heads by increasing interhead forces (*13*, *14*, *41*). In addition to providing simulations supporting a mechanism of hypermotile velocities (Fig 4-6A), this paper focuses on a second possible explanation of how attachment kinetics can influence *V*: if actin movement is not mechanically limited, then a myosin working step can directly contribute to V_{max} (Fig 4-5B).

Significant challenges exist in developing a model of attachment kinetics influencing *V*. If there was no resistance to actin movement on binding, then V_{max} would linearly increase with increased filament overlap in muscle or increased myosin density or actin filament length in in vitro experiments according to Eq 10. Yet, this effect is not observed in muscle or in in vitro experiments (*10*, *42*). If bound myosin heads are stiff in comparison to binding myosin heads, then a detachment limited *V* is reached when the number of actin bound myosin heads is greater than one ($N*r=(N*k_{Att})/k_{Det}>1$), for a k_{Det} determined by ADP release in the AMD -> AM transition (Fig 4-1). A detachment limited *V* is reached even with low stiffness of resistive heads if *N* is increased without limit. Attachment limited *V* can exceed detachment limited *V* at low resistive stiffness.

CONCLUSION

In light of this, the idea that during unloaded shortening myosin heads would battle against each other generating halting internal loads in an otherwise unloaded macroscopic system seems counterintuitive. Why would myosin heads be forced to perform internal mechanical work when no macroscopic work is needed? Moreover, high internal loads in a motility assay shred actin filaments (*7*), and presumably these forces would destabilize contractile proteins in muscle as well.

Our model accurately describes the effects of myosin density and actin filament length observed in in vitro motility assays. It accurately accounts for the observation that the decrease in *V* observed upon addition of inhibitors of actin-myosin binding cannot be recovered by increasing actin filament lengths or myosin densities.

Our model, with an A-M kinetic saturation assumption, shows that unloaded muscle shortening velocities and in vitro motility assay actin filament sliding velocities do not have to be limited by detachment kinetics. Instead, the kinetic saturation of myosin binding sites on actin by weakly bound myosin heads saturates *V*, consistent with Barany's suggestion that *V* is limited by AM ATPase.

REFERENCES

1. Campbell, K. S. (2009) Interactions between Connected Half-Sarcomeres Produce Emergent Mechanical Behavior in a Mathematical Model of Muscle, *PLoS Computational Biology 5*.

2. Walcott, S., Warshaw, D. M., and Debold, E. P. (2012) Mechanical Coupling between Myosin Molecules Causes Differences between Ensemble and Single-Molecule Measurements, *Biophysical Journal 103*, 501–510.

3. Hooft, A. M., Maki, E. J., Cox, K. K., and Baker, J. E. (2007) An accelerated state of myosin-based actin motility., *Biochemistry 46*, 3513–20.

4. Yengo, C. M., Takagi, Y., and Sellers, J. R. (2012) Temperature dependent measurements reveal similarities between muscle and non-muscle myosin motility., *Journal of muscle research and cell motility*.

5. Yengo, C. M., Takagi, Y., and Sellers, J. R. (2012) Temperature dependent measurements reveal similarities between muscle and non-muscle myosin motility., *Journal of muscle research and cell motility 33*, 385–394.

6. Kaya, M., and Higuchi, H. (2010) Nonlinear elasticity and an 8-nm working stroke of single myosin molecules in myofilaments., *Science (New York, N.Y.) 329*, 686–9.

7. Stewart, T. J., Jackson Jr., D. R., Smith, R. D., Shannon, S. F., Cremo, C. R., and Baker, J. E. (2013) Actin sliding velocities are influenced by the driving forces of actin-myosin binding, *Cellular and Molecular Bioengineering*.

8. Greenberg, M. J., Wang, C.-L. a, Lehman, W., and Moore, J. R. (2008) Modulation of actin mechanics by caldesmon and tropomyosin., *Cell motility and the cytoskeleton 65*, 156–64.

9. Ott, A and Magnasco, M and Simon, A and Libchaber, A. (1993) Measurement of the persistence length of polymerized actin using fluorescence microscopy, *Physical Review E 48*, 1642–1645.

10. Harris, D. E., and Warshaw, D. M. (1993) Smooth and skeletal muscle myosin both exhibit low duty cycles at zero load in vitro., *The Journal of biological chemistry 268*, 14764–8.

11. Adelstein, R. S., and Eisenberg, E. (1980) Regulation and kinetics of the actin-myosin-ATP interaction., *Annual review of biochemistry 49*, 921–56.

12. Spudich, J. A. (2001) The myosin swinging cross-bridge model., *Nature reviews. Molecular cell biology 2*, 387–92.

13. Jackson, D. R., and Baker, J. E. (2009) The energetics of allosteric regulation of ADP release from myosin heads., *Physical chemistry chemical physics:PCCP 11*, 4808–14.

14. Baker, J. E. (2004) Free energy transduction in a chemical motor model., *Journal of theoretical biology 228*, 467–76.

15. Jackson, D. R., and Baker, J. E. (2009) The energetics of allosteric regulation of ADP release from myosin heads., *Physical chemistry chemical physics:PCCP 11*, 4808–14.

16. Huxley, A. F. (1957) Muscle structure and theories of contraction., *Progress in biophysics and biophysical chemistry 7*, 255–318.

17. Ninio, J. (1987) Alternative to the steady-state method: derivation of reaction rates from first-passage times and pathway probabilities., *Proceedings of the National Academy of Sciences of the United States of America 84*, 663–7.

18. Walcott, S. (2008) The load dependence of rate constants., *The Journal of chemical physics 128*, 215101.

19. Clemen, A. E.-M., Vilfan, M., Jaud, J., Zhang, J., Bärmann, M., and Rief, M. (2005) Force-dependent stepping kinetics of myosin-V., *Biophysical journal 88*, 4402–10.

20. Bell, G. (1978) Models for the specific adhesion of cells to cells, *Science 200*, 618–627.

21. Uyeda, T. Q., Kron, S. J., and Spudich, J. a. (1990) Myosin step size. Estimation from slow sliding movement of actin over low densities of heavy meromyosin., *Journal of Molecular Biology 214*, 699–710.

22. Stewart, T. J., Jackson Jr., D. R., Smith, R. D., Shannon, S. F., Cremo, C. R., and Baker, J. E. (2013) Actin sliding velocities are influenced by the driving forces of actin-myosin binding, *Cellular and Molecular Bioengineering 6*, 26–37.

23. Huxley, A. F. (1957) Muscle structure and theories of contraction., *Progress in biophysics and biophysical chemistry 7*, 255–318.

24. Siemankowski, R. F., Wiseman, M. O., and White, H. D. (1985) ADP dissociation from actomyosin subfragment 1 is sufficiently slow to limit the unloaded shortening velocity in vertebrate muscle., *Proceedings of the National Academy of Sciences of the United States of America 82*, 658–62.

25. Chase, P. B., Chen, Y., Kulin, K. L., and Daniel, T. L. (2000) Viscosity and solute dependence of F-actin translocation by rabbit skeletal heavy meromyosin., *American journal of physiology. Cell physiology 278*, C1088–98.

26. Tyska, M. J., Hayes, E., Giewat, M., Seidman, C. E., Seidman, J. G., and Warshaw, D. M. (2000) Single-molecule mechanics of R403Q cardiac myosin isolated from the mouse model of familial hypertrophic cardiomyopathy., *Circulation research 86*, 737–44.

27. Baker, J. E., Brosseau, C., Joel, P. B., and Warshaw, D. M. (2002) The biochemical kinetics underlying actin movement generated by one and many skeletal muscle myosin molecules., *Biophysical journal 82*, 2134–47.

28. Gorga, J. a, Fishbaugher, D. E., and VanBuren, P. (2003) Activation of the calcium-regulated thin filament by myosin strong binding., *Biophysical journal*. Elsevier *85*, 2484–91.

29. Kaya, M., and Higuchi, H. (2010) Nonlinear elasticity and an 8-nm working stroke of single myosin molecules in myofilaments., *Science (New York, N.Y.) 329*, 686–9.

30. Guilford, W. H., Dupuis, D. E., Kennedy, G., Wu, J., Patlak, J. B., and Warshaw, D. M. (1997) Smooth muscle and skeletal muscle myosins produce similar unitary forces and displacements in the laser trap., *Biophysical journal*. Elsevier *72*, 1006–21.

31. Howard, J. (2001) Mechanics of Motor Proteins and the Cytoskeleton. Sinauer Associates, Sunderland, MA.

32. Campbell, K. S. (2009) Interactions between connected half-sarcomeres produce emergent mechanical behavior in a mathematical model of muscle., *PLoS computational biology 5*, e1000560.

33. Campbell, K. S. (2006) Filament compliance effects can explain tension overshoots during force development., *Biophysical journal 91*, 4102–9.

34. Tanner, B. C. W., Daniel, T. L., and Regnier, M. (2007) Sarcomere lattice geometry influences cooperative myosin binding in muscle., *PLoS computational biology 3*, e115.

35. Tanner, B. C. W., Daniel, T. L., and Regnier, M. (2012) Filament compliance influences cooperative activation of thin filaments and the dynamics of force production in skeletal muscle., *PLoS computational biology 8*, e1002506.

36. Baker, J. E., Brust-Mascher, I., Ramachandran, S., LaConte, L. E., and Thomas, D. D. (1998) A large and distinct rotation of the myosin light chain domain occurs upon muscle contraction., *Proceedings of the National Academy of Sciences of the United States of America 95*, 2944–9.

37. LaConte, L. E. W., Baker, J. E., and Thomas, D. D. (2003) Transient kinetics and mechanics of myosin's force-generating rotation in muscle: resolution of millisecond rotational transitions in the spin-labeled myosin light-chain domain., *Biochemistry 42*, 9797–803.

38. Debold, E. P., Patlak, J. B., and Warshaw, D. M. (2005) Slip sliding away: load-dependence of velocity generated by skeletal muscle myosin molecules in the laser trap., *Biophysical journal*. Elsevier *89*, L34–6.

39. Bárány, M. (1967) ATPase activity of myosin correlated with speed of muscle shortening., *The Journal of general physiology 50*, Suppl:197–218.

40. Shaw, M. A., Ostap, E. M., and Goldman, Y. E. (2003) Mechanism of inhibition of skeletal muscle actomyosin by N-benzyl-p-toluenesulfonamide., *Biochemistry 42*, 6128–35.

41. Kad, N. M., Kim, S., Warshaw, D. M., VanBuren, P., and Baker, J. E. (2005) Single-myosin crossbridge interactions with actin filaments regulated by troponin-tropomyosin., *Proceedings of the National Academy of Sciences of the United States of America 102*, 16990–5.

42. Granzier, H. L., Burns, D. H., and Pollack, G. H. (1989) Sarcomere length dependence of the force-velocity relation in single frog muscle fibers., *Biophysical journal 55*, 499–507.

Supplement

This chapter supplements the description of the collective force generator model of muscle contraction described in Chapter 4. The previous description outlined the theoretical considerations of the model regarding the basis of interhead forces between myosin molecules determining the potential a myosin head must work against in binding to or detaching from actin, the saturation of myosin binding sites on actin, the efficiency of the transmission of the force generated from a myosin attachment step, and the asymmetric stiffness between binding and bound myosin heads. This chapter provides more details regarding the implementation of the model in an iterative stochastic framework. Specific details of the aforementioned theoretical considerations are maintained in Chapter 4 and not discussed in this supplement to avoid redundancy.

Description of code in model

The model is coded in C++ using an object oriented approach. Simulations can be run to test three different sets of variables for each run. For instance, a series of simulations looking at the effects of varying attachment kinetics can be run at different detachment kinetics at increasing myosin density. The first variable creates a new graph at a value that will be held static while varying the next two parameters. The second variable is shown as different sets of lines at increasing values of the third variable (i.e. the x-ordinate).

The model captures all of the statistics of the system. These include the velocity of actin, average kinetic rates, average time spent in each state, average system stiffness, and the average displacement sizes.

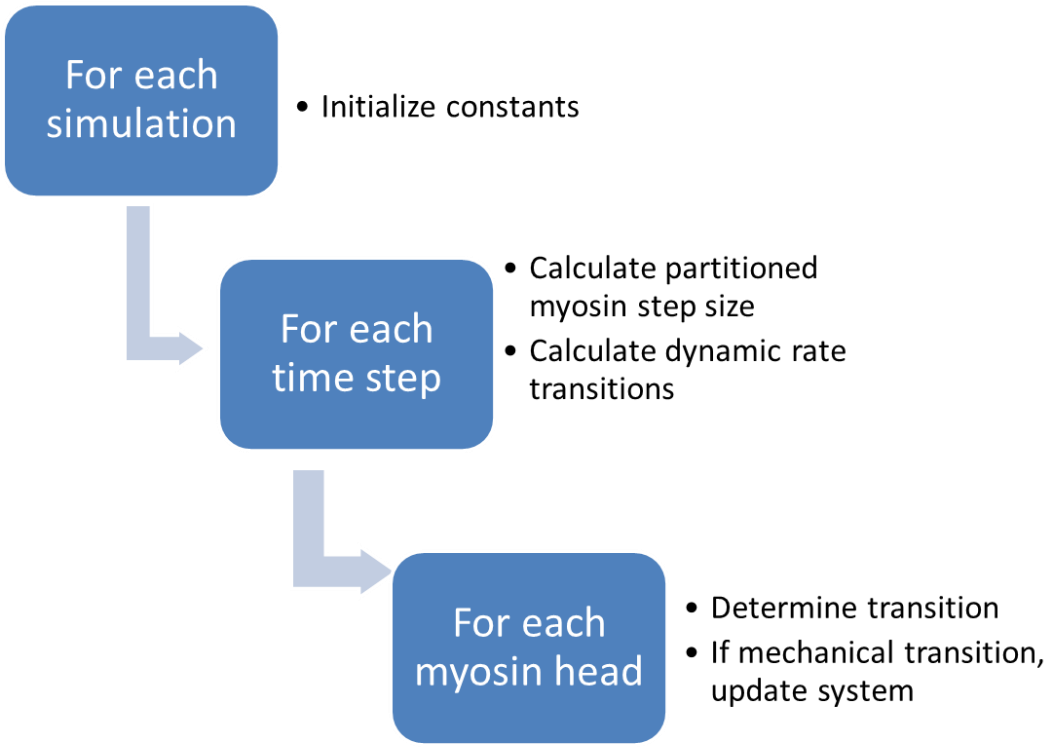

0-1 Algorithm overview of our stochastic collective force generator model of muscle contraction. At the start of each simulation, constants that do not depend on system or dynamic values are initialzed. A list of these are reported in Table 6-1. At the start of each time step in the course of the simulation, the dynamic variables are determined. These are the variables that fluctuate with the stochastic evolution of the system through time. A list of these dynamic time step variables is reported in Table 6-2. At each time step, every head is evaluated to determine if a transition has occurred (Fig. 6-2).

The overall flow of the program is shown in Figure 6-1. At the start of every simulation, the constants are set. These values do not fluctuate during the time evolution of the simulation. Values such as the number of myosin molecules or the

length of actin are examples. All of the simulation constants are reported in Table 6-1. As this is a Markov model, each time step in the course of the simulation is evaluated. This requires the determination of the dynamic variables that change dependent on the state of the system. Examples of these include the work dependent transitions. Since the work potential is a function of the number of bound myosin, this is calculated at the start of every time step if the system has changed in the previous time step. A complete list of the dynamic time step variables is shown in Table 6-2.

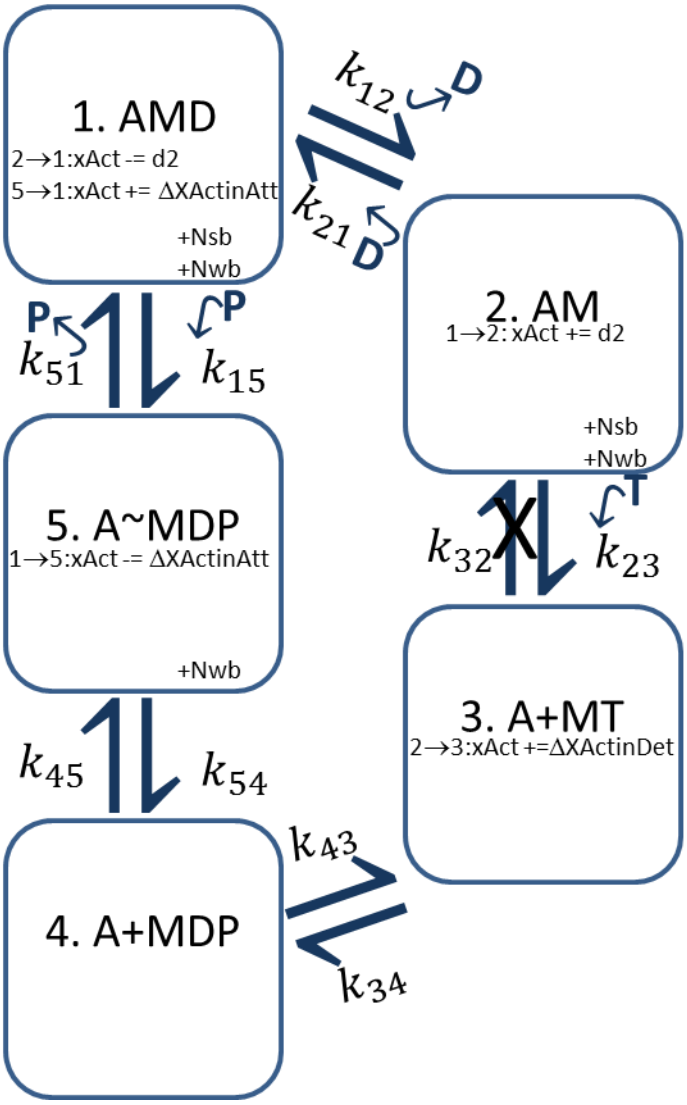

0-2 Kinetic scheme of collective force generator model. Strongly bound states are AMD and AM. The detached states are A+MT, A+MDP, and A~MDP, with the last being the weakly bound state. Values for the transitions between states are listed in Tables 6-1 & 6-2. The displacements, which are calculated as shown in Table 6-2, for the mechanical transitions (k51, k15, k12, k21, k23) are reported in the states.

For each head, transitions are determined at each time step by generating two random variables. The first random variable is used to determine if a transition occurs by comparing the random variable to the sum of the forward and reverse transition probabilities. Transition probabilities are determined by multiplying the appropriate

rates according to the current state the myosin head is in (outlined in Tables 6-1 & 6-2, Fig. 6-2) with the time step, *dt*. If the transition probability is greater than the sum of the forward and reverse transition probabilities, a transition is determined to have occurred. In order to resolve whether the transition is a forward or reverse transition, the second random variable is compared to the ratio of the reverse probability to the sum of the transition probabilities. If it is less than this ratio, it is considered a reverse transition. If it is more, then a forward transition is picked for that myosin. This determination of transitions is checked for every head.

Transitions can be either kinetic or mechanical in terms of having an effect on the mechanical state of the system. Kinetic transitions which do not affect the system mechanics (See Fig. 6-2; k34, k43, k45, k54) are allowed to occur simultaneously from multiple heads. If a transition is mechanical (See Fig. 6-2; k51, k15, k12, k21, k23), then only one is allowed to occur per time step. The number of simultaneous transitions and blocked mechanical transitions are a statistic collected by the program. Upon a mechanical transition, the appropriate displacement modifies the actin filament position (Table 6-2; dXAtt, d2Trans, dXDet).

Simulation Constants	Name	Value	Unit
Experiment time	expTime	1	s
Time step	dt	1.00E-07	s
[ATP]	T	1	mM
[ADP]	D	1	µM
[Pi]	P	1	mM
Actin length	La	1000	nm
Actin persistence length	Lp	20	µm
Myosin density	rho	0.1	#Myosin/nm
Number of myosin	numMyosin	rho*La	-
Binding site density	bsd	0.05	#Binding site/nm
Number of available binding sites	Nabs	bsd*La	-
Myosin weak-to-strong step size	d	8	nm
Myosin ADP release step size	d2	2	nm
Stiffness of driving (binding) myosin	kDri	0.5	pN nm^{-1}
Stiffness of resistive (bound) myosin	kUni	0.5	pN nm^{-1}
[AM] -> [A+MT]	k23	5000 * T	s^{-1}
[A+MT] -> [AM]	k32	0	s^{-1}
[A+MT] -> [A+MDP_i]	k34	100	s^{-1}
[A+MDP_i] -> [A+MT]	k43	100	s^{-1}
[A~MDPi] -> [A+MDP_i]	k54	0.0001	s^{-1} μM^{-1}

Table 0-1 Simulation constants.

Time Step Variables	Name	Value	Unit
Number strong bound myosin	Nsb	Calc.	-
Number weak bound myosin	Nwb	Calc.	-
Total number of bound myosin	Nb	Nsb+Nwb	-
Distance between strong bound myosin	dbsb	La/Nsb	nm
System stiffness	kRes	Nsb*kUni	pN nm^{-1}
Actin slack	s	f(dbsb, Lp)	nm
Transmitted myosin step, d	dTrans	d-s	nm
Transmitted myosin step, d2	d2Trans	d2*(d/dTrans)	nm
Actin displacement on myosin attachment	dXAtt	(kDrive/(kRes+kDri))*dTrans	nm
Distance of binding myosin compliance change	dXMyo	dTrans-dXAtt	nm
Avg. bound myosin compliance length	xUni	(kDri*dXMyo)/(kRes)	nm
Actin displacement on myosin detachment	dXDet	(kRes*xUni-kDri*dXMyo)/(-kDri-kRes)	nm
Free myosin binding sites on actin	NabsFree	Nabs-Nb	nm
$[A+MDP_i] \rightarrow [A\sim MDP_i]$	k45	NabsFree*500	s-1
Boltzmann constant at 25C	kT	4	pN nm
Work of myosin attachment	W51	-partWS * ½kDri*dXmyo²+½kDri*dXmyo*dXAct	-
Work of reverse myosin attachment	W15	(1-partWS) * ½kDri*dXmyo²+½kDri*dXmyo*dXAct	-
$[A\sim MDP_i] \rightarrow [AMD]$	k51	k51°*exp(W51/kT)	s^{-1}
$[AMD] \rightarrow [A\sim MDP_i]$	k15	k15°*exp(W15/kT)*P	s^{-1}
Avg. ratio bound myosin states	ratio	((k23*T)/(k12+(k23*T))-½)/½	-
Partition of ADP release step work	partADP	0.5	-
Work of myosin ADP release	W12	partADP*ratio*(½kRes*d2Trans)	-
Work of reverse myosin ADP release	W21	(1-partADP)*ratio*(½kRes*d2Trans)	-
Basal ADP release rate	k12°	200	s^{-1}
Basal reverse ADP release rate	k21°	1	s^{-1}
$[AMD] \rightarrow [AM]$	k12	k12°*exp(W51/kT)	s^{-1}
$[AM] \rightarrow [AMD]$	k21	k21°*exp(W15/kT)*D	s^{-1}

Table 0-2 Time Step Variables.

Chapter 5

Dissertation conclusion

SUMMARY

We have presented a body of research that fills a void in the current understanding of muscle contraction. By building upon previous observations that were not accounted by the prevailing theory of muscle contraction (*1–4*), we have developed a unified framework for describing various mechanisms that determine muscle contraction (Chapters 2, 4). Since our in vitro and kinetic experimental results were not forced through the lens of the detachment limited model of unloaded shortening velocities, we were able to elucidate the primary mechanism by which an inhibitor of muscle, used for decades experimentally, slows *V* (Chapter 3). In order to measure single molecule myosin kinetics of attachment and detachment to actin, we developed a novel single molecule binding assay, SiMBA (Chapters 1, 3). In total, our work has produced a relatively simple model of muscle contraction that provides mechanisms for how both myosin attachment to and detachment from actin determines unloaded shortening velocities.

CONCLUSIONS

This dissertation covers three related approaches to developing a more complete understanding of how single molecule properties of muscle myosin collectively generate unloaded shortening velocities, *V*. Theory, experimentation, and

simulation results all contributed to answering fundamental muscle research questions. These questions focused on addressing how single myosin molecule properties scale in an ensemble to collectively perform work that results in *V* and how attachment kinetics affect *V*. Our work has resulted in the development of a simple theoretical framework, based on quantifiable kinetic and physical parameters of myosin and actin, which provides a set of mechanisms to describe experimental data that the predominate models of muscle contraction are unable to.

A combination of experimental evidence and theory are used in Chapter 2 to describe how interhead forces in an ensemble of muscle myosin can accelerate ADP release, the primary limiting detachment kinetic step. This theory is extended from the well-established two-headed myosin V system (*5*, *6*) and applied in the setting of muscle myosin with concept that binding to actin couples heads to each other. The force generated between heads is then allowed to act, in effect, as an allosteric regulator of myosin since the chemistry of myosin binding and detachment are mechanically coupled. The energetic cost of this is detailed for both myosin V and muscle myosin II. This theory, of myosin heads being able to act as both force generators and force sensors provides the basis for subsequent development of the collective force generator model discussed in Chapter 4. Initial experimental evidence of changes in interhead forces under different effective detachment rates is presented. This would provide the basis for the development of a more rigorous breaking assay (*4*).

In line with developing a better understanding of how myosin attachment kinetics influences *V*, we characterize the mechanism of sucrose, a well-known inhibitor

of muscle contraction, in Chapter 3. Although used historically in muscle research, first with muscle fiber and then in in vitro studies (*7*–*9*), the specific mechanism of how sucrose reduced muscle force and slowed *V* was not established. Using a combination of stopped flow and steady-state kinetic assays with in vitro and a novel single molecule assay, we show that the primary mechanism by which sucrose affects *V* is by inhibiting attachment of myosin to actin.

Having established that sucrose slowed *V* by slowing attachment and that this effect was not recovered with increased concentrations of myosin, we extended our theoretical model of muscle contraction in Chapter 4 to include three novel assumptions. The first assumption extends the concept of the factors that determine the transmission efficiency of the myosin step along actin. As the basis of Chapter 2, interhead forces are the determining factor for the rate of detachment of myosin from actin. Experimental evidence suggested there was a limit to the efficiency of this force transmission along an actin filament (*10*). Using the persistence length of the actin filament, which is a measure of polymer flexibility, and the distance between strongly bound myosin heads, we develop a formal definition of the efficiency of force transmission. The second assumption applies the well-established principle of myosin saturation of ATPase kinetics (*11*) to our model of in vitro *V*. Finally, we incorporate the recent experimental evidence of asymmetric stiffness of bound and binding myosin heads (*12*). Combining these novel assumptions with the theoretical mechanochemically coupled model described in Chapter 2, we present simulated data that agrees with experimental data showing changes in detachment kinetics and the

inability of increased myosin concentrations to recover reduced *V* due to inhibited attachment rates.

Medical Implications. The development of a collective force generator model grants greater insight into how myosin molecules generate force and the way in which their mechanics are coupled to their chemistry. This is useful in understanding the molecular mechanism s that give rise to some muscle diseases. Familial hypertrophic cardiomyopathy (FHC), which is implicated in sudden cardiac death, has been linked to mutations that alter the mechanical function of cardiac myosin (*13*). Changes in the sarcomere's organization and force generation are known to occur in cases of dilated cardiomyopathy (DCM) (*14*). The calcium sensitivity of the contractile elements of cells is altered by their mechanics (*15*). Our model of muscle contraction provides a fundamental framework required to understand the primary factors involved in tuning muscle function. Although the feasibility of using a muscle myosin attachment inhibitor like sucrose in therapies is low, our work in establishing its primary mechanism enables its utilization as an accessible chemical inhibitor of actin-myosin in studies further probing how attachment kinetics influence muscle function. This could lead to novel therapies that can tune muscle function in to treat various myopathies.

RECOMMENDATIONS

Future work. Our simple model of muscle contraction, which uses macroscopic parameters to approximate system variables, has a minor drawback in that individual molecular mechanical values are not defined. Several models track these mechanical values with a system of connected springs (*16*–*19*). These stochastic implementations

cannot account for simultaneous transitions that involve mechanical changes (i.e. actin movement or myosin binding). An additional challenge is that balancing forces for a collection of springs is highly complex if molecular compliance is non-linear (*12*). An efficient implementation of a graph Laplacian has been developed (*20*). This iterative process of adding edges and rebalancing a graph could to balance system of molecules that have non-linear stiffness.

Our collective force generator model only provides insight into mechanisms under unloaded conditions. Force generation and the effect of external forces are the next areas to extend our model to. Our simple model framework and macroscopic treatment of system variables is well suited to incorporating these important aspects of muscle function.

The regulation of muscle by calcium is an important aspect in the overall mechanisms that determine velocity and force (*21*). Previous work has extended the understanding of the role myosin kinetics play in determining the calcium sensitivity of muscle (*22*). Our collective force generator model can explicitly model actin-myosin kinetics in a regulated muscle system.

Reflections on graduate work in the Baker Lab. All of the work described in this dissertation was done in the lab of Dr. Josh Baker during 2008-2013. This lab fostered a research methodology that relied on both experimental and theoretical techniques to great success. Regardless of the mathematical or computational background of future Baker Lab graduate students, it is highly recommended to adopt this perspective and develop an appreciation of combining modeling and experimentation. Each avenue of

research yields insight into the other, and the combination is a powerful strategy to build upon the conclusions detailed in this dissertation.

Reflections on biological modeling. What is the purpose of a model? Without experimental data to predict or to provide a possible set of mechanisms for, a model exists in pure theoretical space. What is the value of a model? The ability of a model to predict and match experimental data is not the sole determinant of its value, as an unlimited parameter model could fit any set of data and provide zero insight into the mechanisms of the experimental system. Additionally, if the parameters of the model are not representative of measurable components of the system, the insight yielded by the model is significantly diminished. In contrast, if too many variables of inappropriate detail are used, the model loses value. The practical considerations of a model are not solely theoretical exercises, as they are important in determining the scope and applicability of the model to answering questions. In this light, simple models of muscle contraction offer the best framework to be used in conjunction with experimental data to advance our understanding of muscle.

Reflections on muscle modeling. What are the remaining questions of muscle research? There is little doubt that enormous advances in our understanding of muscle contraction have been made since the first major models of muscle were introduced (*23*–*26*). Fenn's model of muscle contraction provided a thermodynamic framework in which to understand the relationship between force and velocity. AV Hill extended this understanding by outlining the contributions of driving and resistive components of muscle. After x-ray crystallography imparted molecular scale images of the muscle

sarcomere, Huxley developed a molecular model of muscle that described the sliding filament in even greater detail. Our collective force generation model provides additional insight into how the mechanics and chemistry of single myosin molecules are coupled in an ensemble and how these affect the attachment and detachment rates. Applying these theories of muscle contraction to developing tangible therapies for muscle related diseases is a high priority goal of publicly funded research. Dilated cardiomyopathy stems from the response of the cardiac tissue to reduced force generation, in which additional numbers of myosin are generated to overcome the decreased force production. It is exciting to consider the potential contribution of our collective force generator model of muscle contraction as a tool for researchers to understand how the various factors of attachment and detachment kinetics, actin polymer flexibility, asymmetric stiffness of myosin heads, and kinetic saturation determine muscle function in the pursuit of developing therapies to treat myopathies.

REFERENCES

1. Baker, J. E., LaConte, L. E., Brust-Mascher, I., and Thomas, D. D. (1999) Mechanochemical coupling in spin-labeled, active, isometric muscle., *Biophysical journal 77*, 2657–64.

2. Baker, J. E., Brosseau, C., Joel, P. B., and Warshaw, D. M. (2002) The biochemical kinetics underlying actin movement generated by one and many skeletal muscle myosin molecules., *Biophysical journal 82*, 2134–47.

3. Hooft, A. M., Maki, E. J., Cox, K. K., and Baker, J. E. (2007) An accelerated state of myosin-based actin motility., *Biochemistry 46*, 3513–20.

4. Stewart, T. J., Jackson Jr., D. R., Smith, R. D., Shannon, S. F., Cremo, C. R., and Baker, J. E. (2013) Actin sliding velocities are influenced by the driving forces of actin-myosin binding, *Cellular and Molecular Bioengineering 6*, 26–37.

5. Rüegg, C., Veigel, C., Molloy, J. E., Schmitz, S., Sparrow, J. C., and Fink, R. H. a. (2002) Molecular motors: force and movement generated by single myosin II molecules., *News in physiological sciences : an international journal of physiology produced jointly by the International Union of Physiological Sciences and the American Physiological Society 17*, 213–8.

6. Sellers, J. R., and Veigel, C. (2006) Walking with myosin V., *Current opinion in cell biology 18*, 68–73.

7. Ando, T., and Asai, H. (1977) The effects of solvent viscosity on the kinetic parameters of myosin and heavy meromyosin ATPase., *Journal of bioenergetics and biomembranes 9*, 283–8.

8. Chase, P. B., Denkinger, T. M., and Kushmerick, M. J. (1998) Effect of viscosity on mechanics of single, skinned fibers from rabbit psoas muscle., *Biophysical journal 74*, 1428–38.

9. Chase, P. B., Chen, Y., Kulin, K. L., and Daniel, T. L. (2000) Viscosity and solute dependence of F-actin translocation by rabbit skeletal heavy meromyosin., *American journal of physiology. Cell physiology 278*, C1088–98.

10. Harris, D. E., and Warshaw, D. M. (1993) Smooth and skeletal muscle myosin both exhibit low duty cycles at zero load in vitro., *The Journal of biological chemistry 268*, 14764–8.

11. Adelstein, R. S., and Eisenberg, E. (1980) Regulation and kinetics of the actin-myosin-ATP interaction., *Annual review of biochemistry 49*, 921–56.

12. Kaya, M., and Higuchi, H. (2010) Nonlinear elasticity and an 8-nm working stroke of single myosin molecules in myofilaments., *Science (New York, N.Y.) 329*, 686–9.

13. Tyska, M. J., Hayes, E., Giewat, M., Seidman, C. E., Seidman, J. G., and Warshaw, D. M. (2000) Single-molecule mechanics of R403Q cardiac myosin isolated from the mouse model of familial hypertrophic cardiomyopathy., *Circulation research 86*, 737–44.

14. Frazier, A. H., Ramirez-Correa, G. a, and Murphy, A. M. (2011) Molecular mechanisms of sarcomere dysfunction in dilated and hypertrophic cardiomyopathy., *Progress in pediatric cardiology*. Elsevier Ireland Ltd *31*, 29–33.

15. Bers, D. M. (2002) Cardiac excitation-contraction coupling., *Nature 415*, 198–205.

16. Campbell, K. S. (2009) Interactions between Connected Half-Sarcomeres Produce Emergent Mechanical Behavior in a Mathematical Model of Muscle, *PLoS Computational Biology 5*.

17. Campbell, K. S. (2006) Filament compliance effects can explain tension overshoots during force development., *Biophysical journal 91*, 4102–9.

18. Tanner, B. C. W., Daniel, T. L., and Regnier, M. (2012) Filament compliance influences cooperative activation of thin filaments and the dynamics of force production in skeletal muscle., *PLoS Computational Biology 8*, e1002506.

19. Tanner, B. C. W., Daniel, T. L., and Regnier, M. (2007) Sarcomere lattice geometry influences cooperative myosin binding in muscle., *PLoS computational biology 3*, e115.

20. Kelner, J. A., Orecchia, L., Sidford, A., and Zhu, Z. A. (2013) A Simple, Combinatorial Algorithm for Solving SDD Systems in Nearly-Linear Time, in *ACM Symposium on the Theory of Computing*, pp 1–32. Data Structures and Algorithms; Numerical Analysis.

21. McKillop, D. F., and Geeves, M. a. (1993) Regulation of the interaction between actin and myosin subfragment 1: evidence for three states of the thin filament., *Biophysical journal*. Elsevier *65*, 693–701.

22. Sich, N. M., O'Donnell, T. J., Coulter, S. a, John, O. a, Carter, M. S., Cremo, C. R., and Baker, J. E. (2010) Effects of actin-myosin kinetics on the calcium sensitivity of regulated thin filaments., *The Journal of biological chemistry 285*, 39150–9.

23. Fenn, W. O. (1923) A quantitative comparison between the energy liberated and the work performed by the isolated sartorius muscle of the frog., *The Journal of physiology 58*, 175–203.

24. Hill, A. V. (1938) The Heat of Shortening and the Dynamic Constants of Muscle, *Proceedings of the Royal Society B: Biological Sciences 126*, 136–195.

25. Huxley, A. F., and Niedergerke, R. (1954) Structural changes in muscle during contraction; interference microscopy of living muscle fibres., *Nature 173*, 971–3.

26. Huxley, A. F. (1957) Muscle structure and theories of contraction., *Progress in biophysics and biophysical chemistry 7*, 255–318.